Investigation of protein secretion in microscale cultivation systems with novel tools

Von der Fakultät für Mathematik, Informatik und Naturwissenschaften der RWTH Aachen University zur Erlangung des akademischen Grades einer Doktorin der Naturwissenschaften genehmigte Dissertation

vorgelegt von

Master of Science (M. Sc.)

Carolin Müller

aus Wolfsburg

Berichter: Univ.-Prof. Dr. rer. nat. Marco Oldiges
Univ.-Prof. Dr.-Ing. Lars Blank

Tag der mündlichen Prüfung: 16.03.2023

„Spaß auf Zellulosebasis“

M. Kennel & J. Frömming

Eidesstattliche Erklärung

Ich, Carolin Müller,

erkläre hiermit, dass diese Dissertation und die darin dargelegten Inhalte die eigenen sind und selbstständig, als Ergebnis der eigenen originären Forschung, generiert wurden.
Hiermit erkläre ich an Eides statt

1. Diese Arbeit wurde vollständig oder größtenteils in der Phase als Doktorandin dieser Fakultät und Universität angefertigt;
2. Sofern irgendein Bestandteil dieser Dissertation zuvor für einen akademischen Abschluss oder eine andere Qualifikation an dieser oder einer anderen Institution verwendet wurde, wurde dies klar angezeigt;
3. Wenn immer andere eigene- oder Veröffentlichungen Dritter herangezogen wurden, wurden diese klar benannt;
4. Wenn aus anderen eigenen- oder Veröffentlichungen Dritter zitiert wurde, wurde stets die Quelle hierfür angegeben. Diese Dissertation ist vollständig meine eigene Arbeit, mit der Ausnahme solcher Zitate;
5. Alle wesentlichen Quellen von Unterstützung wurden benannt;
6. Wenn immer ein Teil dieser Dissertation auf der Zusammenarbeit mit anderen basiert, wurde von mir klar gekennzeichnet, was von anderen und was von mir selbst erarbeitet wurde;
7. Teile dieser Arbeit wurden zuvor veröffentlicht. Eine vollständige Auflistung ist auf den folgenden Seiten zu finden.

Göttingen, April 2023

Carolin Müller

Published work

This work was conducted at the Forschungszentrum Jülich GmbH at the Institute of Bio- and Geosciences, IBG-1: Biotechnology. Parts of this thesis have been published in peer-reviewed journals, were presented at conferences as posters and talks and were parts of supervised student's work.

Figures taken from existing own publications are cited in the text. Any thought, methodology, result, or conclusion that is part of an existing proprietary publication is not specifically mentioned, but is considered properly cited by the following listings.

Journal articles

I. C. Müller, C. L. Igwe, W. Wiechert, and M. Oldiges. "Scaling production of GFP1-10 detector protein in *E. coli* for secretion screening by split GFP assay". In: *Microb Cell Factories* 20.1 (2021). DOI: 10.1186/s12934-021-01672-6

II. C. Müller, P. J. Bakkes, P. Lenz, V. Waffenschmidt, L. M. Helleckes, K.-E. Jaeger, W. Wiechert, A. Knapp, R. Freudl, and M. Oldiges. "Accelerated strain construction and characterization of *C. glutamicum* protein secretion by laboratory automation". In: *Appl Microbiol Biotechnol* 106.12 (2022), pp. 4481–4497. DOI: 10.1007/s00253-022-12017-7

III. L. M. Helleckes, C. Müller, T. Griesbach, M. Moch, M. Osthege, W. Wiechert, and M. Oldiges. "Explore or exploit? A novel screening strategy for PETase secretion by *Corynebacterium glutamicum*". In: *Biotechnol Bioeng* 120.1 (2023), pp. 139–153. DOI: 10.1002/bit.28261
The first two authors contributed equally.

IV. P. J. Bakkes, P. Lenz, C. Müller, A. Bida, D. Dohmen-Olma, A. Knapp, M. Oldiges, K.-E. Jaeger, and R. Freudl. "Biosensor-based optimization of cutinase secretion by *Corynebacterium glutamicum*". In: *Front Microbiol* 12 (2021). DOI: 10.3389/fmicb.2021.750150

V. M. Osthege, N. Tenhaef, R. Zyla, C. Müller, J. Hemmerich, W. Wiechert, S. Noack, and M. Oldiges. "bletl - A Python package for integrating BioLector microcultivation devices in the Design-Build-Test-Learn cycle". In: *Eng Life Sci* 22.3-4 (2022), pp. 242–259. DOI: 10.1002/elsc.202100108

Conference posters

I. C. Müller, C. L. Igwe, V. Waffenschmidt, W. Wiechert, and M. Oldiges. "Screening of signal peptides for secretion of heterologous proteins in *C. glutamicum* using split GFP". 6th Joint Conference of the DGHM & VAAM, Leipzig, Germany, 8.–11.3.2020

II. C. Müller, C. L. Igwe, W. Wiechert, and M. Oldiges. "Application of the split GFP assay in high-throughput screening". 34. DECHEMA-Jahrestagung der Biotechnologen, virtual, 21.–24.09.2020. DOI: 10.1002/cite.202055030

III. C. Müller, V. Waffenschmidt, W. Wiechert, and M. Oldiges. "Automated signal peptide screening workflow for secretion of heterologous proteins in *C. glutamicum*". Himmelfahrtstagung on Bioprocess Engineering 2021 - New Bioprocesses, New Bioproducts, virtual, 10.–12.05.2021

IV. V. Waffenschmidt, C. Müller, W. Wiechert, and M. Oldiges. "Developing a semi-automated cloning workflow: approaches to accelerate strain library generation". German Conference on Synthetic Biology, virtual, 13.–17.09.2021

Conference talks

I. C. Müller, L. M. Helleckes, T. Griesbach, V. Waffenschmidt, M. Osthege, W. Wiechert, and M. Oldiges. "From strain to screening: Automated workflows for identifying the best signal peptide for target protein secretion via split GFP assay". German Conference on Synthetic Biology, virtual, 13.–17.09.2021

II. C. Müller and M. Oldiges. “Automated signal peptide screening workflow for secretion of heterologous proteins in *C. glutamicum*”. Final CKB-Symposium, CLIB-Kompetenzzentrum Biotechnologie, Düsseldorf, Germany, 16.09.2021

III. C. Müller, L. M. Helleckes, V. Waffenschmidt, W. Wiechert, and M. Oldiges. “Automated signal peptide screening workflow for secretion of heterologous proteins in *C. glutamicum*”. ECCE 13 & ECAB 6, virtual, 20.–23.06.2021

Student’s theses and research internships

I. V. Waffenschmidt. “Preparation of a pEKEx-based plasmid for high-throughput screening of signal peptides”. Research internship. University of Bonn, 2019

II. V. Waffenschmidt. “Production and purification of the detector protein GFP1-10 in *Escherichia coli*”. Research internship. University of Bonn, 2020

III. V. Waffenschmidt. “Development and characterisation of an automated routine for the split-GFP assay for monitoring protein secretion”. Research internship. University of Bonn, 2020

IV. C. L. Igwe. “Workflow optimization of split GFP assay for automated screening of cutinase secretion in *Corynebacterium glutamicum*”. Master thesis. RWTH Aachen University, 2020

V. L. Pohlen. “Erstellung und Untersuchung neuer *Corynebacterium glutamicum* Stämme zur Sekretion einer heterologen Cutinase”. Bachelor thesis. FH Aachen University of Applied Sciences, 2020

VI. V. Waffenschmidt. “Development of automated workflows for accelerated generation of *Corynebacterium glutamicum* strains and screening for heterologous protein secretion”. Master thesis. University of Bonn, 2021

VII. T. Griesbach. “Automatisiertes Screening von Sec Signalpeptidenfür die heterologe PETase-Sekretion mit *Corynebacterium glutamicum*”. Master thesis. HTW Berlin University of Applied Sciences, 2022

Acknowledgements

I would like to thank Prof. Dr. Marco Oldiges, who supervised my work and gave me the opportunity to conduct the research project in his group. His valuable feedback during the status seminars, on paper manuscripts, and also on the thesis itself have always been helpful. He gave me a lot of freedom with my research project, but always supported me when I needed advice. Thanks also to Prof. Dr. Wolfgang Wiechert for the opportunity to do my doctoral studies at his institute. I would like to thank Prof. Dr.-Ing. Lars M. Blank and Prof. Dr. Ulrich Schwaneberg for being a members of my examination committee and for examining this work. Furthermore, I am grateful to all my collaborators, who looked at my work from a different angle and discussed new aspects. This includes especially the participants of the frequent secretion meetings from the IBG-1 and the IMET institute. My students have helped to produce so many results in the last few years. Vera Waffenschmidt, Chika L. Igwe, Lutz Pohlen and Tim Griesbach, it was a pleasure to supervise your theses.

A special thanks goes to all members of the BioPro and MicroPhen groups. A PhD always has ups and downs and everything is better with colleagues like I had. You supported me and generally created a pleasant working atmosphere. In the recent years, there have been so many nice conversations during lunch or coffee breaks, as well as countless rounds of Mario Kart on the work-life balance simulator. I would especially like to thank the best office colleagues Kira Küsters and Laura M. Helleckes (the 257er or the MolecuLadies and the Model). I really enjoy thinking back to the many cups of tea or coffee we drank together, the countless situations in which we had professional discussions, but often also simply laughed together and exchanged the latest gossip.

Last but not least, there are some people, who have always accompanied and supported me. These include, of course, my parents, my brother and my grandparents. Without you I would not have become the person I am. Dear Felix, I am infinitely grateful to you for supporting me in the decision to do my doctorate in Jülich. Whatever the future holds for us, I look forward to it.

Contents

Abstract

Until today, it is impossible to predict a suitable signal peptide for Sec-type secretion of heterologous proteins in Gram-positive bacteria. Instead, signal peptides have to be tested for each host and target protein under process conditions. In addition, the ribosome binding site and in particular the spacer between the Shine-Dalgarno sequence and the start codon of the signal peptide can also affect protein secretion. To accelerate the identification of suitable combinations of signal peptides and target proteins, automated workflows for targeted strain construction and high-throughput screening for heterologous protein secretion in *Corynebacterium glutamicum* were established, which can be easily adapted to different target proteins.

A plasmid library with different *Bacillus subtilis* signal peptides was constructed in the newly designed pPBEx2-based plasmid pCMEx12, which allows the exchange of the ribosome binding site including the spacer sequence as well as the signal peptide sequence by cassette mutagenesis. In this method, the inserts are provided as hybridized oligonucleotides that are not fully complementary, but have overhangs that can be ligated to the restriction digested backbone. For target protein secretion with pCMEx-based plasmids, a reporter gene coding for a blue chromoprotein under the control of a constitutive promoter can be exchanged with the gene of interest by Golden Gate assembly, combining restriction and ligation in a one-pot setup. Since the chromoprotein leads to blue colonies after transformation, successful cloning can be detected by a change in colony color from blue to white, in addition to a restriction enzyme digest in which the number and size of DNA fragments depend on the insert. The gene of interest is then expressed in frame with an amino-terminal signal peptide and carboxyl-terminally linked to the 11th β-sheet of the green fluorescent protein (GFP, GFP11-tag) under the control of the inducible tac promoter. The molecular cloning steps of the Golden Gate assembly, the *Escherichia coli* heat-shock transformation, the plasmid purification and the restriction digest were automated using the Opentrons OT-2 liquid handling robot with integrated Temperature or Magnetic Module. This reduced the process time for molecular cloning to about 58% of that for the manual process.

For testing cultivation workflows with online product monitoring, the *C. glutamicum* pPBEx2-PhoD^{Cg}-GFP enabling tightly controlled induction of GFP secretion was successfully prepared. An automated high-throughput screening workflow was developed on a Tecan Freedom EVO® robotic platform with an integrated centrifuge, microplate reader, and BioLector® for microscale cultivation with online measurement of the backscatter signal that correlates to cell dry weight. Automated preculture handling and backscatter-triggered inoculation of main cultures and induction ensure high comparability of bacterial growth. Using this workflow, suitable combinations of ribosome binding sites and *B. subtilis* signal peptides were identified for *Fusarium solani* f. sp. *pisi* cutinase-GFP11 secretion by *C. glutamicum*. Cutinase-GFP11 in the cultivation supernatant was detected 4 h after induction via activity measurement and activity-independently by assembly of the GFP11-tag with GFP1-10 in added detector solution by holo-GFP fluorescence in split GFP assay. The process time from cultivation of up to 12 different strains to detection of the target protein in the supernatant is about 1.5 days, with manual operations only required at the start of cultivation and prior to the assays.

For high-throughput screening approaches, sufficient quantities of detector solution is needed. Therefore, a fed-batch cultivation process for the GFP1-10 production in laboratory-scale bioreactors was established and detector solution for up to 385 screenings in 96-well plates could be obtained. Aspects of GFP1-10 detector protein stability, storage and assay incubation conditions have been investigated.

After a proof-of-concept using the secretion model protein cutinase, a *B. subtilis* signal peptide screening for secretion of polyethylene terephthalate degrading enzymes leaf-branch compost cutinase (LCC) and PE-H was conducted. For this, the cultivation workflow was optimized to allow the comparison of up to 24 different strains in one run. Using a process model combining Bayesian inference and Thompson sampling, the best of 24 signal peptides was identified with a probability of 80% for the PE-H and 75% for the LCC after only three batch cultivations.

Zusammenfassung

Bis heute ist es nicht möglich, ein geeignetes Signalpeptid für die Sec-abhängige Sekretion heterologer Proteine in Gram-positiven Bakterien vorherzusagen. Stattdessen müssen Signalpeptide für jeden Wirt und jedes Zielprotein unter Prozessbedingungen getestet werden. Darüber hinaus können auch die Ribosomen-Bindungsstelle und insbesondere der Spacer zwischen der Shine-Dalgarno-Sequenz und dem Startcodon des Signalpeptids die Proteinsekretion beeinflussen. Um die Identifizierung geeigneter Signalpeptid-Zielprotein-Kombinationen zu beschleunigen, wurden automatisierte Arbeitsabläufe für die gezielte Stammkonstruktion und das Hochdurchsatz-Screening für die heterologe Proteinsekretion in *Corynebacterium glutamicum* etabliert, die an verschiedene Zielproteine angepasst werden können.

Eine Plasmidbibliothek mit verschiedenen *Bacillus subtilis* Signalpeptiden wurde mit dem neu entworfenen pPBEx2-basierten Plasmid pCMEx12 konstruiert, das den Austausch der Ribosomenbindungsstelle einschließlich der Spacer-Sequenz sowie der Signalpeptidsequenz durch Kassettenmutagenese ermöglicht. Bei dieser Methode werden die Inserts als hybridisierte Oligonukleotide bereitgestellt, die nicht vollständig komplementär sind, sondern Überhänge aufweisen, die mit einem entsprechenden restriktionsverdauten pCMEx-Plasmid ligiert werden können. Für die Sekretion des Zielproteins kann in pCMEx-basierten Plasmiden das Reportergen, das für ein blaues Chromoprotein unter der Kontrolle eines konstitutiven Promotors kodiert, durch Golden Gate Assemblierung mit dem gewünschten Gen ausgetauscht werden, wobei Restriktion und Ligation in einem Prozessschritt kombiniert werden. Da das Chromoprotein nach der Transformation zu blauen Kolonien führt, kann eine erfolgreiche Klonierung durch eine Änderung der Koloniefarbe von blau nach weiß nachgewiesen werden, zusätzlich zu einem Restriktionsenzym-Testverdau, bei dem die Anzahl und Größe der DNA-Fragmente vom Insert abhängt. Das Zielgen wird dann zusammen mit einem aminoterminalen Signalpeptid mit einem kurzen Linker und einem Carboxy-terminalen 11. β-Faltblatt des grün fluoreszierenden Proteins (GFP, GFP11-tag) unter der Kontrolle des induzierbaren tac-Promotors exprimiert.

Mit Hilfe eines Opentrons OT-2 Pipettierroboters mit integriertem Temperatur- oder Magnetmodul wurden die Klonierungsschritte Golden Gate Assemblierung, *Escherichia coli* Hitzeschock-Transformation, Plasmidreinigung und Testverdauung automatisiert. Dadurch konnte die Prozesszeit für diese Klonierungsschritte auf etwa 58% der Zeit für den manuellen Prozess reduziert werden.

Zum Testen von Workflows für die Kultivierung mit Online-Produktmessung wurde der Stamm *C. glutamicum* pPBEx2-PhoD^{Cg}-GFP erfolgreich erstellt, der eine streng kontrollierte Induktion der GFP-Sekretion ermöglicht. Ein automatisierter Hochdurchsatz-Screening Workflow wurde auf einer Tecan Freedom EVO® Robotikplattform entwickelt mit integrierter Zentrifuge, Mikroplattenlesegerät und einem BioLector® für die Mikrokultivierung mit Online-Messung des Rückstreusignals, das mit dem Zelltrockengewicht korreliert. Die automatisierte Handhabung der Vorkulturen und die durch Rückstreuung ausgelöste Inokulation der Hauptkulturen und Induktion gewährleisten eine hohe Vergleichbarkeit des Bakterienwachstums. Mit diesem Workflow wurden geeignete Kombinationen von Ribosomenbindungsstellen und *B. subtilis* Signalpeptiden für die Sekretion der *Fusarium solani* f. sp. *pisi* Cutinase-GFP11 mit *C. glutamicum* identifiziert. Cutinase-GFP11 im Kultivierungsüberstand wurde 4 h nach Induktion durch Aktivitätsmessung und aktivitätsunabhängig durch Assemblierung des GFP11-tags mit GFP1-10 in der zugegebenen Detektorlösung mit anschließender Chromophorbildung im Split GFP Assay nachgewiesen. Die Prozessdauer von der Kultivierung von bis zu 12 verschiedenen Stämmen bis zum Nachweis des Zielproteins im Überstand beträgt etwa 1,5 Tage, wobei manuelle Eingriffe nur zu Beginn der Kultivierung und vor den Assays erforderlich sind.

Für Hochdurchsatz-Screenings werden ausreichende Mengen an Detektorlösung benötigt. Daher wurde ein Fed-Batch Kultivierungsprozess für die GFP1-10 Produktion im Labormaßstab in Bioreaktoren etabliert und es konnte Detektorlösung für bis zu 385 Screenings in 96-Well-Platten gewonnen werden. Aspekte der Stabilität des GFP1-10 Detektorproteins, der Lagerung und der Assay-Inkubationsbedingungen wurden untersucht.

Nach einem Proof-of-Concept mit der Cutinase, einem Modellprotein für die heterologe Proteinsekretion, wurde ein *B. subtilis* Signalpeptid-Screening für die Sekretion der Polyethylenterephthalat-abbauenden Enzyme Leaf-branch compost cutinase (LCC) und PE-H durchgeführt. Dafür wurde die Kultivierung optimiert, um den Vergleich von bis zu 24 verschiedenen Stämmen in einem Durchgang zu ermöglichen.

Mit Hilfe eines Prozessmodells, das Bayes'sche Inferenz und Thompson-Sampling kombiniert, wurde das beste von 24 Signalpeptiden mit einer Wahrscheinlichkeit von 80% für die PE-H und 75% für die LCC nach nur drei Batch-Kultivierungen identifiziert.

Abbreviations

4NP	4-nitrophenol
4NPP	4-nitrophenyl palmitate
ATP	adenosine triphosphate
BHI	brain heart infusion
BHIS	BHI with 45.5 g L^{-1} D-sorbitol
CDW	cell dry weight
CPEC	circlar polymerase extension cloning
C-terminal	carboxyl-terminal
dNTP	deoxyribonucleoside triphosphate
DO	dissolved oxygen
DoE	design of experiments
DWP	deepwell plate
EDTA	ethylenediaminetetraacetic acid
ELISA	enzyme-linked immunosorbent assay
GFP	green fluorescence protein
GTP	guanosine triphosphate
HPLC	high-performance liquid chromatography
IPTG	isopropyl β-D-1-thiogalactopyranoside
KPI	key performance indicator
LB	lysogeny broth
LCC	leaf-branch compost cutinase
MCB	master cell bank
MHET	mono(2-hydroxyethyl) terephthalic acid
MOPS	3-(N-morpholino)propanesulfonic acid
MTP	microtiter plate
N-terminal	amino-terminal
OD	optical density
PCA	protocatechuic acid
PCR	polymerase chain reaction
PET	polyethylene terephthalate
PETase	PET hydrolase
PLICing	phosphorothioate-based ligase-independent gene cloning
PTFE	polytetrafluoroethylene
RBS	ribosome binding site

SDS-PAGE	sodium dodecyl sulfate polyacrylamide gel electrophoresis
Sec	general secretion
STR	stirred tank reactor
TAE	tris-acetate-EDTA buffer
Tat	twin-arginine translocation
TCA	trichloroacetic acid
T_M	melting temperature
Tris	tris(hydroxymethyl)aminomethane
WCB	working cell bank
WT	wild type

List of Figures

List of Tables

1. Introduction

1.1. *C. glutamicum*

Corynebacterium glutamicum (see Fig. 1.1) is a Gram-positive, non-sporulating and facultatively anaerobic actinobacterium that was isolated from soil samples in Japan in 1957 [1, 2]. Unlike most other Gram-positive bacteria, *C. glutamicum* comprises an additional outer layer with the mycomembrane [3]. The genome of wild type (WT) strain ATCC 13032 was sequenced in 2003 [4, 5] and *C. glutamicum* is genetically accessible through various vectors for heterologous protein expression [6–8]. Genetic toolboxes for metabolic engineering are available as summarized by Chai et al. [9].

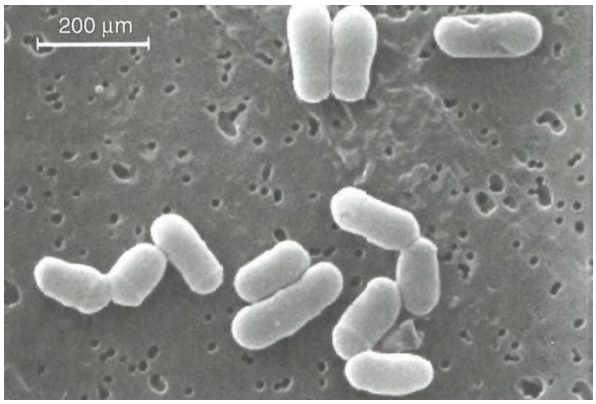

Fig. 1.1. Scanning electron microscopy of *C. glutamicum* on a nucleopore membrane with characteristic snapping division [10]

C. glutamicum is industrially established for the large-scale production of amino acids such as L-glutamate and L-lysine [11, 12], but it is also used for production of other small molecules as summarized elsewhere [13]. It is a robust organism that can produce under aerobic or oxygen-deprivation conditions [14–16] and it is able to utilize a broad spectrum of carbon sources, such as sugars, organic acids, and alcohols [17]. *C. glutamicum* has endotoxin-free properties and some production

processes are generally recognized as safe (GRAS) [18]. Since it exhibits only low extracellular proteolytic activity [19], *C. glutamicum* became of interest as a potential host for recombinant protein production and secretion [20, 21]. Even a commercial protein and peptide expression and secretion system is available with CORYNEX® (Ajinomoto Co., Inc., Japan).

1.2. Protein secretion

Intracellular protein production is not always suitable as overproduction can lead to toxic effects for the host. The reducing environment of the cytoplasm prevents the formation of disulfide bonds and target proteins can aggregate in the polar region of the cells in insoluble inclusion bodies [22, 23]. It is important to note here, that the view on inclusion bodies changed recently. They can retain their residual activity either upon natural aggregation or upon inclusion body formation caused by aggregation-inducing tags and can therefore be used directly as immobilized catalysts [24, 25]. Furthermore, productions have high product yields and target proteins are present with up to 95% purity in the inclusion bodies [26]. However, protein recovery from the inclusion body fraction is still done mainly by trial-and-error [27].

An alternative is the secretion of proteins into the periplasm or supernatant. In particular, the secretion of proteins directly into the supernatant additionally simplifies downstream processing, as the cell disruption step is omitted [20, 28]. The Gram-positive *Bacillus subtilis* that is capable of secreting proteins in the gram-per-liter range is the dominating bacterial host for industrial protein secretion, e.g., detergent enzymes [29, 30]. However, it has high extracellular protease activities that can lead to degradation of target proteins [31]. Protease-reduced *B. subtilis* strains exist [31–33], but switching to other bacterial hosts with generally low extracellular proteolytic activity, such as *C. glutamicum*, might be a reasonable alternative [20].

1.2.1. Secretion pathways

Two protein secretion pathways across the cytoplasmic membrane are highly conserved in bacteria, archaea and eukarya [34]. While the majority of proteins is secreted in an unfolded state by the general secretion (Sec) pathway, intracellularly folded proteins are exported by twin-arginine translocation (Tat) [35].

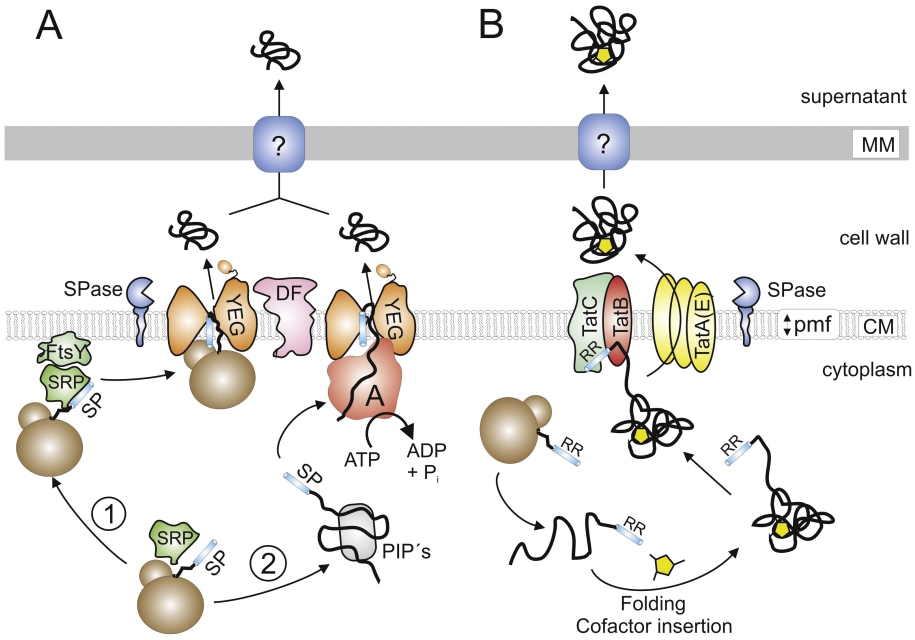

Fig. 1.2. Major secretion pathways in *C. glutamicum*. Unfolded proteins are exported via the Sec pathway (A) in the cotranslational (A1) or posttranslational mode (A2). Folded proteins are secreted via the Tat pathway [20]. SP: signal peptide, SRP: signal recognition particle, SPase: signal peptidase, YEG: SecYEG translocation pore, DF: SecDF, PIP: posttranslationally interacting protein, ATP: adenosine triphosphate, ADP: adenosine diphosphate, P_i: inorganic phosphate, A: SecA, RR: signal peptide with a twin-arginine motif, pmf: proton motive force, CM: cytoplasmic membrane, MM: mycomembrane

Both pathways are summarized for *C. glutamicum* by Freudl [20] (see Fig. 1.2). Briefly, unfolded proteins can be exported via the Sec pathway in two different modes depending on the hydrophobicity of the amino-terminal (N-terminal) signal peptide. In the cotranslational mode, a highly hydrophobic signal peptide is recognized by the signal recognition particle consisting of a Ffh protein and 4.5S RNA during translation [36]. The complex of the ribosome-nascent chain and signal recognition particle is targeted to the membrane. Mediated by 4.5S RNA and regulated by guanosine triphosphate (GTP) hydrolysis, Ffh and the signal recognition particle-receptor FtsY interact through their N-terminal and GTPase domains [37]. The ribosome-nascent chain is subsequently transferred to the translocation pore SecYEG with a three sub-unit core that spans the cytoplasmic membrane [38]. Further elongation at the ribosome provides the energy for translocation [39].

In the posttranslational mode, posttranslationally interacting proteins such as the general chaperones GroEL-GroES/DnaK-DnaJ-GrpE/trigger factor or the soluble form of SecA prevent precursor proteins from folding after translation [40–43]. The

signal peptide is recognized by SecA, which progressively pushes the precursor protein through the SecYEG pore under adenosine triphosphate (ATP) consumption in a power-stroke mechanism [44]. The membrane-bound SecDF is proposed to act as a proton-driven protein-translocation motor utilizing the proton gradient to pull precursor proteins from the SecYEG channel to the *trans* side of the membrane [45, 46]. The signal peptide is removed by a signal peptidase during or directly after export through the cytoplasmic membrane and the protein is released [47].

After intracellular folding, proteins with a signal peptide containing a twin-arginine motif are secreted via the Tat pathway. If necessary, cofactors are inserted prior to the export [48]. The twin-arginine motif is recognized by a Tat-substrate receptor complex consisting of TatC and TatB [49]. Multimers of TatA(E) are subsequently recruited proton motive force-dependently to the substrate-bound Tat-substrate receptor complex [48, 50]. As in *E. coli*, TatE is a cryptic gene duplication of TatA in *C. glutamicum*, but it cannot complement TatA deletion [51]. After protein translocation, the signal peptide is removed by a signal peptidase and the protein is released [47].

The transport across the mycomembrane after Sec- or Tat-dependent translocation across the cytoplasmic membrane still remains unclear. It is unknown whether a protein translocation system exists or not as no potential components of such a system have been yet identified [20].

1.2.2. Signal peptides

Proteins for Sec- and Tat-dependent secretion are recognized by their N-terminal signal peptide that is usually 20–40 amino acids long. As depicted in Fig. 1.3, these signal peptides share a characteristic tripartite structure consisting of a positively charged n-region, a hydrophobic h-region in the core and the c-region with the signal peptidase type I recognition site [52]. This recognition site adjacent to the protein targeted for secretion is characterized by the presence of amino acids with small neutral side chains such as alanine at positions –3 and –1 with respect to the signal peptidase cleavage site, and the preferred consensus motif is A–X–A [53].

In contrast to Sec signal peptides, Tat signal peptides have a longer n-region with the highly conserved Tat consensus motif S/T-RR-X-F-L-K including the eponymous two arginine residues [54]. This motif is adjacent to a comparably less hydrophobic

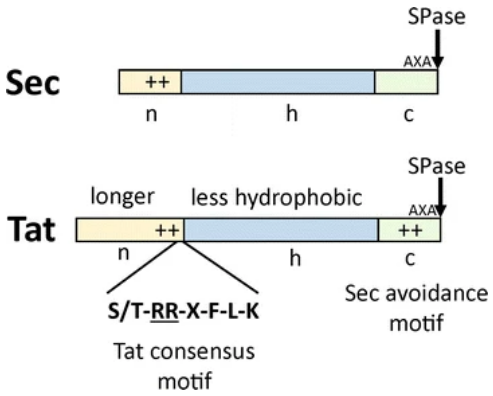

Fig. 1.3. Signal peptides for Sec- or Tat-dependent secretion. Both share a tripartite structure, but Tat signal peptides can be distinguished by a Tat consensus motif, length of the n-region, reduced hydrophobicity and Sec avoidance motif only [52]

h-region [55]. Some Tat signal peptides have an additional Sec avoidance motif with positively charged amino acids in the c-region that, together with the less hydrophobic h-region, prevent targeting to the Sec pathway [55, 56].

In addition, there are N-terminal lipoprotein signal peptides that are recognized and cleaved by type II signal peptidases after export via Sec or Tat immediately before the conserved +1 cysteine residue of the four-amino-acid lipobox motif [57]. Besides, type IV pilin-like signal peptides share a signal sequence motif that is recognized and cleaved by type III signal peptidase after export by the Sec translocon [58].

Signal peptide sequences, their cleavage sites and the positions of their n-, h- and c-region can be predicted by the bioinformatics tool SignalP 6.0. This tool assigns a score indicating the likelihood of a sequence being a signal peptide, but it cannot predict secretion efficiencies. SignalP 6.0 can be used for proteins from archaea, Gram-positive and -negative bacteria as well as eukarya. Except for the latter, the newest version does not exclusively discriminate between the pathways, but also the signal peptidases I–III used for cleavage and thus can discriminate between five types of signal peptides: Sec pathway with cleavage by signal peptidases I–III and Tat pathway with cleavage by signal peptidases I or II [59]. SignalP is based on pretrained language models for proteins provided by ProtTrans [60].

Data on the secretion efficiency of signal peptides for specific target proteins can be obtained from the recently published Signal Peptide Secretion Efficiency Database

(SPSED). This tool also allows to find homologous secreted proteins or signal peptides by using the Basic Local Alignment Search Tool (BLAST). However, about 80% of the data are based on *Bacillus* strains and so far only data for 18 target proteins have been deposited as of August 2022 [61].

1.2.3. Heterologous protein secretion

To secrete a heterologous protein, a suitable pathway must first be identified. Although the majority of homologous proteins are secreted Sec-dependently, it is not necessarily possible to secrete a heterologous protein via this pathway or useful, e.g., when enzymes require the incorporation of cofactors [20, 62]. One example is the green fluorescence protein (GFP), which can only be secreted by *C. glutamicum* in an active conformation via the Tat pathway [51, 63].

Improvements in heterologous secretion can be achieved by host selection or by using optimized hosts, such as protease-reduced strains [31–33]. Proteins involved in the respective secretion process may be over-expressed. Examples include genomic integration of an additional copy of the groESL operon for improved post-translational Sec secretion [64] or plasmid-based additional expression of TatABC for improved Tat-dependent secretion [65].

Since all homologous proteins have a unique signal peptide, finding a suitable signal peptide for heterologous secretion via the chosen pathway with a specific host is another challenging task. So far, it is not possible to predict a suitable combination of signal peptide, target protein and host, and this choice is additionally influenced by cultivation conditions [66]. One untargeted approach would be to systematically screen libraries of homologous [67–69] or heterologous signal peptides of closely related strains [70]. For *C. glutamicum*, it was shown that even signal peptides from *B. subtilis* are suitable for sufficient secretion of heterologous proteins [71, 72]. In another approach, a selected signal peptide sequence could be optimized for the secretion of a target protein through semi-targeted modifications, such as site saturation mutagenesis of the positively charged N-domain [73]. However, prior knowledge is limited and so far the data could not be transferred to other secretion processes [74]. A third approach could be the untargeted random mutagenesis of a selected signal peptide by error-prone polymerase chain reaction (PCR), which can produce many different variants in a short time [75]. To screen in high-throughput

for improved secretion, Bakkes et al. [75] used fluorescence-activated cell sorting of a *C. glutamicum* secretion stress biosensor strain K9. In this strain, the *htrA* gene coding for an extracytosolic protease was replaced by an *eyfp* gene leading to a dose-dependent fluorescence response on target protein secretion [76].

In addition to the signal peptide sequence itself, the promoter and the 5' untranslated region have an impact on secretion performance. There, e.g., the spacer between Shine-Dalgarno sequence and start codon can influence translation initiation presumably by secondary mRNA structures [77, 78]. The first amino acids of the heterologous protein itself can affect cleavage by signal peptidases and thus also secretion [69, 79]. Watanabe et al. [69] observed that +1 glutamine residues adjacent to the signal peptidase cleavage site have an influence on amylase secretion with *C. glutamicum* R.

All of these optimization approaches, alone or in combination, result in a large number of variants for each heterologous target protein. Since predictions are currently not possible, these variants should ideally be tested under process conditions [66].

1.3. Carboxylic ester hydrolases

Carboxylic ester hydrolases (EC 3.1.1) are ubiquitous and catalyze the hydrolysis of esters to alcohols and carboxylic acids. They are further divided into more than 100 classes by substrate and product of catalysis and are of interest for various biotechnological applications [80, 81]. Some carboxylic ester hydrolases such as the *Fusarium solani* f. sp. *pisi* cutinase are secreted by their native host [82].

1.3.1. Cutinase

Cutinases (EC 3.1.1.74) were discovered in studies on plant pathogens as they catalyze the hydrolization of cutin ester bonds of plant cuticles [83]. They belong to the α/β-hydrolase fold superfamily [84]. One of the first characterized cutinases originates from the plant pathogen *F. solani* f. sp. *pisi* [82]. It consists of five β-sheets and four α-helices with an active site triad with serine, histidine and aspartate acid on positions 120, 188 and 175, respectively [85]. Particularly the *F. solani* f. sp. *pisi* cutinase was used as a model enzyme for several studies on cutinase structure,

function and reactivity [82, 86, 87], as well as for studies on heterologous protein secretion with bacteria [67, 72, 75, 88, 89]. The latter is not only due to the eukaryotic origin of the enzyme, but also to the possibility to determine cutinase activity spectrophotometrically by degradation of 4-nitrophenyl palmitate (4NPP) as a substrate analogue and detection of 4-nitrophenol (4NP) by absorption measurement at 410 nm [90] (see Fig. 1.4).

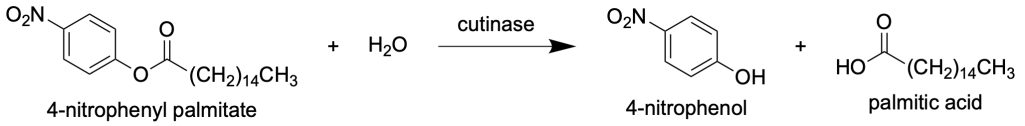

Fig. 1.4. Cutinase activity assay with 4NPP as substrate analogue. Formation of 4NP can be detected by absorption measurement at 410 nm

The ability of cutinases to catalyze the hydrolization of cutin, as well as polyesters and triglycerides leads to potential applications in laundry detergent and textile industries, among others [91–93].

1.3.2. Polyethylene terephthalate hydrolases

Plastics including polyethylene terephthalates (PETs) are widely used in everyday life and the enormous amounts of plastic waste are a growing environmental problem. In 2020, 511.8 tons of PET were produced in Germany [94]. In the same year, the European Union, Norway, Switzerland and the United Kingdom had a combined demand of 49.1 million tons of plastic, of which PET accounted for 8.4%. 29 million tons of post-consumer plastic waste was collected in these countries, of which only 34.6% were recycled, 42% were used for energy recovery, and still 23.4% were sent to landfill [95].

The discovery of the bacterium *Ideonella sakaiensis* that can degrade and assimilate amorphous PET in 2016 revealed a new potential of biotechnological plastic degradation. *I. sakaiensis* produces a PET hydrolase (PETase) that converts PET mainly to mono(2-hydroxyethyl) terephthalic acids (MHETs), that can be further enzymatically degraded by MHETases [96] (Fig. 1.5). Numerous reviews on PETases and their application in plastic degradation [97, 98] as well as plastic upcycling [99–101] have been recently published.

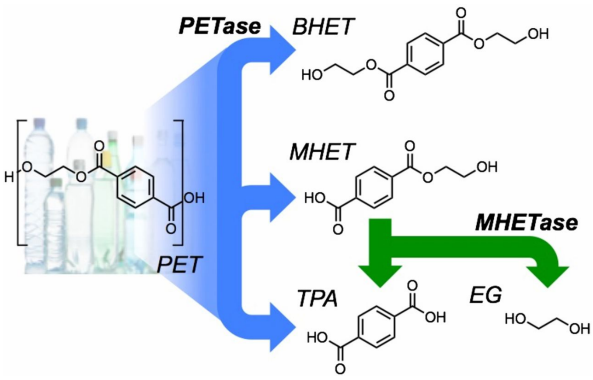

Fig. 1.5. PETases degrade PET to MHETs and byproducts terephthalic acid (TPA) and bis(2-hydroxyethyl)-TPA (BHET). MHET can be converted to TPA and ethylene glycol (EG) by MHET-degrading enzymes (MHETase) [102]

Like cutinases, PETases (EC 3.1.1.101) have a highly conserved catalytic triad consisting of serine, histidin and aspartate [103]. The *F. solani* f. sp. *pisi* cutinase can also degrade PET [104], albeit with low activity compared to other PETases such as the leaf-branch compost cutinase (LCC) [105]. The LCC was discovered in a metagenomic approach and originates most likely from an unknown thermophilic bacterium [106, 107]. At temperatures above 40 °C, the LCC outperforms the *I. sakaiensis* PETase [96]. Like the *F. solani* f. sp. *pisi* cutinase, the LCC can also degrade 4-nitrophenyl ester, preferentially short-chain substrates such as 4-nitrophenyl butyrate [106]. It was further engineered for improved activity and heat stability resulting in the mutant ICCG. 90% depolymerization of pre-treated post-consumer PET waste were shown with 3 mg LCC^{ICCG} per gram PET in 10 h at 72 °C with a mean productivity of 16.7 $g_{terephtalate} L^{-1} h^{-1}$ [105]. Another PETase used in this study is the PE-H that was discovered by Bollinger et al. [108] from the marine mesophilic bacterium *Pseudomonas aestusnigri*. Whereas the LCC is a member of the Type I family of PETases, the PE-H has another disulfide bond and an extended loop region and thus belongs to the Type IIa family. Only the rationally engineered mutant $PE\text{-}H^{Y250S}$ is able to hydrolyze a PET film substrate obtained from a commercial PET bottle. Although hydrolysis of amorphous PET could also be increased by this single amino acid exchange, MHET formation is still lower than with the *I. sakaiensis* PETase [108]. LCC and PE-H both are presumably secreted by their native host, as an N-terminal signal peptide sequence was predicted for both [106, 108].

1.4. Split GFP assay

If no established activity assays exist, target proteins can be detected by covalent linking to a fluorescence reporter. The most prominent one is the GFP that was isolated from the jellyfish *Aequorea victoria* [109]. It is a widely used reporter for gene expression and protein localization [110, 111] and a superfolder variant was developed that allows robust folding even when fused with other proteins [112].

However, a full-size reporter protein could affect the solubility, folding and secretion of a target protein. To minimize this effect, the split GFP assay was developed. Here, only the 16 amino acids long 11th β-sheet of a superfolder GFP (GFP11) and a small peptide linker are used as a protein tag [113]. Since residue E222 from the 11th β-sheet is necessary for GFP chromophore formation [114], the remaining part of the GFP (GFP1-10) is non-fluorescent. Only in presence of both parts, fluorescence of superfolder GFP can be measured after self-assembly and chromophore maturation [113]. A comprehensive review of recent developments, such as the extension to other split fluorescence proteins [115, 116], and *in vivo* or *in vitro* applications of the split GFP assay [117] can be found elsewhere.

For *in vitro* protein detection, a GFP1-10 detector solution must be added. GFP1-10 can be produced intracellulary with *E. coli* BL21(DE3), purified and refolded from the inclusion body fraction after cell disruption [89, 118, 119]. For reduced incubation times in split GFP assays, GFP1-10 can be prematurated in additional purification steps [120, 121].

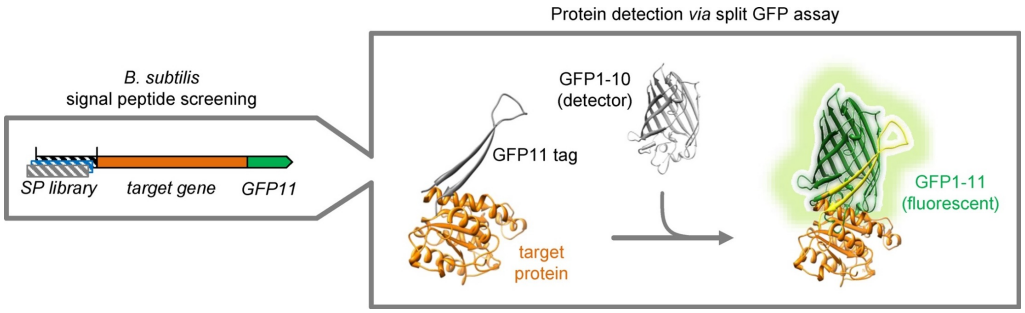

Fig. 1.6. Split GFP assay for detection of secreted proteins. The C-terminal GFP11-tag of the folded target protein in the supernatant assembles with the non-fluorescent GFP1-10 detector to a functional fluorescent GFP [88]

The split GFP assay was used by Knapp et al. [88] for screening of Sec-dependent signal peptides for secretion of a heterologous cutinase and homologous lipase as

well as the non-enzymatic swollenin EXLX1 in *B. subtilis* (see Fig. 1.6). For the enzymes, the carboxyl-terminal (C-terminal) GFP11-tag did not negatively impact protein secretion and split GFP assay results correlate to enzymatic activities [122]. The split GFP assay can also be used in a quantitative manner by combination with activity measurements and is easily applicable in high-throughput screenings [119].

1.5. Bioprocess development

Especially in semi-targeted or untargeted approaches of strain development, many different genetic variants can be generated. In addition, the automation of molecular biology workflows has also accelerated targeted strain construction, enabling the generation of numerous variants on a short time scale as well [123, 124]. These variants must be tested and compared with each other in order to develop a suitable bioprocess with the best performing strains.

1.5.1. Miniaturization and automation

In standard process development as shown in Fig. 1.7, strain variants are tested in primary screenings conducted in microtiter plate (MTP) format with high throughput and low cultivation volume. MTP screenings are therefore cost-effective, and these parallelized cultivations can often be integrated into automated workflows to accelerate them, but standard MTPs provide few process insights and less process control [125–127]. Interesting candidates are screened in further rounds in MTPs or flasks and only a fraction is cultivated in laboratory-scale bioreactors for process development and optimization. The best performing strains are then used for process validation and production in pilot scale [127, 128]. With lower throughput, insights into the process increase compared to MTPs or flasks. Bioreactors allow for feeding, more targeted monitoring and regulation of the process by an active pH control [129].

To overcome the limitations in small scale, flask-based cultivations have been improved in terms of process insights and variability. Optical online measurements of backscatter and, based on fluorophores, also of pH and dissolved oxygen (DO) are

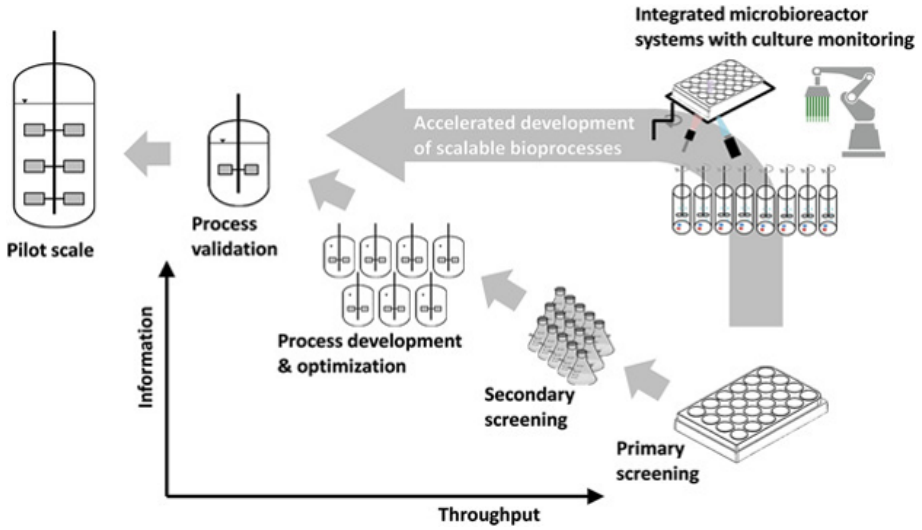

Fig. 1.7. Bioprocess development. In traditional bioprocess development, process information increase with reduced throughput by bioreactor-based cultivation. Microbioreactor systems integrated into robotic platforms can deliver both high throughput and information while being scalable, accelerating bioprocess development [128]

possible [130, 131]. Additionally, devices for off-gas analytics are available [132–134] and different strategies for feeding were tested [135, 136].

In addition, the development of microbioreactors is of particular interest. In contrast to flask-based systems, these can often be automated by integration in liquid handling robotic systems. Microbioreactor systems provide improved process insights and are scalable [126, 128, 137]. Different stirred or shaken cultivation systems in micro- or milliliter scale have been reviewed by Hemmerich et al. [128]. Stirred microbioreactors are usually operated in milliliter scale and resemble typical bioreactors. Examples are the automated Ambr® 15 system (Sartorius, Germany) for 24 or 48 parallel cell culture cultivations with 10–15 mL working volume or the bioREACTOR 48 (2mag, Germany) with up to 48 parallelized cultivation vessels and 8–15 mL working volume. In the Ambr® 15, feeding and sampling can be performed by automated liquid handling. This is only possible with the bioREACTOR 48 if the device is integrated into a robotic platform from other manufacturers. Although the above mentioned systems provide only bolus feeding in contrast to continuous feeding strategies used in other stirred tank reactors (STRs), they show high reproducibility and comparability with laboratory-scale STR cultivation [138, 139]. Microfluidic devices for milliliter scale cultivation were investigated to allow for continuous feeding in 48 parallel milliliter scale bioreactors [140].

Shaken microbioreactors can also be fed with substrate via automated liquid handling if they are integrated into an automation platform [137, 141]. One example is the BioLector® (Beckman Coulter, USA) that allows for online measurement of biomass by backscatter as well as pH, DO and fluorescence in up to 48 wells of a MTP with up to 800–2 400 µL working volume depending on well geometry and shaking frequencies. In addition to round well plates, FlowerPlates® are available, where the flower-shape of the well mimics baffled flasks and allows higher oxygen transfer rates compared to round wells according to the manufacturer. The measurement principle is depicted in Fig. 1.8a and is comparable to optical measurements in flasks. While the plate is shaken during incubation, an optic fiber moves along underneath the plate measuring scattered light, fluorescence, pH and DO signal in defined measurement intervals using corresponding LED modules. For DO and pH measurement, plates with optodes are required [142].

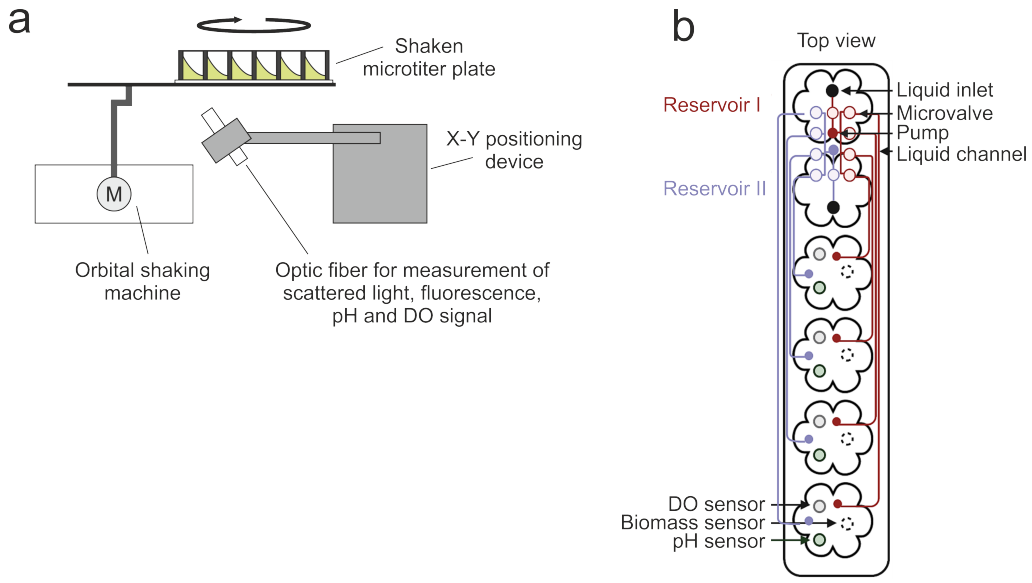

Fig. 1.8. BioLector® measurement principle. (a) Scheme of BioLector®, adapted from [142]. While the cultivation plate is shaken, an optic fiber can move along the wells underneath and take measurements at intervals. (b) Top view on a microfluidic FlowerPlate® column, adapted from [143]. The flower-shaped wells may contain optodes for pH and DO measurement. Backscatter as an equivalent to biomass can be measured through the bottom of the well. Reservoir wells in the upper two rows are connected to the cultivation wells underneath by membrane valves and microfluidic channels

A BioLector® integrated into a robotic platform was successfully used for screening of protein variants in different studies [71, 72]. It has been shown for various microbial cell factories including *C. glutamicum* that the processes are scalable from

microbioreactor to laboratory bioreactor [71, 144, 145]. The BioLector® Pro (Beckman Coulter, USA) additionally enables feeding via microfluidic channels with various feeding modes and rates [146]. The wells in the upper two rows of a microfluidic plate are used as reservoirs connected to the cultivation wells underneath, e.g., for substrate feeding and one-sided pH adjustment (see Fig. 1.8b) [143].

The advantage of shaken microbioreactors is the easy set-up compared to stirred solutions. In return, some parameters such as cultivation temperature or headspace oxygen can only be controlled globally in one experiment. In addition, frequent liquid handling in the cultivation plate by the robotic system will affect the cultivation by opening the lid and the resulting change in temperature and gas mixture in the headspace [128, 137]. This effect is particularly noticeable when the shaking is stopped [147].

In summary, bioprocess development can be accelerated using microbioreactors integrated into laboratory automation systems enabling automated, miniaturized and parallelized experiments. This setup can combine high throughput with high process information and insights [128].

1.5.2. Strategic experimental design

Even though screening throughput can be increased by miniaturization, parallelization and automation, there is a limit, i.e., the 48 wells in a BioLector® cultivation. The goal is therefore to gain the best possible and statistically sound insights in a cultivation and screening process with the least possible expenditure of time and material. This can be achieved by combination with algorithms for evaluation and planning of cultivation and screening experiments.

The method of classical design of experiments (DoE) has been first described in 1936 [148], but it was not applied for bioprocess development until much later. Now, DoE is widely used to optimize cultivation media, among other applications in bioprocess development, as summarized by Mandenius and Brundin [149]. Here, more than one variable is varied simultaneously, since they can also have combinatorial effects on the desired output. This makes it less likely to get stuck in a local optimum than compared to optimizing one variable after the other (see Fig. 1.9).

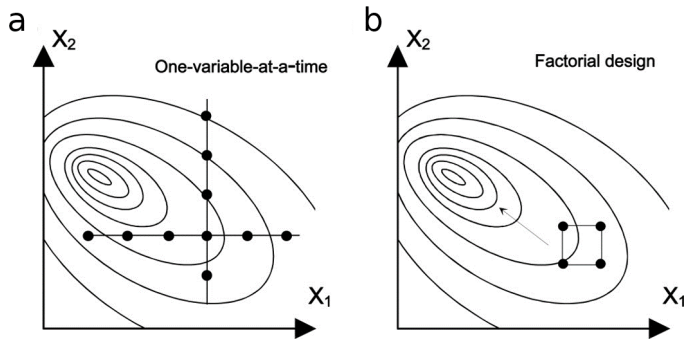

Fig. 1.9. Design of experiments with two factors X1 and X2 (modified from [149]). By varying one variable at a time (a), only a local optimum can be reached, since both variables are dependent on each other. Using factorial design (b), X1 and X2 are simultaneously varied. With the evaluation by an experimental design software the direction of the global optimum can be predicted

With a full factorial design, the upper and lower limits of a factor are usually set and all factors are examined in combination with each other, resulting in a large amount of data that needs to be collected. Alternatively, fractional factorial design can be used, in which only a subset of the factors is examined [150]. Results from fractional or full factorial design are evaluated mostly by a response surface model to identify the optimum to be achieved, e.g., the product yield or enzymatic activity [149, 151]. These response surface methods attempt to describe the relationship between independent variables and a response variable to identify the optimum conditions within the tested space and visualize the direction to the optimum [149].

An alternative to response surface methodology is Kriging that is known to model complex nonlinear behavior more accurately [152]. Freier et al. [153] combined classical DoE with the Kriging algorithm to successfully accelerate media optimization for GFP secretion with *C. glutamicum*.

Process models can be used to improve experimental design in an alternative approach. For example, a key performance indicator (KPI) such as the maximum product formation rate is used for a strain library ranking. For this purpose, parameters such as the growth rate have to be estimated, e.g., by ordinary differential equations or other reaction kinetics models. Likelihood functions can be used to take measurement noise or bias into account [154]. The measurement noise is often assumed to be normally distributed for all time points and thus can be described by the probability density function of the normal distribution [155]. Additionally, a measure of the quality of an estimate is also important in this context so that the experimenter

knows whether further data need to be collected in screening rounds. This requires probability distributions instead of point estimates of the model parameters, and this can be obtained by using Bayesian inference (see Eq 1.1).

$$p(\theta|\mathcal{D}) = \frac{p(\mathcal{D}|\theta) \cdot p(\theta)}{p(\mathcal{D})} \tag{1.1}$$

In this equation, θ are all model parameters including the KPI, e.g., the product formation rate, $\mathcal{D}$ is the experimental data, $p(\theta|\mathcal{D})$ is the posterior distribution, $p(\mathcal{D}|\theta)$ is the likelihood, $p(\theta)$ is the prior distribution before collecting another round of experimental data and $p(\mathcal{D})$ is the evidence of the data. The prior distribution $p(\theta)$ is therefore needed to calculate the posterior distribution $p(\theta|\mathcal{D})$ that describes the KPI by taking into account the collected data. In the following experiments, the posterior of the previous experiment is used as prior and thus the prior knowledge is extended in each round. Posterior distributions can be calculated, for example, by Markov chain Monte Carlo algorithms [154, 155].

Bioprocess development often involves a trade-off between exploitation and exploration, i.e., making the best decision based on the current information or gathering more information. Using the example of signal peptide screening for heterologous protein secretion, this would be the decision to continue testing the most suitable signal peptide to date to collect even more statistically valid data (exploitation), or to test additional signal peptides, one of which may be even more suitable, but without wasting resources unnecessarily (exploration). So in addition to calculating posterior distributions, a decision policy is needed to choose which strains to test in the next screening round and for this Thompson sampling can be implemented. Thompson sampling was described in 1933 [156] and is nowadays widely used, e.g., in online advertisement [157] or online network revenue management [158].

L. M. Helleckes (Forschungszentrum Jülich GmbH) combined a decision algorithm with a process model for PETase secretion screening, and it works as shown in Fig. 1.10a. The Thompson sampling decides which action to play, i.e., which PETase secretion strains to be tested in the next screening round by drawing random samples from a posterior distribution provided by a model based on Bayesian inference. Observations from screening, i.e., absorption from activity measurements with cultivation supernatant samples, are used by the model to calculate the probability distribution of a performance indicator, i.e., the reaction rate coefficient k of the enzymatic

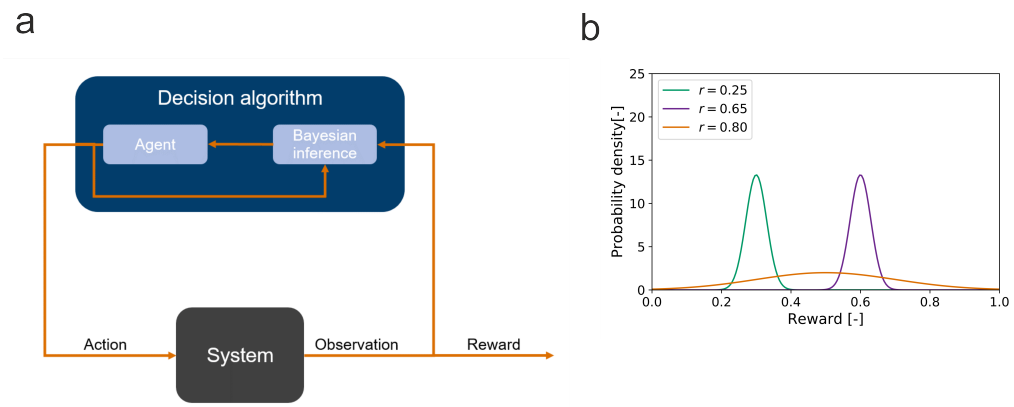

Fig. 1.10. Bayesian inference and Thompson sampling. (a) Overview of the decision algorithm combining a Bayesian inference based model for posterior distribution calculation and Thompson sampling for playing the action with the highest posterior out of random samples from posterior distribution. (b) Probability densities over rewards of three exemplary candidates. The real mean rewards in the legend indicate that the orange candidate has the highest reward, but a great uncertainty. Based solely on the highest mean probability density, the violet candidate would be chosen despite having a lower real mean reward than the orange candidate (both adapted from [154] which in turn were modified from [159])

conversion. The Thompson sampling algorithm then draws random samples from this posterior distribution and chooses the strains with the highest posterior for the next round with the aim of achieving the highest reward, i.e., the highest reaction rate coefficient k. As described, the Thompson sampling does not select the action with the highest mean, i.e., the secretion strain with the highest mean probability density of the reaction rate coefficient k for the next screening round. Instead, it draws a random sample from the posterior distributions of each candidate and chooses the action with the highest sample next. This can maximize the reward in long term as visualized in Fig. 1.10b. By choosing actions based on the highest mean probability density, only the violet candidate would be chosen. With Thompson sampling, also the orange candidate would be taken into account, because despite the great uncertainty it could still yield a higher reward than the violet candidate with the narrow probability density. In this example, the orange candidate has indeed the highest real mean reward with r = 0.8. The green candidate would not be tested further, as it is clearly worse than the purple one based on the the posterior distributions [154, 159].

1.6. Aim of this thesis

In this work, the split GFP assay will be evaluated as an activity-independent detection method for GFP11-tagged target proteins secreted by *C. glutamicum*. The split GFP assay will be standardized and implemented on a Tecan Freedom EVO® robotic platform with an integrated BioLector® for microscale cultivation with online measurement of the dissolved oxygen, pH and backscatter signal that correlates with cell densities. With the additionally integrated centrifuge, a cooled sample storage and microplate reader, this screening platform is equipped for the entire workflow from the cultivation to the detection of proteins in the supernatant. The impact of environmental conditions on the split GFP assay, such as pH and temperature, will be investigated. To validate the split GFP assay as a suitable detection method, a heterologous cutinase secreted by *C. glutamicum* will be detected by the split GFP assay, and holo-GFP fluorescence will be correlated with enzymatic activities. To provide high quantities of GFP1-10 for automated high-throughput screenings, the GFP1-10 detector protein production in *E. coli* will be scaled from flasks to a fed-batch process in defined medium in laboratory-scale bioreactors.

A new pPBEx2-based plasmid will be constructed that allows for easy exchange of the ribosome binding site spacer and signal peptide sequence by cassette mutagenesis. Integration of the target gene into this plasmid will be enabled via Golden Gate assembly. The generation of *C. glutamicum* expression vectors will be accelerated using the low-cost Opentrons OT-2 liquid handling robot. Unit operations such as plasmid purification, *E. coli* heat-shock transformation and restriction digestion will be automated.

A fully automated screening workflow will be established with integrated pre-culture handling and backscatter-triggered decision making for main culture inoculation and the induction of target gene expression, as well as cell harvesting triggered by a predefined time period since induction. The split GFP and the cutinase activity assay will be tested for detection of secreted target proteins. Target protein secretion in the microbioreactor operated in batch mode will be compared with fed-batch mode and with a laboratory-scale batch experiment in a stirred-tank reactor.

The automated secretion screening workflow will be used to investigate the impact of the ribosome binding site spacer on cutinase secretion mediated with four signal peptides. Secretion performance with *C. glutamicum* will be compared to those

with *B. subtilis* as a secretion host. Using the automated plasmid generation and secretion screening workflow, a library of different *B. subtilis* signal peptides will be tested for secretion of a heterologous cutinase and two PETase mutants, LCC^{ICCG} and PE-H^{Y250S}, by *C. glutamicum*. In collaboration with a colleague, a process model will be developed that, in combination with a decision algorithm, will allow a statistically sound analysis of *C. glutamicum* PETase secretion performance.

In addition, the *C. glutamicum* pCGPhoD^{Cg}-GFP will be optimized. This strain can secrete GFP_{uv} mediated by the Tat-dependent signal peptide sequence of PhoD and enables online product monitoring by fluorescence measurement in BioLector® cultivations. The *phoD-GFP$_{uv}$* will be amplified from the original pEKEx2-based plasmid and ligated with the pPBEx2. In this plasmid, a repressor gene was restored and intraplasmid duplicate sequences were removed. Thus, pPBEx2-PhoD^{Cg}-GFP should allow for low basal and tightly controlled gene expression using the tac promoter and a higher plasmid stability.

2. Material and methods

2.1. Materials

2.1.1. Devices, consumables and software

The devices used in this study for which the model may be relevant are listed in Tab. 2.1. Software used for experiments and data analysis is shown in Tab. 2.2 and consumables and kits in Tab. 2.3.

Tab. 2.1. Devices used in this work

Device	Model	Manufacturer
Bioreactor	1.5 L DASGIP® reactor	Eppendorf, Germany
Capillary electrophoresis	MCE-202 MultiNA	Shimadzu, Japan
Centrifuges	Allegra X-30R	Beckman Coulter, USA
	Biofuge pico	Heraeus, Germany
	GS-15R	Beckman Coulter, USA
	Himac CT15RE	Hitachi, Japan
	Rotanta 460 Robotic	Hettich, Germany
DO optodes	VisiFerm DO 225	Hamilton, Switzerland
Electroporator	Gene Pulser Xcell	Bio-Rad Laboratories, USA
	ECM™ 630	BTX, USA
French press	HTU Digi-F-Press	G. Heinemann Ultraschall- und Labortechnik, Germany
HPLC system	HP/Agilent 110	Agilent Technologies, USA
HPLC column	Metab ACC, Organic Acid resin, 300 x 8 mm	ISERA, Germany
Laboratory automation	Freedom EVO® 200	Tecan, Switzerland
	OT-2	Opentrons, USA
Microbioreactor	Biolector® Pro	Beckman Coulter, USA
Microplate reader	Infinite® M Nano	Tecan, Switzerland
Microscope	Nikon Eclipse Ti2	Nikon, Japan
Online biomass monitor	SFR vario	PreSense Precision Sensing, Germany
pH electrode	405-DPAS-SC-K8S	Mettler Toledo, USA

Device	Model	Manufacturer
	Metrohm 6.0234.110	Metrohm, Switzerland
Pipettes	Research® Plus	Eppendorf, Germany
	VOYAGER (electronic, multichannel with adjustable tip space)	Integra Biosciences, Switzerland
Plate pourer	Universal Plate Pourer	KREO Technologies, Canada
Thermal cycler	Termocycler Module	Opentrons, USA
Temperature control systems	Heratherm incubator	Thermo Fisher Scientific, USA
	Microcool MC 600	LAUDA DR. R. WOBSER, Germany
	Temperature Module	Opentrons, USA
Tempered shakers	ISF-4-W	Adolf Kühner AG, Switzerland
	Multitron Pro	Infors HT, Switzerland
	Multitron Standard	Infors HT, Switzerland
	ThermoMixer® comfort	Eppendorf, Germany
Spectrophotometer	NanoDrop™ 1000	Thermo Fisher Scientific, USA
	UV-1800	Shimadzu, Japan

Tab. 2.2. Software used in this work

Software	Application	Reference
ArviZ $\geq$0.11.4	Exploratory analysis of Bayesian models	[160]
BioLection® 3.18	BioLector® control	Beckman Coulter, USA
Bletl v1.0.4	Parsing of BioLector® data and analysis	[161, 162]
Calibr8 $\geq$6.2.1	Calibration models	[163, 164]
ChemDraw 20.0.0.38	Visualization of chemical structures and reactions	PerkinElmer, USA
DASware®	Bioreactor control	Eppendorf, Germany
Detl 0.4.0	Parsing of bioreactor raw data	[165]
EnvManager v1.5.0.5	Application for creating Python environments	M. Osthege, Forschungszentrum Jülich GmbH, unpublished
Freedom EVOware® 2.7	Tecan robotic system	Tecan, Switzerland
i-control™ 2.0	Reader	Tecan, Switzerland

Software	Application	Reference
Matplotlib ≥3.4.3	Data visualization	[166, 167]
Microsoft Excel 2016	Data processing	Microsoft, USA
MultiNA Control Software 1.13.0	Capillary electrophoresis	Shimadzu, Japan
NumPy ≥1.20	Scientific computing	[168]
Opentrons App 4.5.0	Opentrons robotic system	Opentrons, USA
OT-2 Python Protocol API 2.8	Opentrons robotic system	Opentrons, USA
Pandas ≥1.3	Data analysis and manipulation	[169, 170]
PreSense Flask Studio 3.1.2.35	Online biomass measurement in flasks	PreSense Precision Sensing, Germany
PyMC ≥4.0.0b2	Bayesian statistical modeling and probabilistic machine learning	[171]
Python 3.8.1	Experiment scripts and data processing	Python Software Foundation, USA
Retl 0.3.1	Parsing of microplate reader data	M. Osthege and N. Tenhaef, Forschungszentrum Jülich GmbH, unpublished
Robotools v1.3.0	Writing of worklist files for Tecan robotic systems	[172]
SciPy ≥1.6.3	Data manipulation and analysis	[173]
SnapGene® software 5.3.2	DNA cloning (planning, visualization, documentation)	Insightful Science, USA
ThorCam™	Microscopic image acquisition	Thorlabs, USA

Tab. 2.3. Consumables and kits used in this work. PP: polypropylene, PS: polystyrene

Consumable	Model	Manufacturer
12-column plate	Reservoir, 12 column, PP	Agilent Technologies, USA
24-well deepwell plate (DWP)	Square well, riplate® SW	Ritter, Germany
48-well FlowerPlate	MTP-48-BOH 1	Beckman Coulter, USA
	MTP-MF32C-BOH 1 (microfluidic)	Beckman Coulter, USA
96-well DWP	Riplate® RW, PP (1 mL)	Ritter, Germany
	Riplate® RW, PP (2 mL)	Ritter, Germany
	Square well collection plate, 2.2 mL, u-buttom, PP	Brand, Germany
96-well MTP	μCLEAR®, f-bottom, PS	Greiner Bio-One, Austria
	μCLEAR®, f-bottom, black, PS	Greiner Bio-One, Austria

Consumable	Model	Manufacturer
	Clear, v-bottom, PS	Greiner Bio-One, Austria
	Clear, u-bottom, PS, 320 µL	Greiner Bio-One, Austria
96-well PCR plate	0.2 mL skirted, robotic	Thermo Fisher Scientific, USA
	0.2 mL low profile, non-skirted	Thermo Fisher Scientific, USA
	0.2 mL non-skirted	Thermo Fisher Scientific, USA
Cuvettes	Q-VETTES semi-micro, PS	Ratiolab, Germany
DNA purification kit	NucleoSpin Gel and PCR Clean-up	Macherey Nagel, Germany
	NucleoSpin Plasmid (No Lid)	Macherey Nagel, Germany
	Wizard® MagneSil® Plasmid DNA Purification System	Promega, USA
Electroporation accessories	96-Well Plate, 2 mm Gap, 150 µL well capacity	BTX, USA
	Cuvettes with 2 mm gap size	VWR, USA
MultiNA kit	DNA-12000 Reagent Kit	Shimadzu, Japan
SDS-PAGE Gel	4–12% Criterion™ XT Bis-Tris Precast Gel	Bio-Rad Laboratories, USA
Sealing foil	Gas permeable (silicone foil + non-woven foil) for automation	Beckman Coulter, USA
	Gas permeable (silicone foil + non-woven foil) for microfluidic MTP	Beckman Coulter, USA
	Gas-permeable	Beckman Coulter, USA
	SILVERseal™ adhesive aluminium foil	Greiner Bio-One, Austria
Single-well plate	Nunc™ OmniTray™, PS	Thermo Fisher Scientific, USA

2.1.2. Laboratory-scale bioreactors

Cultivation in laboratory-scale STRs was done in four parallel 1.5 L DASGIP® bioreactors equipped with two Rushton-type impellers (6 blades, 1 cm height, 3 cm distance). Included DASGIP® modules were TC4SC4 for temperature and agitation control, PH4PO4 for control of DO and pH, MF4 for mass flow controlled gassing, MP8 for control of feed flow rates and GA4 exhaust analyzer. DO was measured with VisiFerm DO 225 optodes and pH with 405-DPAS-SC-K8S electrodes. The plan view of the setup is shown in Fig. 2.1.

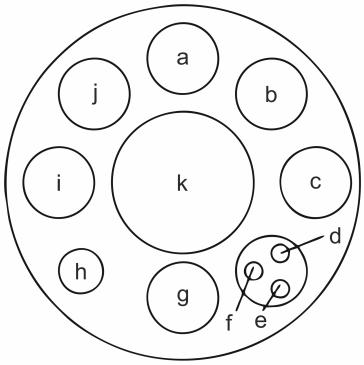

Fig. 2.1. Plan view on DASGIP® bioreactor setup. (a) pH electrode, (b) septum, (c) sampling and inoculation port, feed inlet, (d) acid inlet, (e) base inlet, (f) sampling and inoculation port, feed inlet, (g) sparger, (h) thermometer, (i) exhaust gas cooler, (j) DO electrode and (k) stirring unit. Adapted from [174]

2.1.3. Robotic system for molecular biology applications

Workflows for automating plasmid construction were implemented on the low-cost liquid handling system Opentrons OT-2 with open source based software. It includes two different pipettes for liquid handling with disposable tips that can be exchanged. The multichannel pipettes P20 GEN2, P300 and P300 GEN2 were used in different applications of this work, as well as the Thermocycler and the Magnetic Module.

2.1.4. Robotic system for cultivation and screening

For secretion screenings and other applications involving cultivation, the Tecan Freedom EVO® 200 with integrated BioLector® Pro for cultivation was used as shown in Fig. 2.2. This liquid handling system uses fixed stainless steel tips coated with polytetrafluoroethylene (PTFE) and is capable of moving plates with the robotic manipulator along the axis. In addition to the Biolector® Pro, this system also includes the Rotanta 460 Robotic centrifuge for cell harvest, a cooling carrier connected to the Microcool MC 600 for cooled sample storage, deck space for preparing cultivation and assays and an Infinite® M Nano microplate reader. A sterile environment is ensured by a laminar flow hood with high-efficiency particulate air filtration.

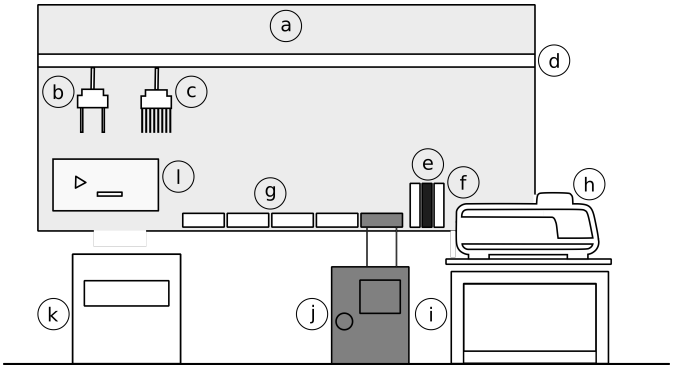

Fig. 2.2. Schematic of the robotic screening platform used in this work. The Tecan Freedom EVO® with a 200 base unit is equipped with (a) a sterile hood, (b) a liquid handler and (c) robotic manipulator that can move along the (d) axis in X–Y–Z-directions, (e) a washing station, (f) trough carriers, (g) plate carriers, (h) a BioLector® Pro with (i) control unit, (j) a cooling system and cooling carrier for plates, (k) a plate centrifuge and (l) microplate reader [175]

Microbioreactor

The BioLector® Pro for cultivation in microliter-scale enables online measurement of biomass by backscatter, pH, DO and fluorescence. Depending on the application, LED modules in Tab. 2.4 were used. Bacteria were cultivated in MTP-48-BOH 1 plates with optodes HP8/Pst3 for DO and pH measurement unless otherwise indicated.

Tab. 2.4. BioLector® LED modules used for online measurement during cultivation

LED module	**Details**
Biomass	Excitation at 620 nm (bandpass: 10 nm), scattered light measurement
DO (Pst3)	Excitation 520 nm (bandpass: 10 nm) / Emission 600 nm (longpass), BOH 1 plates
eYFP and Citrine	Excitation 508 nm (bandpass: 10 nm) / Emission 532 nm (bandpass: 10 nm)
GFP / Gemini	Excitation 480 nm (bandpass: 10 nm) / Emission 520 nm (bandpass: 25 nm)
pH (HP8)	Excitation 470 nm (bandpass: 10 nm) / Emission 525 nm (longpass), BOH 1 plates, pH 5.0–7.0

System control

For autonomous experiments on the screening platform, a process control system designed by M. Osthege and J. Hemmerich (Forschungszentrum Jülich GmbH,

[176]) in the context of the BMBF-funded DigInBio project was used, where access to the Freedom EVO® and BioLector® is enabled by gateways.

In an experiment script programmed in Python, protocols of the Freedom EVOware® and the BioLector® can be started and BioLector® data can be parsed during the experiment using the BLETL package [161, 162]. During the experiment, worklists are written with robotools [172] based on backscatter measurements that can be loaded and executed in EVOware® scripts. Cultivation wells are divided into the categories listed in Tab. 2.5. At the beginning of a new cultivation, only preculture_wells (experiment with automated pre-culture) or active_wells (experiment without automated pre-culture) are defined. After all active wells are harvested and no pre-culture wells remain, the cultivation is finished.

Tab. 2.5. Categories of cultivation wells in the cultivation plate during automated screenings
*Only for cultivations with automated pre-culture

Name	**Type**	**Details**
preculture_wells*	List	Wells of the pre-culture, inoculated from cryo-conserved cultures by the robotic system
wells_for_main*	List	Pre-culture wells that have reached the trigger for inoculation of main cultures in the current cycle. After inoculation of main cultures, respective pre-culture wells are removed from preculture_wells
main_wells*	List	Wells of the main culture that are inoculated from the respective pre-culture. These wells are added to the active_wells
active_wells	List	All main culture wells that are not yet harvested
wells_to_induce	List	Active wells that are selected for induction in the current cycle
induced_wells	Dictionary	Active wells that are already induced but not harvested. The dictionary includes the name of the well and the time of cultivation at which this well is harvested (induction time + 4 h)
sampled_wells	List	Wells that were harvested. After harvest, these wells are removed from active_wells

As an example, the method for making induction decisions is shown in Fig. 2.3. When this method is executed, it will be checked if the backscatter signal of the active wells has exceeded the threshold of 5.82. If this is the case and the well is not in the list induced_wells already, the well name is added to the list wells_to_induce. This also applies if the cultivation time exceeds 24 h. The execution of induction is defined in another method.

```
def _select_for_induction(self, latest_cycle:int, bldata:bletl.BLData) -> list:
    """Method for making induction decisions.
    Args:
        latest_cycle (int): number of the current cycle (used to slice data)
        bldata (bletl.BLData): current BioLector data for making decisions
    Returns:
        wells_to_induce (list): list of wells that were triggered in this cycle
    """
    # The -> list: defines that a list is returned

    wells_to_induce = []
    for well in self.active_wells:
        # get backscatter data for this well, x_BS = time, y_BS = BS data
        x_BS, y_BS = bldata['BS3'].get_timeseries(well)

        x_BS = x_BS[:latest_cycle]
        y_BS = y_BS[:latest_cycle]

        # BS trigger:
        if y_BS[latest_cycle - 1] >= 5.82 and not well in self.induced_wells:
            wells_to_induce.append(well)

        # Induction without trigger, if it takes too long!
        if self.cultivator.cultivation_time > 24 and not well in self.induced_wells:
            wells_to_induce.append(well)

    return wells_to_induce
```

Fig. 2.3. Method for making induction decisions in the experiment script. Based on the backscatter data, wells will be selected for induction. For this, the well must not already be included in the induced_wells list and the backscatter or cultivation time threshold must have been reached

2.1.5. Bacterial strains and plasmids

Bacterial strains are listed in Tab. 2.6 and plasmids used in this study in Tab. 2.7.

Tab. 2.6. Bacterial strains used in this work. *B. subtilis* was exclusively used by a cooperation partner in the Knapp lab (Heinrich Heine University Düsseldorf/Forschungszentrum Jülich GmbH)

Strain	Genotype	Reference
B. subtilis TEB1030	*his nprE aprE bpf ispI lipA lipB*	[177]
C. glutamicum ATCC 13032	WT	[1]
C. glutamicum K9	*htrA* replaced by *htrA'* (first 51 bp of *htrA*), TAG stop codon, 16 bp spacer containing a ribosome binding site (RBS) and *eyfp* gene	[76]
E. coli BL21(DE3)	F^- *ompT gal dcm lon hsdS*$_B$(r_B^- m_B^-) λ(DE3 [*lacI lacUV5-T7p07 ind1 sam7 nin5*]) [*malB*$^+$]$_{K\text{-}12}$(λ^S)	[178]
E. coli DH5α	F^- *endA1 glnV44 thi-1 recA1 relA1 gyrA96 deoR nupG purB20* φ80d*lacZ*ΔM15 Δ(*lacZYA-argF*)U169, hsdR17($r_K^-m_K^+$), λ^-	[179]

Strain	Genotype	Reference
E. coli TOP10	F⁻ *mcrA* Δ*(mrr-hsdRMS-mcrBC)* φ*80lacZ*Δ*M15* Δ*lacX74 nupG recA1 araD139* Δ*(ara-leu)7697 galE15 galK16 rpsL*(Str^R) *endA1* λ^-	Thermo Fisher Scientific, USA

Tab. 2.7. Plasmids used in this work. All plasmids contain resistance genes for ampicillin (Amp^r) or kanamycin (Km^r)

Plasmid	Description	Reference
pET22b-sfGFP1-10	pET22b(+) with *sfgfp1-10* gene under control of P_{T7}, Amp^r	[88]
pBS-4nt-SPPel-Cut11	pBSMul1[180]-based *E. coli*/*B. subtilis* shuttle vector with 4 nt spacer length and NdeI/XbaI inserted fragment containing Pel signal peptide sequence, *F. solani* f. sp. *pisi cut1* gene and C-terminal GFP11-tag sequence, Km^r	[78]
pBS-Xnt-SPNprE-Cut11	pBSMul1[180]-based *E. coli*/*B. subtilis* shuttle vector with X nt spacer length (X = 4–12) and NdeI/XbaI inserted fragment containing NprE signal peptide sequence, *F. solani* f. sp. *pisi cut1* gene and C-terminal GFP11-tag sequence, Km^r	P. Lenz, published in [175]
pBSMul-SPMix-SPNprE-YoaJ-GFP11	pBSMul3[67]-based *E. coli*/*B. subtilis* shuttle vector with 5 nt spacer length, HindIII/EcoRI inserted fragment containing NprE signal peptide sequence and EcoRI/XbaI inserted fragment containing *B. subtilis yoaJ* gene and GFP11-tag sequence, Km^r	K. Volkenborn, unpublished
pUC57-Insert-Amp	pUC57 with insert consisting of P_{tac}, 12 nt spacer with sequence $[a]_9$cat, *B. subtilis* signal peptide sequence from *yncM*, *Actinia equina blue chromoprotein aeCP597* under the control of the constitutive P_{em7} and GFP11-tag sequence, Amp^r	Synthesized (Synbio Technologies, USA), published in [175]
pUC57-Cutinase-Amp	pUC57 with *F. solani* f. sp. *pisi cut1* gene, Amp^r	Synthesized (Synbio Technologies, USA), published in [175]
pUC57-LCC-Amp	pUC57 with *lcc*^{ICCG} gene, Amp^r	Synthesized (Synbio Technologies, USA), published in [181]

Plasmid	Description	Reference
pUC57-PE-H-Amp	pUC57 with *P. aestusnigri PE-H*^{Y250S} gene, Amp^r	Synthesized (Synbio Technologies, USA), published in [181]
pPBEx2	Cured pEKEx2[182]-derivative, *E. coli*/*C. glutamicum* shuttle vector, pUC18 *oriV*$_{Cg}$, pBL1 *oriV*$_{Ec}$, P$_{tac}$, corrected *lacI*^{q} allele, lacking destabilizing replicate sequences (Δ930-1140 nucleotides), ΔEcoRI site in the mcs, Km^r	[8]
pPBEx2-NprE-cutinase-GFP11	Insert from pEKEx2-NprE-cutinase-GFP11[8, 66] excised with PstI/SacI and ligated into pPBEx2, Km^r	[75, 89]
pPBEx2-Pel-cutinase-GFP11	Insert from pEKEx2-Pel-cutinase[75] excised with PstI/SacI and ligated into pPBEx2, Km^r	[75, 89]
pPBEx2-Pel(F11I)-cuti11	Pel^{SP} mutant F11I fused to cutinase-GFP11, Km^r	[75]
pPBEx2-Pel(P16S)-cuti11	Pel^{SP} mutant P16S fused to cutinase-GFP11 (V7 from Pel^{L1}), Km^r	[75]
pPBEx2-Pel(F11I/P16S)-cuti11	Pel^{SP} mutant F11I/P16S fused to cutinase-GFP11, Km^r	[75]
pPBEx2-Pel(F11I/G13A/P16S)-cuti11	Pel^{SP} mutant F11I/G13A/P16S fused to cutinase-GFP11, Km^r	[75]
pCMEx12	pPBEx2[8]-based *E. coli*/*C. glutamicum* shuttle vector with NdeI restriction site removed by blunting, new insert consisting of P$_{tac}$, 12 nt spacer with sequence [a]$_9$cat, *B. subtilis* signal peptide sequence from *yncM*, *A. equina blue chromoprotein aeCP597* under the control of the constitutive P$_{em7}$ and GFP11-tag sequence via circlar polymerase extension cloning (CPEC), Km^r	This work, published in [175]
pCMEx[4-11]	pCMEx12-based *E. coli*/*C. glutamicum* shuttle vector with [4-11] nt spacer length with sequence [a]$_{1\text{-}9}$cat cloned into pCMEx12 via PstI/NdeI, Km^r	This work, published in [175]
pCMEx[4-12]-[SP]	pCMEx[4-12] with *B. subtilis* signal peptide sequence from *yncM* exchanged with other *B. subtilis* signal peptide sequences via NdeI/EcoRI, Km^r	This work, published in [175]

Plasmid	Description	Reference
pCMEx[4-12]-[SP]-Cutinase	pCMEx[4-12]-[SP] with P_{em7}-*aeCP597* exchanged with *F. solani* f. sp. *pisi cut1* by Golden Gate assembly using BsaI, *cut1* gene in frame with N-terminal *B. subtilis* signal peptide and C-terminal GFP11-tag sequence, P_{tac}, [4-12] nt spacer length, Km^r	This work, published in [175]
pCMEx8-[SP]-LCC	pCMEx[4-12]-[SP] with P_{em7}-*aeCP597* exchanged with lcc^{ICCG} by Golden Gate assembly using BsaI, *cut1* gene in frame with N-terminal *B. subtilis* signal peptide and C-terminal GFP11-tag sequence, P_{tac}, [4-12] nt spacer length, Km^r	This work, published in [181]
pCMEx-[SP]-PE-H	pCMEx[4-12]-[SP] with P_{em7}-*aeCP597* exchanged with *P. aestusnigri PE-H*^{Y250S} by Golden Gate assembly using BsaI, *cut1* gene in frame with N-terminal *B. subtilis* signal peptide and C-terminal GFP11-tag sequence, P_{tac}, [4-12] nt spacer length, Km^r	This work, published in [181]
pEKEx2-$PhoD^{Cg}$-GFP	(=pCGPhoD^{Cg}-GFP), *E. coli*/*C. glutamicum* shuttle vector pEKEx2 [182] (pUC18 $oriV_{Cg}$, pBL1 $oriV_{Ec}$, P_{tac}, $lacI^q$ with modified C-terminus with $phoD^{Cg}$-gfp_{uv}, Km^r	[63]
pPBEx2-$PhoD^{Cg}$-GFP	pPBEx2-based *E. coli*/*C. glutamicum* shuttle vector with $phoD^{Cg}$-gfp_{uv} from pEKEx2-$PhoD^{Cg}$-GFP inserted via SbfI/KpnI, Km^r	This work

2.1.6. Oligonucleotides

All oligonucleotides that were used are grouped by application and listed in Tab. 2.8. Oligonucleotides were synthesized by Eurofins Genomics (Germany).

Tab. 2.8. Oligonucleotides used in this work

Oligonucleotide	5'→ 3' sequence
Primers for sequencing:	
sCM-Insert_for	gtggtatggctgtgcag
sCM-Insert_rev	gttttatcagaccgcttctg
sCM-lacI_for	cggtatcgtcgtatcccac
sCM_1f	ctcaatacactggccgtcttc

Oligonucleotide	**5'→3' sequence**
sCM_2f	gtattatcccgtgttgacg
sCM_3f	ccggtaactatcgtcttgag
sCM_4f	gcatggttactcaccactgc
sCM_5f	ggtccacctacaacaaagctc
sCM_6f	agtgcttcgatggtggcttg
sCM_7f	tcaatgagggttctaaggtcac
sCM_8f	cgtgagtatgaggttggttc
sCM_9f	gtagtgggcagtgtgcaca
sCM_10f	gttgggaatgtaattcagctcc
CPEC for construction of pCMEx12:	
CPEC-Backbone_for	acgaaaggctcagtcgaaagactgg
CPEC-Backbone_rev	ctcatgttatatcccgccgttaacc
CPEC-Insert_for	ggttaacggcgggatataacatgag
CPEC-Insert_rev	ccagtctttcgactgagcctttcgt
Oligonucleotide hybridization, exchange of spacer sequence for pCMEx[4-11]:	
4nt_Spacer_for	gagaagacaggagaca
4nt_Spacer_rev	tatgtctcctgtcttctctgca
5nt_Spacer_for	gagaagacaggagaaca
5nt_Spacer_rev	tatgttctcctgtcttctctgca
6nt_Spacer_for	gagaagacaggagaaaca
6nt_Spacer_rev	tatgtttctcctgtcttctctgca
7nt_Spacer_for	gagaagacaggagaaaaca
7nt_Spacer_rev	tatgttttctcctgtcttctctgca
8nt_Spacer_for	gagaagacaggagaaaaaca
8nt_Spacer_rev	tatgtttttctcctgtcttctctgca
9nt_Spacer_for	gagaagacaggagaaaaaaca
9nt_Spacer_rev	tatgtttttctcctgtcttctctgca
10nt_Spacer_for	gagaagacaggagaaaaaaaca
10nt_Spacer_rev	tatgtttttttctcctgtcttctctgca
11nt_Spacer_for	gagaagacaggagaaaaaaaaca
11nt_Spacer_rev	tatgtttttttctcctgtcttctctgca
Oligonucleotide hybridization, exchange of signal peptide sequence for pCMEx[4-12]-[SP]:	
AbnA_for	tatgaagaagaagaagacctggaagcgcttcctgcacttctcctccgcagcactggcagca ggcctgatcttcacctccgcagcaccagcagaagcag
AbnA_rev	aattctgcttctgctggtgctgcggaggtgaagatcaggcctgctgccagtgctgcggagg agaagtgcaggaagcgcttccaggtcttcttcttcttca
AmyE_for	tatgttcgcaaagcgcttcaagacctccctgctgccactgttcgcaggcttcctgctgctg ttccacctggtgctggcaggcccagcagcagcatccgcag
AmyE_rev	aattctgcggatgctgctgctgggcctgccagcaccaggtggaacagcagcaggaagcctg cgaacagtggcagcagggaggtcttgaagcgctttgcgaaca

Oligonucleotide	5'→3' sequence
AprE_for	tatgcgctccaagaagctgtggatctccctgctgttcgcactgaccctgatcttcaccatg gcattctccaacatgtccgtgcaggcag
AprE_rev	aattctgcctgcacggacatgttggagaatgccatggtgaagatcagggtcagtgcgaaca gcagggagatccacagcttcttggagcgca
Bpr_for	tatgcgcaagaagaccaagaaccgcctgatctcctccgtgctgtccaccgtggtgatctcc tccctgctgttcccaggcgcagcaggcgcag
Bpr_rev	aattctgcgcctgctgcgcctgggaacagcagggaggagatcaccacggtggacagcacgg aggagatcaggcggttcttggtcttcttgcgca
Bsn_for	tatgaccaagaaggcatggttcctgccactggtgtgcgtgctgctgatctccggctggctg gcaccagcagcatccgcatccgcag
Bsn_rev	aattctgcggatgcggatgctgctggtgccagccagccggagatcagcagcacgcacacca gtggcaggaaccatgccttcttggtca
CwlS_for	tatgaagaagaagatcgtggcaggcctggcagtgtccgcagtggtgggctcctccatggca gcagcaccagcagaagcag
CwlS_rev	aattctgcttctgctggtgctgctgccatggaggagcccaccactgcggacactgccaggc ctgccacgatcttcttcttca
Epr_for	tatgaagaacatgtcctgcaagctggtggtgtccgtgaccctgttcttctccttcctgacc atcggcccactggcacacgcag
Epr_rev	aattctgcgtgtgccagtgggccgatggtcaggaaggagaagaacagggtcacggacacca ccagcttgcaggacatgttcttca
LipA_for	tatgaagttcgtgaagcgccgcatcatcgcactggtgaccatcctgatgctgtccgtgacc tccctgttcgcactgcagccatccgcaaaggcag
LipA_rev	aattctgcctttgcggatggctgcagtgcgaacagggaggtcacggacagcatcaggatgg tcaccagtgcgatgatgcggcgcttcacgaacttca
LipB_for	tatgaagaaggtgctgatggcattcatcatctgcctgtccctgatcctgtccgtgctggca gcaccaccatccggcgcaaaggcag
LipB_rev	aattctgcctttgcgccggatggtggtgctgccagcacggacaggatcagggacaggcaga tgatgaatgccatcagcaccttcttca
Mpr_for	tatgaagctggtgccacgcttccgcaagcagtggttcgcatacctgaccgtgctgtgcctg gcactggcagcagcagtgtccttcggcgtgccagcaaaggcag
Mpr_rev	aattctgcctttgctggcacgccgaaggacactgctgctgccagtgccaggcacagcacgg tcaggtatgcgaaccactgcttgcggaagcgtggcaccagcttca
NprB_for	tatgcgcaacctgaccaagacctccctgctgctggcaggcctgtgcaccgcagcacagatg gtgttcgtgacccacgcatccgcag
NprB_rev	aattctgcggatgcgtgggtcacgaacaccatctgtgctgcggtgcacaggcctgccagca gcagggaggtcttggtcaggttgcgca
NprE_for	tatgggtttaggtaagaaattgtctgttgctgtcgctgcttcgtttatgagtttatcaatc agcctgccaggtgttcaggctg
NprE_rev	aattcagcctgaacacctggcaggctgattgataaactcataaacgaagcagcgacagcaa cagacaatttcttacctaaaccca
Pel_for	tatgaaaaaagtgatgttagctacggctttgtttttaggattgactccagctggcgcgaac gcag

Oligonucleotide	5'→3' sequence
Pel_rev	aattctgcgttcgcgccagctggagtcaatcctaaaaacaaagccgtagctaacatcactttttca
PelB_for	tatgaagcgcctgtgcctgtggttcaccgtgttctccctgttcctggtgctgctgccaggcaaggcactgggcg
PelB_rev	aattcgcccagtgccttgcctggcagcagcaccaggaacagggagaacacggtgaaccacaggcacaggcgcttca
PhoB_for	tatgaagaagttcccaaagaagctgctgccaatcgcagtgctgtcctccatcgcattctcctccctggcatccggctccgtgccagaagcatccgcag
PhoB_rev	aattctgcggatgcttctggcacggagccggatgccagggaggagaatgcgatggaggacagcactgcgattggcagcagcttctttgggaacttcttca
SacB_for	tatgaacatcaagaagttcgcaaagcaggcaaccgtgctgaccttcaccaccgcactgctggcaggcggcgcaacccaggcattcgcag
SacB_rev	aattctgcgaatgcctgggttgcgccgcctgccagcagtgcggtggtgaaggtcagcacggttgcctgctttgcgaacttcttgatgttca
SacC_for	tatgaagaagcgcctgatccaggtgatgatcatgttcaccctgctgctgaccatggcattctccgcagatgcag
SacC_rev	aattctgcatctgcggagaatgccatggtcagcagcagggtgaacatgatcatcacctggatcaggcgcttcttca
Vpr_for	tatgaagaagggcatcatccgcttcctgctggtgtccttcgtgctgttcttcgcactgtccaccggcatcaccggcgtgcaggcagcaccagcag
Vpr_rev	aattctgctggtgctgcctgcacgccggtgatgccggtggacagtgcgaagaacagcacgaaggacaccagcaggaagcggatgatgcccttcttca
YoaW_for	tatgaagaagatgctgatgctggcattcaccttcctgctggcactgaccatccacgtgggcgaagcatccgcag
YoaW_rev	aattctgcggatgcttcgcccacgtggatggtcagtgccagcaggaaggtgaatgccagcatcagcatcttcttca
YolA_for	tatgaagaagcgcatcacctactccctgctggcactgctggcagtggtggcattcgcattccaccgattcctccaaggcaaaggcag
YolA_rev	aattctgcctttgccttggaggaatcggtgaatgcgaatgccaccactgccagcagtgccagcagggagtaggtgatgcgcttcttca
YpjP_for	tatgaagctgtggatgcgcaagaccctggtggtgctgttcaccatcgtgaccttcggcctggtgtccccaccagcagcactgatggcag
YpjP_rev	aattctgccatcagtgctgctggtggggacaccaggccgaaggtcacgatggtgaacagccaccaccagggtcttgcgcatccacagcttca
YwaD_for	tatgaagaagctgctgaccgtgatgaccatggcagtgctgaccgcaggcaccctgctgctgccagcacagtccgtgaccccagcagcacacgcag
YwaD_rev	aattctgcgtgtgctgctggggtcacggactgtgctggcagcagcagggtgcctgcggtcagcactgccatggtcatcacggtcagcagcttcttca
YwmC_for	tatgaagaagcgcttctccctgatcatgatgaccggcctgctgttcggcctgacctccccagcattcgcag
YwmC_rev	aattctgcgaatgctggggaggtcaggccgaacagcaggccggtcatcatgatcagggagaagcgcttcttca

Oligonucleotide	5'→3' sequence
Oligonucleotide hybridization, exchange of RBS in pCMEx8-NprE-Cutinase:	
RBS-PB_for	gaaggagatataca
RBS-PB_rev	tatgtatatctccttctgca
RBS-PB-BbsI_for	gaagacgaaggagatataca
RBS-PB-BbsI_rev	tatgtatatctccttcgtcttctgca
RBS-CM_for	gaaggagaaaaaca
RBS-CM_rev	tatgtttttctccttctgca
RBS-CM-BbsI-GA_for	gagaagacgaaggagaaaaaca
RBS-CM-BbsI-GA_rev	tatgtttttctccttcgtcttctctgca
PCR amplification of phoD^{Cg}-gfp$_{UV}$:	
PhoD_for	atcacctgcaggaaggagatatagatatgccacagttaagcagacg
GFPuv_rev	atcaggtaccttatttgtagagctcatccatgccatgtg

2.1.7. Chemicals and enzymes

Chemicals were obtained from Carl Roth (Germany), Sigma-Aldrich (USA) or Merck (Germany) and restriction enzymes from New England Biolabs (USA). Chemicals from other manufacturers, other enzymes and size standards are listed in Tab. 2.9.

Tab. 2.9. Chemicals from other manufacturers, other enzymes and size standards used in this work

Product	Manufacturer
1 kb Plus DNA Ladder	New England Biolabs, USA
CutSmart® Buffer(10x)	New England Biolabs, USA
DNA Polymerase I, Large (Klenow) Fragment	New England Biolabs, USA
Deoxyribonucleoside triphosphate (dNTP) Mix Conc. 40 mM (10 mM each)	VWR, USA
Gel Loading Dye, Purple (6x)	New England Biolabs, USA
GelStar™ Nucleic Acid Gel Stain (10 000x)	Lonza, Switzerland
NEBuffer (10x)	New England Biolabs, USA
NuPAGE™ MES SDS Running Buffer (20x)	Thermo Fisher Scientific, USA
PageRuler™ Prestained Protein Ladder, 10 to 180 kDa	Thermo Fisher Scientific, USA
Q5® High-Fidelity DNA Polymerase	New England Biolabs, USA
Q5® Reaction Buffer (5x)	New England Biolabs, USA
Sample Buffer, Laemmli (2x)	Sigma-Aldrich, USA
SimplyBlue™ SafeStain	Thermo Fischer Scientific, USA
T4 DNA Ligase	New England Biolabs, USA
T4 DNA Ligase Buffer (10x)	New England Biolabs, USA

2.2. Microbiological methods

2.2.1. Sterilization

Materials and solutions were sterilized by autoclaving at 121 °C and 2 bar for 20 min, if necessary. Heat-sensitive solutions were sterile filtered with 0.22 µm pore size.

2.2.2. Cultivation media and supplements

Unless stated otherwise, media components were dissolved in deionized water, sterilized by autoclaving and stored at room temperature.

For cultivation of *E. coli* in complex medium, SOC medium was prepared with the final concentrations listed in Tab. 2.10 and lysogeny broth (LB) with Miller's modifications [183] with final concentrations listed in Tab. 2.11. For cultivation on plates, 15 g L^{-1} agar were added to LB medium before autoclaving.

Tab. 2.10. SOC medium; sterilized by filtration

Concentration	Component
20 g L^{-1}	Peptone *ex* soya, papainic digested
5 g L^{-1}	Yeast extract
0.6 g L^{-1}	NaCl
0.2 g L^{-1}	KCl
0.95 g L^{-1}	$MgCl_2$, anhydrous
1.2 g L^{-1}	$MgSO_4$, anhydrous
3.95 g L^{-1}	Glucose · $1H_2O$

Tab. 2.11. LB medium with Miller's modifications [183]; pH = 7.0±0.2; sterilized by autoclaving

Concentration	Component
10 g L^{-1}	Trypton
5 g L^{-1}	Yeast extract
10 g L^{-1}	NaCl

Defined medium for cultivation of *E. coli* was prepared according to [184] with final concentrations listed in Tab. 2.12. 10x stocks of ethylenediaminetetraacetic acid

(EDTA), KH_2PO_4, $(NH_4)_2HPO_4$, citric acid, Fe(III) citrate and Thiamine · HCl as well as a 50x stock of $MgSO_4 \cdot 7H_2O$ were prepared separately. Stock solutions of Fe(III) citrate and Thiamine · HCl were sterile filtered and stored at 4 °C and –20 °C, respectively. A 100x concentrated salt solution with $CoCl_2 \cdot 6H_2O$, $MnCl_2 \cdot 4H_2O$, $CuCl_2 \cdot 4H_2O$, boric acid, $Na_2MoO_4 \cdot 2H_2O$ and zinc acetate · $2H_2O$ was adjusted with 10 M NaOH to a pH value of 1 for autosterility. 500 g L^{-1} glucose were prepared as a stock solution.

Tab. 2.12. DeLisa defined medium according to [184] with 20 g L^{-1} glucose

Concentration	Component
20 g L^{-1}	Glucose
13.3 g L^{-1}	KH_2PO_4
4 g L^{-1}	$(NH_4)_2HPO_4$
1.2 g L^{-1}	$MgSO_4 \cdot 7H_2O$
1.7 g L^{-1}	Citric acid
8.4 mg L^{-1}	EDTA
2.5 mg L^{-1}	$CoCl_2 \cdot 6H_2O$
15 mg L^{-1}	$MnCl_2 \cdot 4H_2O$
1.5 mg L^{-1}	$CuCl_2 \cdot 4H_2O$
3 mg L^{-1}	Boric acid
2.5 mg L^{-1}	$Na_2MoO_4 \cdot 2H_2O$
13 mg L^{-1}	Zinc acetate · $2H_2O$
0.1 g L^{-1}	Fe(III) citrate
4.5 mg L^{-1}	Thiamine · HCl

Cultivation of *C. glutamicum* was done in brain heart infusion (BHI), BHI with 45.5 g L^{-1} D-sorbitol (BHIS) or in CGXII medium. Final concentrations are given in Tab. 2.13 and Tab. 2.14. For cultivation on plates, 10 g L^{-1} agar were added to BHIS medium before autoclaving.

Tab. 2.13. BHI and BHIS medium; D-sorbitol was autoclaved separately to prevent a Maillard reaction and added only for BHIS medium

Concentration	Component
37 g L^{-1}	BHI
91 g L^{-1}	D-sorbitol

Tab. 2.14. CGXII medium according to [185]

Concentration	Component
20 g L^{-1}	D-glucose
42 g L^{-1}	3-(N-morpholino)propanesulfonic acid (MOPS)
20 g L^{-1}	$(NH_4)_2SO_4$
1 g L^{-1}	K_2HPO_4
1 g L^{-1}	KH_2PO_4
5 g L^{-1}	Urea
13.25 mg L^{-1}	$CaCl_2 \cdot 2H_2O$
0.25 g L^{-1}	$MgSO_4 \cdot 7H_2O$
10 mg L^{-1}	$FeSO_4 \cdot 7H_2O$
10 mg L^{-1}	$MnSO_4 \cdot H_2O$
0.02 mg L^{-1}	$NiCl_2 \cdot 6H_2O$
0.313 mg L^{-1}	$CuSO_4 \cdot 5H_2O$
1 mg L^{-1}	$ZnSO_4 \cdot 7H_2O$
0.2 mg L^{-1}	Biotin
30 mg L^{-1}	Protocatechuic acid (PCA)

For CGXII medium, stock solutions were prepared in two ways. For the first, 1.25x shake flask salts consisting of $(NH_4)_2SO_4$, urea, K_2HPO_4, KH_2PO_4, MOPS were mixed and the pH was adjusted to 7 with 4 M NaOH. A 500 g L^{-1} glucose stock solution and 1 000x stock solutions of $CaCl_2 \cdot 2H_2O$, $MgSO_4 \cdot 7H_2O$ were separately prepared. 1 000x concentrated PCA and biotin were dissolved in 1 M NaOH for autosterility and stored at –20 °C. For a 1 000x stock of trace element solution, $FeSO_4 \cdot 7H_2O$, $MnSO_4 \cdot H_2O$, $ZnSO_4 \cdot 7H_2O$, $CuSO_4 \cdot 5H_2O$ and $NiCl_2 \cdot 6H_2O$ were mixed and HCl was added for complete dissolution before sterile filtration.

To adjust the concentration of the media components, separate stock solutions of 440 g L^{-1} glucose, 500 g L^{-1} urea and 209.26 g L^{-1} MOPS with the pH adjusted to 7 with NaOH were filter sterilized. The trace element solution was prepared as described above, but the pH was adjusted to 1 with sulfuric acid. 500 g L^{-1} $(NH_4)_2SO_4$ stock solution, a phosphate stock solution with 100 g L^{-1} K_2HPO_4 and KH_2PO_4 and stock solutions with 3.312 5 g L^{-1} $CaCl_2 \cdot 2H_2O$ and 62.5 g L^{-1} $MgSO_4 \cdot 7H_2O$ were separately prepared.

Antibiotics were added to cultivation media as required for plasmid stabilization (see Tab. 2.7) and isopropyl β-D-1-thiogalactopyranoside (IPTG) for induction of target gene expression (Tab. 2.15).

Tab. 2.15. Media supplements. All stock solutions were prepared with deionized water, sterile filtered and stored at –20 °C

Supplement	Bacteria	Stock concentration	Final concentration
Ampicillin	*E. coli*	100 g L^{-1}	100 µg mL^{-1}
IPTG	*E. coli*, *C. glutamicum*	100 mM	100–1 000 µM
Kanamycin	*E. coli*	50 g L^{-1}	50 µg mL^{-1}
	C. glutamicum	30 g L^{-1}	30 µg mL^{-1}

2.2.3. Bacterial cultivation

C. glutamicum was cultivated at 30 °C and *E. coli* at 37 °C unless otherwise indicated. Cultivation in flasks was done in baffled flasks with a filling volume of 0.1x flask volume and a shaking diameter of 25 mm.

24- and 96-well DWPs for cultivation were sealed with gas-permeable sealing foils and incubated in tempered shakers at 900 rpm with a shaking diameter of 3 mm and humidity control or at 250 rpm with a shaking diameter of 25 mm without humidity control. Test tubes were incubated at 170 rpm with 50 mm shaking diameter.

2.2.4. Determination of cell density

The cell density was either determined by measurement of optical density (OD) or by cell dry weight (CDW). The $OD_{580\,nm}$ or $OD_{578\,nm}$ was measured for *E. coli* samples and the $OD_{600\,nm}$ for *C. glutamicum* samples. 0.9% (w/v) NaCl were used as a blank and for sample dilution to fit 0.1–0.3 in the linear range.

For CDW determination, weighed 2 mL reaction tubes were dried at 90 °C for 24 h and put into a desiccator. 2 mL cultivation samples were transferred into these reaction tubes and centrifuged at 21 500 x*g* and 4 °C for 10 min. The supernatant was discarded, and the remaining cells were dried at 90 °C for 24 h before weight determination. For samples from LCC secretion in STRs, 1.5 mL reaction tubes were used and the sample volume was reduced tot 1.5 mL. Before drying, cells were washed with 0.9% (w/v) NaCl.

2.2.5. Strain maintenance

Bacterial cultures streaked on agar plates were stored at 4 °C for up to 2 weeks. For long time storage, cryo-conserved cultures were prepared with final concentrations of 25–50% (w/v) glycerol as described below and stored at –80 °C in cryogenic vials, unless otherwise specified.

For *E. coli*, 6 mL LB in test tubes were inoculated from a single colony from agar plates. After overnight incubation at 37 °C and 170 rpm, 750 µL culture were mixed with 750 µL 50% (w/v) glycerol.

For master cell banks (MCBs) of *C. glutamicum*, 10 mL BHI in a flask or 3.5 mL in a 24-well DWP were inoculated from single colonies and incubated overnight at 30 °C and 250 rpm. 750 µL culture were mixed with 750 µL 100% (w/v) glycerol to a final glycerol concentration of 50% (w/v). For the preparation of *C. glutamicum* working cell banks (WCBs) in flasks, 50 mL CGXII were inoculated with 250 µL of a MCB. *C. glutamicum* was incubated for around 15 h at 250–300 rpm and 30 °C with online biomass monitoring (SFR vario, PreSense Precision Sensing). The cells were harvested by centrifuging with 9 283 x*g* for 5 min before reaching the stationary phase and resuspended to an $OD_{600\,nm}$ of 60 with 0.9% (w/v) NaCl. After diluting the samples 2x with 50% (w/v) glycerol, 1 mL aliquots were stored at –80 °C.

Additionally, cryo-conserved cultures of PETase-secreting *C. glutamicum* strains were prepared in 96-well MTPs. For this, 3.5 mL CGXII per well of a 24-well plate were inoculated with 100 µL MCB and incubated overnight at 30 °C and 900 rpm. Cultures were centrifuged for 5 min at 2 000 x*g* and the supernatant was discarded. Cells were washed with 1.5 mL CGXII, resuspended in 3.5 mL fresh medium and incubated for 5 h at 30 °C and 900 rpm. Each 100 µL culture was mixed with 100 µL 50% (w/v) glycerol in a 96-well MTP, the MTP was sealed with aluminium foil and stored at –80 °C.

2.3. Molecular biological methods

2.3.1. Preparation and transformation of competent *E. coli*

5 mL LB in a test tube or 10 mL in a baffled flask were inoculated from a single colony of *E. coli* DH5α or TOP10 streaked on LB agar. After cultivation overnight at 37 °C and 170–180 rpm, 1–2 mL were used to inoculate 100–200 mL LB in a baffled flask with 5x volume compared to filling volume, respectively. Cells were incubated at 37 °C and 250 rpm until an $OD_{578\,nm}$ of 0.6–0.8 was reached. The culture was transferred to 50 mL centrifugation tubes and incubated on ice for 10 min. After centrifugation for 10 min at 3 300 x*g* and 4 °C, the supernatant was discarded and cells were resuspended in 10 mL sterile and ice-cold 0.1 M $CaCl_2$ with 10% (w/v) glycerol per centrifugation tube. After incubation on ice for 15 min with subsequent centrifugation (10 min, 3 300 x*g*, 4 °C), the supernatant was discarded and cells were resuspended in 1 mL sterile and ice-cold 0.1 M $CaCl_2$ with 10% (w/v) glycerol per centrifugation tube. 104 µL competent cells in 1.5 mL centrifugation tubes or 20 µL per well of a low-profile and non-skirted PCR plate sealed with aluminium foil were stored at –80 °C until transformation.

For manual heat-shock transformation of $CaCl_2$-competent *E. coli*, 1 µL (plasmid purified from *E. coli*) or 5 µL (ligated plasmid) were carefully mixed with 20 µL or 50 µL competent cells, respectively. After incubation on ice for 20 min, heat-shock was performed for 30 s at 42 °C with subsequent incubation on ice for 2 min. 250 µL LB were added and cells were regenerated for 1 h at 37 °C and 300 rpm in a ThermoMixer®. Cells were streaked on LB agar with appropriate antibiotic and incubated overnight at 37 °C or for 72 h at room temperature in the dark. For improved transformation efficiencies, the first incubation on ice was elongated to 30 min and SOC medium was used for regeneration of cells. For transformation of plasmids already purified from *E. coli*, regeneration in LB was shortened to 30 min.

Automated heat-shock transformation was done with the Opentrons OT-2 with Thermocycler Module. The protocol for improved transformation efficiency was modified to mixing 2 µL plasmid DNA with 20 µL competent cells. Only 178 µL SOC medium were added for regeneration and minimum 4x 8 µL cell suspension were pipetted onto single-well plates with LB agar filled by a plate pourer to ensure uniform filling levels. The OT-2 script was deposited in a repository [186].

2.3.2. Preparation and transformation of competent *C. glutamicum*

C. glutamicum was streaked on BHIS agar and incubated for 48 h at 30 °C. 50 mL BHIS were inoculated from a single colony and incubated overnight at 30 °C and 250 rpm. 1.5 mL of this culture were used to inoculate 100 mL fresh BHIS and cells were incubated at 30 °C and 250 rpm until the $OD_{600\,nm}$ exceeded 1.5. Cells were harvested for 20 min at 4 500 x*g* and 4 °C and resuspended in 2 mL ice-cold TG buffer (Tab. 2.16). Further 4 mL TG buffer were added followed by centrifugation (10 min, 4 500 x*g*, 4 °C). Cells were washed with TG buffer again and 2x with 6 mL ice-cold 10% (w/v) glycerol. Afterwards, cell pellets were resuspended in 1 mL ice-cold 10% (w/v) glycerol and 100 µL aliquots were stored at –80 °C until transformation.

Tab. 2.16. TG buffer for preparation of competent *C. glutamicum*. A 1 000x stock solution of sterile Tris(2-hydroxyethyl)amine hydrochloride was prepared. The pH of TG buffer was adjusted to 7.5 with NaOH before autoclaving

Concentration	Component
185.5 mg L^{-1}	Tris(2-hydroxyethyl)amine hydrochloride ($C_6H_{15}NO_3 \cdot HCl$)
101.26 g L^{-1}	Glycerol

Transformation by electroporation was done as described elsewhere [187]. Briefly, 4 mL BHIS were pre-warmed to 46 °C in sterile 15 mL centrifugation tubes. Competent cells were thawed on ice and 50 µL were mixed with 1–2 µL plasmid DNA in an electroporation cuvette. The cell solution was overlaid with 800 µL sterile 10% (w/v) glycerol and electroporated (25 µF, 2 500 V, 12.5 kV cm^{-1}, 200 Ω). Cells were transferred to the pre-warmed BHIS, incubated at 46 °C for 6 min and cooled to 30 °C on ice. After incubation at 30 °C and 170 rpm with 50 mm shaking diameter for 90 min, cells were centrifuged (10 min, 2 800 x*g*) and resuspended in a greatly reduced amount of supernatant. Cells were streaked on BHIS agar and incubated at 30 °C for 48 h.

For high-throughput electroporation in an electroporation plate, cells and DNA were overlaid with only 50 µL sterile 10% (w/v) glycerol. Cell regeneration was done in 1 mL BHIS in a 96-well DWP with 2 mL filling volume and cells were incubated at 30 °C and 900 rpm. Instead of streaking, 8 µL cell suspension were pipetted on BHIS agar. After centrifugation for 10 min at 2 800 x*g*, cells were resuspended in

a reduced amount of supernatant and again pipetted on BHIS agar to ensure that individual colonies grow for each strain.

2.3.3. Plasmid purification

For plasmid purification of up to 24 samples, 6 mL LB in a test tube were inoculated from a single colony of *E. coli* DH5α or TOP10 on LB agar. After overnight cultivation at 37 °C and 170 rpm, the culture was transferred to a 5 mL centrifugation tube. Cells were harvested by centrifugation (9 283 x*g*, 4 °C, 5 min) and stored at –20 °C, if purification was not immediately carried out. DNA was purified with the NucleoSpin Plasmid (NoLid) kit and a vacuum manifold. Deviating, the silica membrane was dried in an additional centrifugation step with subsequent incubation at 70 °C for 5 min. Elution buffer or ultrapure water was heated to 70 °C and incubated for 5 min on the membrane prior to elution.

With up to 96 samples, 1.5 mL LB in a 96-well DWP with square wells were inoculated from a single *E. coli* colony. Cells were cultivated overnight at 37 °C and 250 rpm and harvested by centrifuging for 15 min at 2 500 x*g*. Plasmids were automatically purified using the Wizard® MagneSil® Plasmid on the Opentrons OT-2 with the Magnetic Module according to manufacturer's instructions. Since shaken incubation was not possible, the mixing was done by pipetting up and down. The complete script can be found in the aforementioned repository [186]. Manual work was only involved to prepare the robot and fill reagents into a 12-column plate as indicated in Tab. 2.17. While running the experiment, only the trash can had to be emptied in between and used pipette tips had to be exchanged with new ones.

Tab. 2.17. Reagents in a 12-column plate for automated plasmid purification using the Wizard® MagneSil® Plasmid on the Opentrons OT-2 with the Magnetic Module

Column	Minimum (recommended) volume for:		Reagent
	One column	One plate	
1	0.72 mL (2 mL)	8.64 mL (12 mL)	Cell resuspension solution
2	0.96 mL (2 mL)	11.52 mL (14 mL)	Cell lysis solution
3	0.96 mL (2 mL)	11.52 mL (14 mL)	Neutralisation solution
4	0.2 mL (2 mL)	2.4 mL (5 mL)	Magnesil Blue
5	0.4 mL (2 mL)	4.8 mL (7 mL)	Magnesil Red
6	0.8 mL (2 mL)	9.6 mL (13 mL)	80% (v/v) Ethanol
7	0.8 mL (2 mL)	9.6 mL (13 mL)	80% (v/v) Ethanol
8	0.8 mL (2 mL)	9.6 mL (13 mL)	80% (v/v) Ethanol

Column	Minimum (recommended) volume for:		Reagent
	One column	One plate	
9	0.8 mL (2 mL)	9.6 mL (13 mL)	Elution Buffer
10	–	–	–
11	–	–	–
12	–	–	–

2.3.4. Determination of DNA concentration

The concentration of double-stranded DNA was determined by absorbance measurement at 260 nm with a NanoDrop™ 1000 spectrophotometer according to the manufacturer's instructions. Protein impurities were identified by absorbance measurement at 280 nm. The quotient of absorbance at 260 nm and 280 nm indicates the purity of the DNA and should ideally be around 1.8 according to the manufacturer.

2.3.5. Restriction digestion

DNA was digested with restriction enzymes at 37 °C for 2 h. Heat inactivation after digestion was omitted as DNA was subsequently purified by gel extraction (subsection 2.3.6) unless otherwise stated.

For generation of the pPBEx2-based pCMEx12, the NdeI restriction site in the backbone of pPBEx2 had to be removed by blunting (see subsection 2.3.7). For this, pPBEx2 was digested with NdeI with the reaction mix in Tab. 2.18 before subsequent gel extraction and blunting.

Tab. 2.18. Reaction mix for restriction digestion of pPBEx2 for NdeI blunting

Volume	Component
2.63 µL	Plasmid DNA (pPBEx2, 1 µg final)
5 µL	10x CutSmart®
1 µL	NdeI
Filled to 50 µL	Ultrapure water

The composition of the reaction mix for digestion of pCMEx[4-12] to exchange the spacer or signal peptide sequences is listed in Tab. 2.19. In Tab. 2.20, the reaction

mix for digestion of pCMEx8-NprE-Cutinase for exchange of the RBS sequence or for digestion of pPBEx2 and PCR-amplified *phoD*^{Cg}*-gfp* (see subsection 2.3.8) prior to ligation is shown.

Tab. 2.19. Reaction mix for restriction digestion of pCMEx12 before exchange of spacer sequence or of pCMEx[4-12] for exchange of signal peptide sequence

Volume	Component for sequence exchange of:	
	spacer	**signal peptide**
20 µL	Plasmid DNA	
4 µL	10x CutSmart˚	
1–2 µL	PstI-HF	EcoRI-HF
1–2 µL	NdeI	
Filled to 40 µL	Ultrapure water	

Tab. 2.20. Reaction mix for restriction digestion of pCMEx8-NprE-Cutinase for exchange of RBS or of pPBEx2 and PCR-amplified *phoD*^{Cg}*-gfp* prior to ligation

Volume	Component for restriction digestion of:	
	pCMEx8-NprE-Cutinase	**pPBEx2 and *phoD*^{Cg}*-gfp***
30 µL	Plasmid DNA or PCR product	
5 µL	10x CutSmart˚	
2 µL	PstI-HF	SbfI-HF
2 µL	NdeI	KpnI-HF
Filled to 50 µL	Ultrapure water	

As a control after Golden Gate assembly (subsection 2.3.11) or DNA blunting (subsection 2.3.7), DNA samples were digested at 37 °C for 1 h (Tab. 2.21). Enzymes were heat-inactivated for 20 min at 65 °C or at 80 °C, if NcoI-HF was used.

Tab. 2.21. Reaction mix for restriction digestion as a control of successful DNA blunting of pPBEx2 or target gene insertion by Golden Gate assembly. For the latter, different restriction enzymes were used depending on the inserted target gene

Volume	Component for inserted gene:			Component for
	cutinase	***pe-h***	***lcc***	**NdeI blunting**
3 µL	Plasmid DNA			
1 µL	10x CutSmart®			
0.2 µL	NotI-HF	NcoI-HF	EagI-HF	NdeI
0.2 µL	EcoRI-HF	EcoRI-HF	EagI-HF	PstI-HF
Filled to 10 µL	Ultrapure water			

This restriction digestion was automated with the Opentrons OT-2 with Thermocycler Module and the script was deposited elsewhere [186]. Plasmid DNA was placed on the robotic deck directly in the elution plate after plasmid purification. The remaining reaction mix was provided in another plate and both were automatically mixed in a fresh PCR plate in the Thermocycler Module. After incubation and heat-inactivation of the enzymes, plasmids were directly diluted in deionized water for analysis of DNA fragment number and size by capillary electrophoresis (subsection 2.3.12). With successful NdeI removal by DNA blunting, only EcoRI-HF would digest pPBEx2 resulting in only one DNA fragment. For Golden Gate assembly samples, restriction enzymes would cut twice in total with inserted gene of interest and only once without.

2.3.6. Gel electrophoresis and DNA extraction

A 1% (w/v) agarose gel (agarose in 1x tris-acetate-EDTA buffer (TAE) buffer, see Tab. 2.22) was prepared and covered with 1x TAE buffer. DNA was mixed with 6x Purple Loading Dye and applied to the agarose gel with 7 µL 1 kb Plus DNA Ladder for size comparison. Depending on the size of the gel, DNA fragments were separated for 70 min at 90–110 V and stained with ethidium bromide. Respective DNA fragments were excised under UV light and purified using the Nucleospin Gel & PCR Cleanup kit according to manufacturer's instructions. Deviating from this, the DNA was eluted with 30 µL ultrapure water.

Tab. 2.22. 10x TAE buffer. The pH was adjusted to 8 with acetic acid

Concentration	Component
48.40 g L^{-1}	Tris(hydroxymethyl)aminomethane (Tris)
2.94 g L^{-1}	EDTA

2.3.7. DNA blunting

The NdeI restriction site in the backbone of pPBEx2 had to be removed before circlar polymerase extension cloning (CPEC) of pCMEx12 (subsection 2.3.8). 3' overhangs of NdeI-digested pPBEx2 were removed and 5' overhangs were filled by the DNA Polymerase I, Large (Klenow) Fragment. Samples were prepared according

to Tab. 2.23 and incubated for 15 min at 25 °C. Reaction was stopped by addition of EDTA with 10 mM final concentration and heating to 75 °C for 20 min before DNA purification by gel extraction.

Tab. 2.23. Reaction mix for DNA blunting of NdeI-digested pPBEx2

Volume	Component
29 µL	NdeI-digested pPBEx2 (571 ng final)
4 µL	10x NEBuffer
1.32 µL	10x diluted dNTP Mix (33 µM final concentration each)
0.5 µL	DNA Polymerase I, Large (Klenow) Fragment
Filled to 40 µL	Ultrapure water

2.3.8. PCR and circular polymerase extension cloning

Polymerase chain reaction (PCR) is used for *in vitro* amplification of DNA and is the basis of CPEC. For CPEC-based generation of pCMEx12, the backbone of pPBEx2 without NdeI restriction site and the insert from pUC57-Insert-Amp were separately amplified by PCR (reaction mix in Tab. 2.24) with the respective CPEC primers listed in Tab. 2.8. Amplified DNA fragments were purified by gel electrophoresis and used for CPEC (reaction mix in Tab. 2.25).

For preparation of pPBEx2-phoD^{Cg}-GFP for Tat-dependent GFP-secretion, *phoD^{Cg}-gfp* was amplified from pEKEx2-phoD^{Cg}-GFP with respective primers (Tab. 2.8) and the reaction mix listed in Tab. 2.26. All thermocycler protocols are listed in Tab. 2.27.

Tab. 2.24. Reaction mix for PCR amplification of insert and backbone for CPEC

Volume	Component for amplification of:	
	Backbone	Insert
10 µL	5x Q5 Reaction Buffer	
1 µL	10 mM dNTPs (200 µM final)	
2.5 µL	10 µM forward primer (0.5 µM final)	
2.5 µL	10 µM reverse primer (0.5 µM final)	
2 µL	1, 4 or 10 ng µL^{-1} pUC57-Insert-Amp	1, 5 or 10 ng µL^{-1} pPBEx2 without NdeI restriction site
0.5 µL	Q5® High-Fidelity DNA Polymerase	
Filled to 50 µL	Ultrapure water	

Tab. 2.25. Reaction mix for CPEC of pCMEx12 with insert-to-vector molar ratio of 2:1 and 500 ng backbone

Volume	Component
10 µL	5x Q5 Reaction Buffer
1 µL	10 mM dNTPs (200 µM final)
20 µL	DNA backbone (approx. 500 ng final)
10 µL	DNA insert (approx. 404 ng final)
0.5 µL	Q5® High-Fidelity DNA Polymerase
Filled to 50 µL	Ultrapure water

Tab. 2.26. Reaction mix for amplification of *phoD^{Cg}-gfp* from pEKEx2-phoD^{Cg}-GFP

Volume	**Component**
5 µL	5x Q5 Reaction Buffer
0.5 µL	10 mM dNTPs
1.25 µL	10 pmol µL^{-1} forward primer
1.25 µL	10 pmol µL^{-1} reverse primer
1 µL	DNA diluted to 5 ng µL^{-1} (5 ng final)
0.25 µL	Q5® High-Fidelity DNA Polymerase
Filled to 25 µL	Ultrapure water

Tab. 2.27. Thermocycler protocols for *in vitro* DNA amplification

Cycles	**Step**	**Temperature**	**Time**
Amplification of the pUC57-Insert-Amp insert for CPEC:			
1	Initial denaturation	98 °C	30 s
30	Denaturation	98 °C	10 s
	Primer annealing	68 °C	30 s
	Elongation	72 °C	77 s
1	Final elongation	72 °C	120 s
Amplification of the pPBEx2 backbone without NdeI restriction site for CPEC:			
1	Initial denaturation	98 °C	30 s
30	Denaturation	98 °C	10 s
	Primer annealing	68 °C	30 s
	Elongation	72 °C	256 s
1	Final elongation	72 °C	120 s

Cycles	Step	Temperature	Time
CPEC of pCMEx12 with separately amplified insert and backbone:			
1	Initial denaturation	98 °C	30 s
5	Denaturation	98 °C	10 s
	Primer annealing	68 °C	30 s
	Elongation	72 °C	128 s
1	Final elongation	72 °C	120 s
Amplification of phoD^{Cg}-gfp:			
1	Initial denaturation	98 °C	30 s
30	Denaturation	98 °C	10 s
	Primer annealing	68 °C	30 s
	Elongation	72 °C	25 s
1	Final elongation	72 °C	120 s

2.3.9. Oligonucleotide hybridization

Partly complementary oligonucleotides (see Tab. 2.8) were hybridized to obtain double-stranded DNA with overhangs that can be ligated with digested plasmids. Components listed in Tab. 2.29 were mixed in a robotic PCR plate and incubated in the Opentrons OT-2 Thermocycler Module as described in Tab. 2.29. Temperature profiles are based on the melting temperature (T_M) of the oligonucleotides, which correlates with the length. Therefore, temperature profile for hybridization of the shorter spacer oligonucleotides was adjusted.

Tab. 2.28. Reaction mix for annealing of complementary oligonucleotides

Volume	Component	Stock concentration	Final concentration
3.5 µL	Oligonucleotide 1 (for)	100 pmol µL^{-1}	5 µM
3.5 µL	Oligonucleotide 2 (rev)	100 pmol µL^{-1}	5 µM
7 µL	T4 DNA Ligase Buffer	10x	1x
Filled to 70 µL (56 µL)	Ultrapure water	–	–

Tab. 2.29. Thermocycler protocol for annealing of complementary oligonucleotides

Step	Time	Temperature	
		Spacer	Signal peptides, RBS
Denaturation	5 min	90 °C	
Annealing 1 (T_M)	20 min	56.2 °C	85 °C

Step	Time	Temperature	
		Spacer	Signal peptides, RBS
Annealing 2 (T_M–5)	120 min	51.2 °C	80 °C
Cooling	–0.2 °C min^{-1}	to 24 °C	

2.3.10. Ligation

DNA fragments with blunt ends or compatible cohesive ends were ligated with the T4 DNA Ligase by incubating at room temperature for 15–65 min or overnight at 16 °C for improved ligation efficiencies (reaction mix in Tab. 2.30). Prior to *E. coli* transformation, the ligase was heat-inactivated at 65 °C for 10 min.

Tab. 2.30. Reaction mix for ligation

Volume for ligation of:			Component
pPBEx2 after DNA blunting	pCMEx[4-11] and pCMEx[4-11]-[SP]	pPBEx2-*phoD^{Cg}-gfp*	
15 µL (= 84 ng)	1.5 µL	18 µL	Backbone DNA
–	7 µL	0.5 µL	Insert DNA
2 µL	1 µL	2.5 µL	10x T4 DNA Ligase Buffer
1 µL	0.5 µL	1.25 µL	T4 DNA Ligase
Filled to 20 µL	Filled to 10 µL	Filled to 25 µL	Ultrapure water

2.3.11. Golden Gate assembly

The gene of interest was cloned into pCMEx[4-12]-[SP] by Golden Gate assembly. This technique uses type IIS restriction enzymes such as BsaI that cut outside their recognition site. The plasmids containing the genes of interest and the backbone were designed to have compatible cohesive ends. After ligation, no recognition site is present in the final plasmid, thus digestion and ligation can be performed in a one-pot setup. The reaction mix is listed in Tab. 2.31 and the thermocycler protocol in Tab. 2.32. For automated Golden Gate assembly on the Opentrons OT-2 with the Thermocycler Module, the backbone plasmids were provided in a PCR plate and the remaining reaction mix provided in a 12-column plate was automatically added [186].

Tab. 2.31. Reaction mix for Golden Gate assembly

Volume	Component
3 µL	200 ng µL^{-1} backbone plasmid (pCMEx[4-12]-[SP])
1 µL	200 ng µL^{-1} plasmid with gene of interest (pUC57-[Cutinase/LCC/PE-H]-Amp)
2 µL	10x T4 DNA Ligase Buffer
0.5 µL	T4 DNA Ligase
0.5 µL	BsaI-HF® v2
Filled to 20 µL	Ultrapure water

Tab. 2.32. Thermocycler protocol for Golden Gate assembly

Cycles	Step	Temperature	Time
30	Enzymes active	37 °C	1 min
	Only ligase active	16 °C	5 min
1	Enzymes active	37 °C	10 min
1	Heat-inactivation	80 °C	20 min

2.3.12. Capillary electrophoresis

DNA samples with heat-inactivated enzymes were appropriately diluted with ultrapure water before analysis with the MCE-202 MultiNA and the DNA-12000 Reagent Kit. Capillary electrophoresis was done according to manufacturer's instructions with the 1 kb Plus DNA Ladder for size comparison. Results were analyzed using the MultiNA control software.

2.3.13. DNA sequencing

Purified DNA plasmids were sequenced by Eurofins Genomics (Germany) with the respective sequencing oligonucleotides (Tab. 2.8). The obtained DNA sequences were analyzed with the SnapGene® software.

2.4. Heterologous protein production and purification

2.4.1. Low-throughput heterologous protein secretion

C. glutamicum pre-cultivation in shake flasks

10 mL BHI were inoculated with 1 mL cryo-conserved *C. glutamicum* pPBEx2-NprE-Cutinase-GFP11 or pPBEx2-Pel-Cutinase-GFP11. After incubation for 6 h at 30 °C and 250 rpm, 100 µL were used to inoculate a second pre-culture with fresh 10 mL CGXII with 10% (v/v) BHI and incubated for further 16 h.

C. glutamicum BioLector® cultivation

For main cultures in a BioLector® Pro integrated into a Tecan Freedom EVO® robotic platform (subsection 2.1.4), 800 µL CGXII were inoculated from the second pre-culture to an $OD_{600\,nm}$ of 0.2 in a FlowerPlate® with optodes. Standard cultivation conditions were 30 °C, 1 400 rpm and $\geq$85% relative humidity with measurement of backscatter, pH and DO every 13 min. Cutinase-GFP11 expression was induced individually in each well by addition of IPTG to a final concentration of 100 µM at a backscatter value corresponding to 4 g L^{-1} CDW. Cells were harvested after 4 h for 6 min at 3 756 x*g* and 4 °C and supernatant was stored in a 1 mL DWP on a cooling carrier. After all cultivations were finished, an automated cutinase activity and split GFP assay was conducted.

The pCMEx-based cutinase-GFP11 secretion with *C. glutamicum* ATCC 13032 K9 biosensor cells was done in the Freudl lab (Forschungszentrum Jülich GmbH) essentially as described elsewhere [75] with media supplemented with 25 µg mL^{-1} kanamycin. Briefly, biosensor cells were grown in BHIS and 50 µL were transferred to a FlowerPlate® with wells containing 800 µL CGXII with 10 g L^{-1} glucose. The plate was covered with gas-permeable sealing foil and incubated in a BioLector® I at 30 °C, 1 200 rpm and $\geq$85% relative humidity with online measurement of backscatter and eYFP fluorescence. After overnight cultivation, the $OD_{600\,nm}$ was measured and fresh medium in a new FlowerPlate® was inoculated to an $OD_{600\,nm}$ of 1. After 4 h cultivation in the BioLector®, gene expression was induced by addition of IPTG to a final concentration of 250 µM and cultivation was sustained for another 20 h.

Specific fluorescence of the biosensor cells was calculated by dividing the eYFP fluorescence by the corresponding backscatter.

C. glutamicum cultivation in shake flasks

50 mL CGXII in baffled flasks were inoculated with 300 µL of the second pre-culture. IPTG was added at an $OD_{600\,nm}$ of 0.3–0.4 to a final concentration of 100 µM. Cells were harvested in 50 mL centrifugation tubes after 6 h of cutinase-GFP11 expression for 10 min at 4 000 x*g* and 4 °C. Supernatant was stored at –20 °C until use. If cutinase-GFP11 expression lasted for 16 h, the first pre-culture was inoculated with 50 µL cryo-conserved *C. glutamicum*, incubated for 16 h. The second pre-culture was cultivated for 6 h and 500 µL were used for inoculation of main cultures. Cutinase-GFP11 expression in shake flasks was done for 16 h unless stated otherwise.

2.4.2. *B. subtilis* cultivation

In the Knapp lab (Heinrich Heine University Düsseldorf/Forschungszentrum Jülich GmbH), secretion studies with *B. subtilis* were carried out. A 10 mL overnight culture was inoculated with a single colony from transformation and incubated at 37 °C. 10 mL LB were inoculated from the previous culture to an $OD_{580\,nm}$ of 0.05 and cultivated at 37 °C and 130 rpm for 6 h. Cutinase-GFP11 was expressed under control of the strong constitutive P_{HpaII} promoter [188].

2.4.3. High-throughput protein secretion screening

For automated secretion screening, the robotic workflow in subsection 2.4.1 was extended to automated pre-culture handling. 12 cryo-conserved cultures in cryogenic vials as well as CGXII medium in a trough were placed on deck of the robotic platform. For pre-cultures, 780 µL CGXII were transferred to 12 wells of a FlowerPlate® with optodes covered with a sealing foil for automation. 20 µL of each cryo-conserved culture were used to inoculate one of the pre-culture wells in the outer columns of the plate. As soon as a pre-culture exceeded a certain device-dependent backscatter threshold in the exponential phase, the three adjacent wells in the same row

were filled with 780 µL CGXII for main cultures and each inoculated with 20 µL of the respective pre-culture. Target gene expression was induced in the early exponential phase triggered by a device-dependant backscatter signal by addition of IPTG to a final concentration of 200 µM unless otherwise indicated. Cell harvest was conducted as in subsection 2.4.1.

As cryo-conserved PETase secretion strains in MTPs had a lower $OD_{600\,nm}$ than those in cryogenic vials, 40 µL were used to inoculate 760 µL CGXII for pre-cultures. Remaining cryo-conserved cultures in the MTP were discarded. Deviating from above, target gene expression in main cultures was induced with IPTG added to a final concentration of 500 µM. In addition to the cultivation and screening workflow with up to 12 different strains, a similar workflow with one main culture per pre-culture was established to compare up to 24 different strains. A scheme of all different workflows including positions of supernatants on assay MTPs is depicted in Fig. 2.4.

2.4.4. Protein secretion in laboratory-scale bioreactors

Protein secretion in a laboratory-scale batch bioreactor setup as described in subsection 2.1.2 and subsequent cutinase activity assays with supernatant samples was done by Matthias Moch with the support of Petra Geilenkirchen (Oldiges lab, Forschungszentrum Jülich GmbH).

50 mL CGXII medium in a baffled flask was inoculated from a cryo-conserved *C. glutamicum* PETase secretion strain and incubated for 16 h at 30 °C and 300 rpm with online biomass monitoring (SFR vario, PreSense Precision Sensing). Cells were harvested in the late exponential growth phase by centrifugation with 9 283 x*g* for 5 min at 4 °C. Cells were resuspended in 0.9% (w/v) NaCl and used for inoculation of 1 L CGXII in a bioreactor to an $OD_{600\,nm}$ of 0.3. The CGXII medium for bioreactor cultivations with 20 g L^{-1} glucose does not contain MOPS and urea, and the kanamycin content was changed to 50 µg mL^{-1}. An appropriate amount of Antifoam 204 (Sigma-Aldrich, USA) was added to prevent foaming. Cells were incubated in batch mode at 30 °C, and the DO was kept $\geq$ 40% with a constant air flow rate q_{in} = 1 vvm by adjusting the agitation speed n = 400–1 500 rpm. The pH was set to 7 by addition of 18% (w/w) NH_4OH and 30% (w/w) H_3PO_4. PETase gene expression was induced around $OD_{600\,nm}$ = 1 by adding IPTG to a final concentration of 200 µM.

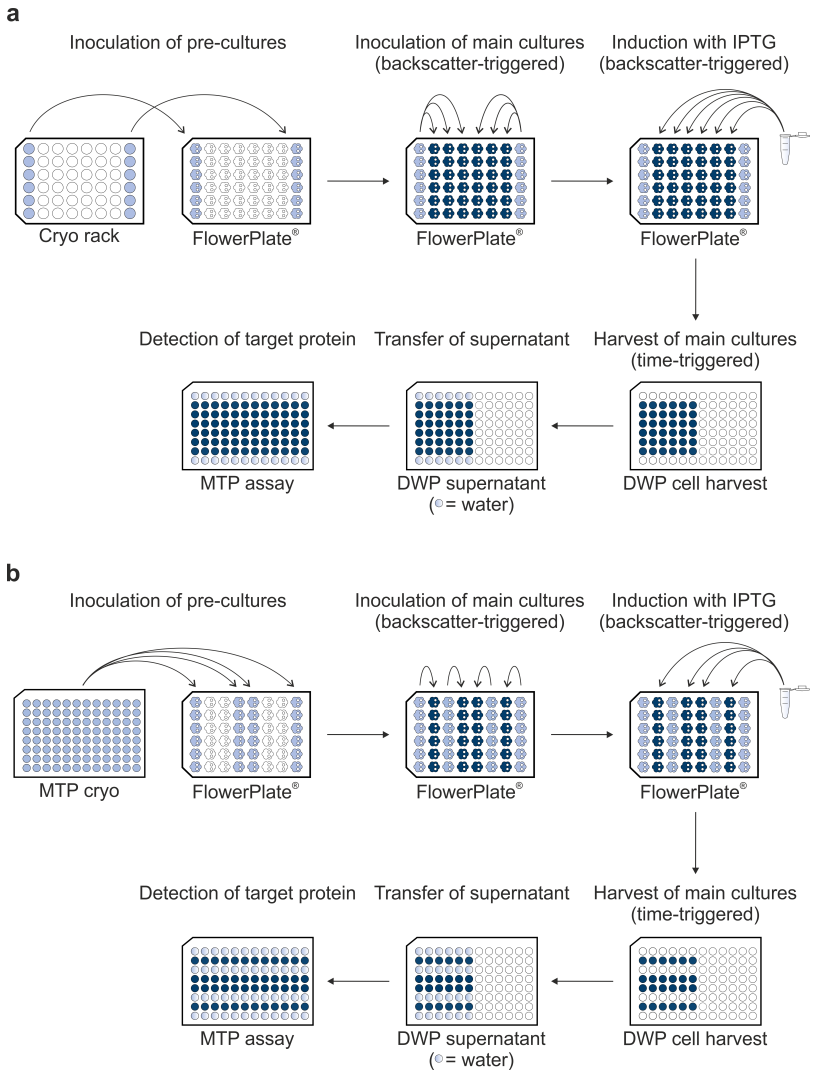

Fig. 2.4. Schematic workflows for cultivation and screening. For comparison of up to 12 different strains, the pre-culture wells in the outer columns of a FlowerPlate® are automatically filled with medium and inoculated from thawed cryo-conserved cultures in vials or in a MTP. Triggered by the individual backscatter signal of a pre-culture in the exponential phase, three main culture wells are filled with medium and inoculated by the respective pre-culture. If a main culture exceeds a specific backscatter threshold indicating the early exponential phase, cells are induced with IPTG and harvested in a DWP after 4 h of target protein production. The supernatant is stored in a DWP on the cooled position until all cultivations are finished. Target proteins in the supernatant samples are detected by the activity (and split GFP) assay in technical duplicates in a MTPs (a, adapted from [175]). For comparison of up to 24 different strains that are stored as cryo-conserved cultures in a MTP, the workflow was changed to inoculation of one main culture per pre-culture (b, adapted from [181])

Further sterile Antifoam 204 (Sigma-Aldrich, USA) was added if needed. Samples for measuring the $OD_{600\,nm}$, CDW and activity were taken.

2.4.5. Fed-batch cultivation of *C. glutamicum* K9 biosensor strains

C. glutamicum K9 biosensor cells were grown in 50 mL CGXII medium at 30 °C and 300 rpm. Cells were harvested in the late exponential phase by centrifugation in 50 mL tubes (5 min, 9 283 x*g*, 4 °C) and resuspended in 0.9% (w/v) NaCl. The fed-batch cultivation was conducted in a MTP-MF32-BOH 1 FlowerPlate® covered with sealing foil for microfluidic MTP in a BioLector® Pro. Cultivation conditions were 30 °C, 1 400 rpm, $\geq$30% headspace oxygen and $\geq$85% relative humidity. Biomass and pH were measured every 13 min. 800 µL CGXII medium containing 22 mg L^{-1} PCA, 30 µg mL^{-1} kanamycin, 5 g L^{-1} glucose and no urea were inoculated with the corresponding pre-cultures to an $OD_{600\,nm}$ of 0.5. Starting after 10 h, 400 g L^{-1} glucose were fed with 0.16 µL pump volume and a constant feed rate of 5.22 µL h^{-1} into fed-batch cultivation wells. After one hour cultivation time, the pH in all wells was one-sided adjusted to 6.8 with 3 M KOH with medium PI setting and 0.3 µL pump volume. Cutinase gene expression was induced by adding IPTG to a final concentration of 250 µM after 8 h. Cells were harvested after around 25 h and the supernatants were stored at 4 °C until the end of the cultivation before analysis of cutinase content and activity by the Freudl lab (Forschungszentrum Jülich GmbH).

2.4.6. GFP1-10 production in flasks

GFP1-10 was produced intracellulary in *E. coli* BL21(DE3) and purified from the inclusion body fraction. 10 mL LB in baffled flasks were inoculated with a single colony from agar plate and cultivated at 37 °C and 250 rpm. 50 mL or 100 mL LB in baffled flasks were inoculated to an $OD_{580\,nm}$ of 0.05 and cultivated at 37 °C and 250 rpm. GFP1-10 gene expression was induced by adding IPTG to a final concentration of 200 µM. Cells were harvested after another 5 h by centrifugation in 50 mL tubes (5 min, 9 283 x*g*, 4 °C). The supernatant was discarded and the pellets were stored at –20 °C before cell disruption and GFP1-10 purification (subsection 2.4.8).

2.4.7. GFP1-10 production to laboratory-scale bioreactors

GFP1-10 production in a laboratory-scale bioreactor setup as described in subsection 2.1.2 was done with LB or DeLisa medium and compared to production in 50 mL of the same medium in baffled flasks.

A first pre-culture was done as described in subsection 2.4.6. Depending on the main culture medium, a second pre-culture in 100 mL LB or DeLisa medium was incubated under the same conditions as before. In batch experiments, the first pre-culture was incubated for 4 h and 1 mL was used to inoculate a second pre-culture that was incubated for another 16 h. For fed-batch experiments, the first pre-culture was incubated for about 10 h and a second pre-culture inoculated with 300 µL of the first pre-culture was then incubated for another 6 h. Main cultures were inoculated to an $OD_{580\,nm}$ of 0.05 and laboratory-scale bioreactors were operated in batch or fed-batch mode.

In batch-mode, 1 L LB or DeLisa medium was incubated at 37 °C with an initial agitation speed of n_0 = 400 rpm and air flow rate of $q_{in,\,0}$ = 0.1 vvm. The pH was adjusted to 6.7 with 1 M sodium hydroxide and 1 M hydrochloric acid. The DO was kept $\geq$ 30% by adjusting the agitation speed n = 400–1 200 rpm and air flow rate q_{in} = 0.10–2 vvm. For comparison to bioreactor production in batch-mode, 50 mL main cultures in baffled flasks were incubated with the same settings of the pre-cultures and GFP1-10 gene expression was induced as in the bioreactor by adding IPTG to a final concentration of 200 µM.

Fed-batch experiments with an initial volume of 800 mL DeLisa medium with 20 g L^{-1} glucose comprised a batch phase conducted the same way as batch fermentations. Deviating from batch fermentations, 30% (v/v) phosphoric acid and ammonium hydroxide were used for pH control. At the end of the batch phase with DO $\geq$ 60%, 500 g L^{-1} glucose and inducer solution (10 mM IPTG or 100 g L^{-1} lactose) were constantly fed with 30 mL h^{-1} pump rate. Feeding of inducer solution was stopped once a final concentration of 1 mM IPTG or 10 g L^{-1} lactose were reached. The glucose pump was operated under on-off control with limits set to 10–35% DO and sterile Antifoam 204 (Sigma-Aldrich, USA) was added if necessary. Cells were harvested for GFP1-10 purification by centrifugation in 50 mL tubes (5 min, 9 283 x*g*, 4 °C), the supernatant was discarded and the pellets were stored at –20 °C until use.

2.4.8. GFP1-10 purification from inclusion bodies

Cells after GFP1-10 production in inclusion bodies were resuspended in TNG buffer (Tab. 2.33) to an $OD_{580\,nm}$ of 20 before cell disruption with a French press (15 000 psi, 4x). After centrifugation for 10 min at 4 °C and 4 000 x*g*, pellets containing GFP1-10 inclusion bodies were washed three times by resuspension in TNG buffer and subsequent centrifugation. As described by Santos-Aberturas et al. [119], inclusion bodies were completely unfolded by resuspending them in 1 mL urea each 75 mg pellet. After centrifugation for 20 min at 4 000 x*g* and 4 °C, 400 µL supernatant each were mixed with 10 mL TNG buffer for GFP1-10 refolding. The solutions were stored at –20 °C until use in split GFP assay.

Tab. 2.33. TNG buffer for cell disruption and GFP1-10 purification

Concentration	Component
100 mM	Tris-HCl pH 7.4
100 mM	NaCl
10% (v/v)	Glycerol

2.5. Analytical methods

2.5.1. Microscopy

Samples from GFP1-10 production were analyzed by microscopy with 100x oil immersion objective to detect inclusion body formation.

2.5.2. pH

The offline pH was measured with an electrode calibrated by two points (pH 4 and pH 7).

2.5.3. Split GFP assay

For the final GFP1-10 detector solution, additional 10 mL TNG buffer (Tab. 2.33) were added and 180 µL detector solution were mixed with 20 µL supernatant containing GFP11-tagged target proteins in a black MTP with clear bottom. Self-assembly of holo-GFP was measured in a microplate reader at an excitation wavelength of 485 nm and an emission wavelength of 535 nm over a time period of at least 13 h. Between measurements, the MTP was shaken inside the microplate reader (linear mode, 887 rpm) at 20 °C unless stated otherwise.

The split GFP assay was additionally conducted by cooperation partners with the following modifications. Both added 10 mM EDTA (pH 8) the final GFP1-10 detector solution. In the Knapp lab (Heinrich Heine University Düsseldorf/Forschungszentrum Jülich GmbH), the MTP was covered with the respective lid and incubated for 16 h before fluorescence measurement with a SpectraMax 250 (Molecular devices, Germany). Fluorescence emission was measured from 505–550 nm in 5 nm steps using an appropriate gain factor with biological and technical triplicates. The GFP-specific emission maximum at 510 nm was used for subsequent calculations. In the Freudl lab (Forschungszentrum Jülich GmbH), the MTP was covered with a gas-permeable membrane and incubated for 24 h at 20 °C under gentle agitation. Holo-GFP emission was measured at 510 nm using an Infinite M1000 Pro (Tecan, Switzerland). For each cultivated recombinant strain, at least two independent clones were tested and assay measurements were performed in duplicates.

2.5.4. Cutinase activity assay

Activity of GFP11-tagged cutinase and PETases in supernatant samples was determined spectrophotometrically by degradation of 4NPP as substrate analogue [90] as described by Hemmerich et al. [147]. Briefly, 9 parts reaction buffer (Tab. 2.34) were mixed with 1 part 3 g L^{-1} 4NPP in 2-propanol. 200 µL were filled into MTP wells and pre-warmed to 37 °C. Supernatant samples were appropriately diluted with 50 mM potassium phosphate buffer pH 8 (pPBEx-based cutinase secretion: 500x, pCMEx-based cutinase secretion: 160x, pCMEx-based PETase secretion: 72x for BioLector® samples and 12x for bioreactor samples). 40 µL diluted supernatant were pipetted into two wells filled with the reaction mix for technical duplicates. 4NP formation was measured at 410 nm and 37 °C for 40 min in a microplate reader.

40 µL 0–2.3 mM 4NP were mixed with 200 µL reaction mix in triplicates and absorption was measured to convert absorption into product concentration. Enzymatic activities were calculated using Eq 2.1 with enzymatic activity EA in U = µmol min^{-1} or in relation to the assay volume in U mL^{-1}, absorption A_{410} in a.u., slope of the 4NP standard m_{standard} in a.u. mM^{-1} and the unitless supernatant dilution factor DF. By default, standard deviations were calculated from replicates. If the 95% confidence interval calculated with t-values was displayed instead, this is marked accordingly.

$$\text{EA} = \Delta A_{410} \cdot \frac{1}{m_{\text{standard}}} \cdot \text{DF} \tag{2.1}$$

The cutinase activity assay was additionally conducted by cooperation partners with the following modifications. Supernatant samples were appropriately diluted in 66.5 mM Sørensen buffer pH 8 and this buffer was also used instead of potassium phosphate buffer pH 8 in the reaction buffer. In the Knapp lab (Heinrich Heine University Düsseldorf/Forschungszentrum Jülich GmbH), 10 µL diluted *B. subtilis* supernatant were filled into wells of a MTP and 20 µL *C. glutamicum* supernatant in the Freudl lab (Forschungszentrum Jülich GmbH). Reaction buffer and substrate were mixed and added to a final well volume of 200 µL. The absorption of replicates as described for split GFP assay was measured for 15 min with 1 min or 30 s intervals with supernatant samples from *C. glutamicum* or *B. subtilis*, respectively. The cutinase activity was calculated from the linear slope using a molar extinction coefficient of 15 000 M^{-1} cm^{-1}.

Tab. 2.34. Reaction buffer for cutinase activity assay

Concentration	Component
2.3 g L^{-1}	Na-desoxycholate
1.1 g L^{-1}	Gum arabic
50 mM	Potassium phosphate buffer pH 8

2.5.5. Process model and Thompson sampling

The process model development, implementation of Thompson sampling as a decision policy and the application in evaluating the PETase secretion performance originate from a cooperation and are solely the work of L. M. Helleckes (Forschungszentrum Jülich GmbH) published in Helleckes et al. [181].

A Bayesian hierarchical process model was developed with the PyMC Python package [171], and prior distributions were chosen for each parameter. To convert 4NP product absorbance into concentration, a calibration model assuming a linear relationship between absorbance and concentration and a measurement noise following a Student's t-distribution was fitted using the calibr8 Python package [164] (refer to Fig. A.11 for a visualization). The measured 4NP product absorbance was then evaluated against the modeled concentration using a customized likelihood. It was assumed that the product concentration follows a first order mass action law during the activity assay as shown in Eq 2.2 with the product concentration P_t at time t, S_0 as the initial substrate concentration and k_{assay} as the rate constant.

$$P_t = S_0 \cdot \left(1 - e^{(-k_{\text{assay}} \cdot t)}\right), \tag{2.2}$$

An initial absorbance offset was observed in the activity assay, that was modeled by `absorbance_intercept`. From each activity assay sample, the parameter k_{assay} was observed. However, the KPI used for the secretion performance ranking is the actual rate k_{strain} of each PETase-secreting strain. The k_{strain} is impacted by several biological and technical effects such as the position in the assay MTP (`column_effect`) or batch effects between runs. These batch effects can be caused at different stages of the screening, during the cultivation, e.g., by quality differences of the cryo-conserved cultures or during the assay preparation, e.g., due to pipetting errors. A visualization of the process model is depicted in Fig. 2.5, a mathematical notation of the model is shown in the appendix (see Eq A.1) and the code for the process model can be found on the accompanying GitHub repository [189].

Markov chain Monte Carlo sampling was applied to obtain posterior probability distributions by using the No-U-Turn sampler [190] in PyMC. ArviZ was used for convergence checks and inspection of the traces. The posterior probabilities after each cultivation and screening round were used for Thompson sampling. By parallel Thompson sampling [191] using the `sample_batch` function from the pyrff package [192], a batch of strain replicates for the following round was drawn and randomly assigned to positions in the FlowerPlate® pre-culture wells. The process model was re-run after each round with the obtained process data to obtain posterior probabilities of the KPIs for the next cultivation and screening round.

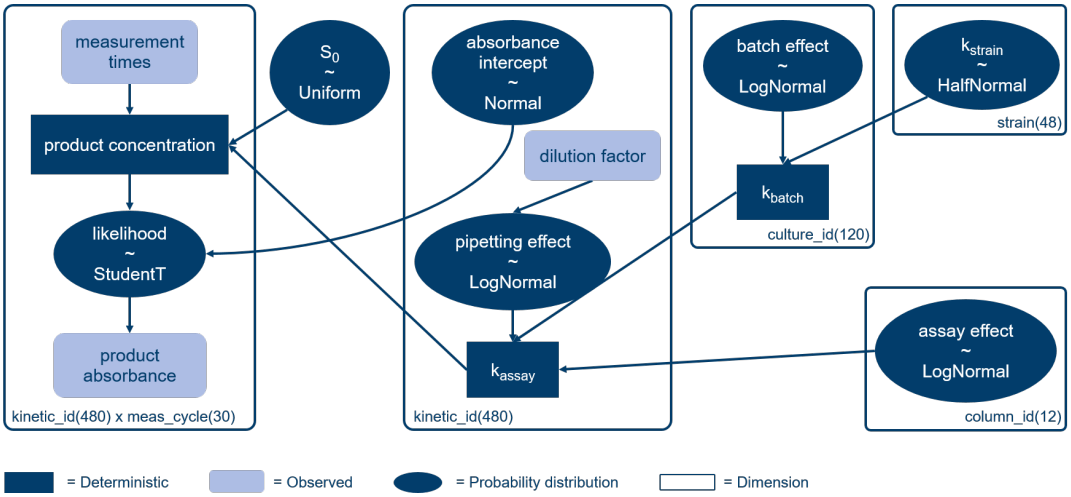

Fig. 2.5. Graphical representation of the process model developed by L. M. Helleckes. The rate constant k_{strain} (upper right) is used as a KPI for PETase secretion performance ranking of *C. glutamicum* strains [181]

2.5.6. Protein precipitation with TCA

Proteins in BioLector® cultivation supernatants of *C. glutamicum* were precipitated with trichloroacetic acid (TCA) as described by Bakkes et al. [8]. Briefly, 500 µL supernatant were mixed with 60 µL 100% (w/v) TCA. After incubation in a ThermoMixer® at 4 °C and 600 rpm for at least 1 h, samples were centrifuged for 30 min at 20 000 x*g* and 4 °C. Precipitated proteins were resuspended in 100 µL 1x Laemmli sample buffer and the pH was adjusted by adding 12 µL 1 M Tris solution for analysis by sodium dodecyl sulfate polyacrylamide gel electrophoresis (SDS-PAGE).

2.5.7. SDS-PAGE

Samples for SDS-PAGE in 1x Laemmli sample buffer were boiled at 99 °C for 5 min and stored at –20 °C until use. 10 µL samples from TCA precipitation or from final detector solution were analyzed on a 4–12% Criterion™ XT Bis-Tris Protein Gel with 7 µL PageRuler™ Prestained Protein Ladder (10 to 180 kDa) for size comparison. Proteins were separated at 200 V with NuPAGE™ MES SDS Running Buffer and stained with SimplyBlue™ SafeStain according to manufacturer's instructions.

2.5.8. Sugar quantification by HPLC

Glucose and lactose concentration in fermentation samples were measured by high-performance liquid chromatography (HPLC) with an organic acid resin at 25 °C. Cultivation supernatant that was stored at –20 °C until use was 10x diluted and sterile filtered. Standard solutions of 0.1–20 g L^{-1} glucose and lactose were freshly prepared. 20 µL sample or standard were injected and sugars were detected with a refractometer. Elution was done with 0.1 M sulfuric acid and a flow rate of 0.6 mL min^{-1}.

3. Results and discussion

3.1. Split GFP assay and scaling production of GFP1-10

In this chapter, the intracellular production of β-sheets 1-10 of the GFP in inclusion bodies in *E. coli* and the application of GFP1-10 in split GFP assay for detection of secreted proteins was comprehensively studied. GFP1-10 production in flasks in complex and defined medium was compared to production in laboratory-scale bioreactors resulting in a standardized fed-batch process providing high quantities of GFP1-10. After cell disruption and purification, GFP1-10 was applied in automated split GFP assays to detect cutinase-GFP11 secreted by *C. glutamicum* with the two *B. subtilis* signal peptides NprE and Pel. The impact of environmental conditions, such as pH and temperature on the split GFP assay was investigated. This chapter is based on data collected during student projects III–V and parts were published in conference posters I & II, conference talks I & III and publication I.

Author's contributions:
C. Müller established the automated cutinase activity assay on the screening platform, did the supervision of the student projects and wrote the publication. She contributed to the experimental data and analysis for long-term storage of GFP1-10 detector solution and the comparison of split GFP and activity assay results with supernatant containing cutinase-GFP11 diluted to different degrees. V. Waffenschmidt established the split GFP assay on the screening platform and contributed to the cultivation workflow. P. Lenz provided plasmids and protocols for split GFP assay and P. J. Bakkes provided *C. glutamicum* strains for pPBEx-based cutinase-GFP11 secretion. C. L. Igwe did all bioreactor fermentations as well as the comparison to flask-based production. She established the purification based on cell disruption by French press and investigated the environmental impact on the split GFP assay. M. Oldiges contributed to the study design and the writing of the manuscript of publication I. W. Wiechert helped to finalize the publication.

The split GFP assay is based on the self-assembly of GFP1-10 and GFP11. For *in vitro* assays, a protein is tagged with the short amino acid sequence of GFP11 (GFP11-tag) and GFP1-10 is usually produced intracellularly in *E. coli* in inclusion

bodies. After cell disruption, the GFP1-10 detector protein can be purified and refolded from the inclusion body fraction with high purity [113, 118] (see Fig. A.1).

3.1.1. Scaling from flask to laboratory-scale bioreactor

Production of GFP1-10 with *E. coli* BL21(DE3) pET22b-sfGFP1-10 in inclusion bodies was done in 50 mL LB in baffled flasks and in 1 L LB in STRs as batch processes. Besides LB, DeLisa defined medium [184] was tested, since it provides improved process control in the bioreactor at lower cost and was successfully used for GFP production in inclusion bodies with *E. coli* as host [193].

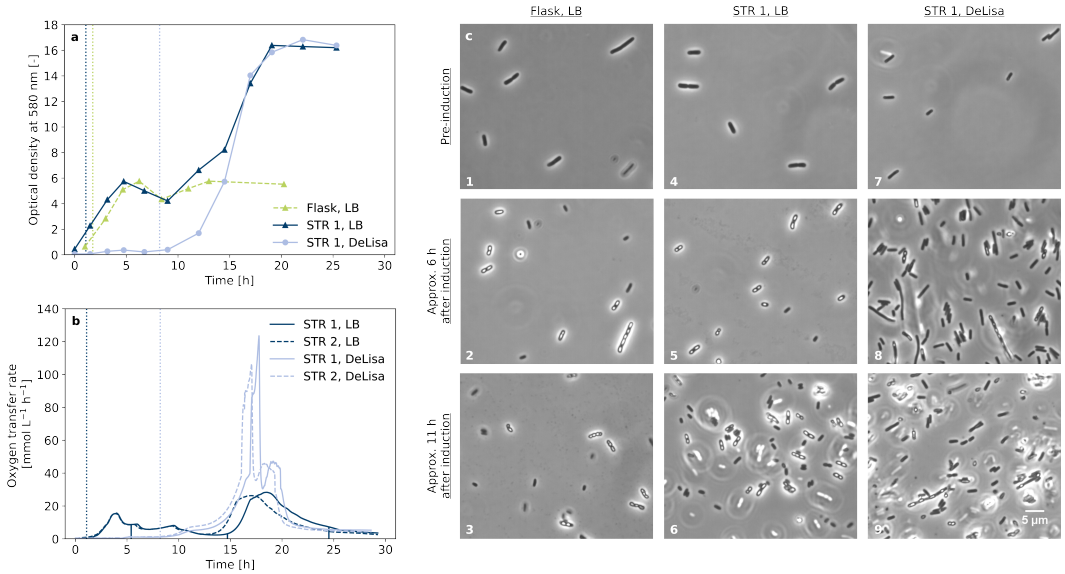

Fig. 3.1. Batch-production of GFP1-10 in shake flasks and laboratory-scale bioreactors. Dotted lines indicate induction with IPTG to a final concentration of 200 µM. (a) $OD_{580\,nm}$ during cultivation of *E. coli* BL21(DE3) pET22b-sfGFP1-10 in shake flask or STR with LB or DeLisa medium. (b) Oxygen transfer rate in STRs during batch fermentation from two biological replicates in LB and DeLisa medium. (c) Microscopic images taken during cultivation at different time points from shake flask with LB (1–3) and STRs with LB (4–6) or with DeLisa medium (7–9). Inclusion bodies are the bright spots mainly located at the cell poles. Only $OD_{580\,nm}$ and microscope images of STR 1 are shown due to the good comparability of the biological replicates from STRs. Modified from [89]

In LB shake flask culture low ODs of about 6 were reached, while OD in batch bioreactor cultures with LB and DeLisa medium was more than twice as high with approximately 17 (Fig. 3.1a). In LB medium growth started immediately, while there is a lag-phase of about 8 h for the DeLisa defined medium which is followed by exponential growth until OD 17. Although both media exhibit different growth rates, final OD

for both media is reached after process time of 18 h. The oxygen transfer rate was calculated from off-gas analytics for the two biological replicates in LB and DeLisa medium (Fig. 3.1b) showing good reproducibility between biological replicates with only a slight time offset visible in the oxygen uptake rate. Maximum oxygen transfer rates with DeLisa medium were above 100 mmol L^{-1} h^{-1} and thus significantly higher than with LB medium which is a consequence of faster growth in this phase. Inclusion body formation was monitored by microscopy (Fig. 3.1c). In samples before induction, no inclusion bodies were visible under the microscope. For cultivations with LB medium more than 50% of the cells seem to contain one or more inclusion bodies 6 h after induction with IPTG. With DeLisa medium, slightly less cells containing inclusion bodies are visible. After 11 h, the number of cells with inclusion bodies dropped, indicating that the harvest time might be a relevant factor.

In terms of batch process time and final biomass concentration, there was no difference between LB and DeLisa medium. Thus, it was decided to select DeLisa medium for the fed-batch process development although slightly reduced inclusion body formation, since it showed higher growth rate with better process control in the bioreactor and reduced media cost.

3.1.2. GFP1-10 production in bioreactors in fed-batch mode

After the batch process was successfully transferred from shake flasks to STRs, glucose feeding was tested to further increase cell densities with DeLisa defined medium. Fed-batch strategy was based on a triggered glucose feed control using the online signal of DO with on-off setting for the glucose feed pump. Hence, glucose feed pump was activated with a constant feed rate if increased DO indicates substrate depletion and stops if the DO is below a threshold level. With the first start of the glucose feed, the inducer was also constantly fed into the reactor until final inducer concentrations of 1 mM IPTG or 10 g L^{-1} lactose were reached. Both inducers were compared for induction of GFP1-10 expression (Fig. 3.2).

After an initial batch phase the raise of DO above 60% indicated total consumption of batch glucose after 13.5 h and the fed-batch phase was initiated by starting glucose feed control. The added glucose is consumed by the bacteria which increases the oxygen consumption and decreases the DO content, until the glucose feeding

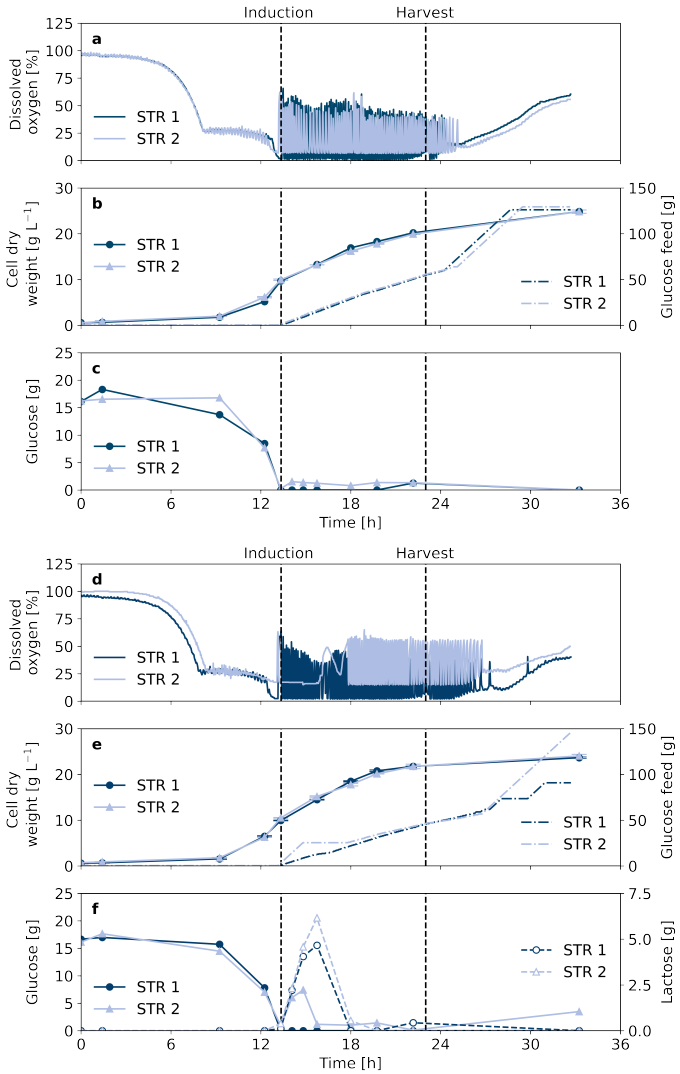

Fig. 3.2. Fed-batch fermentation for production of GFP1-10. GFP1-10 expression in *E. coli* BL21(DE3) pET22b-sfGFP1-10 was induced by constant feeding of IPTG (a–c) or lactose (d–f) until calculated inducer concentrations of 1 mM IPTG or 10 g/L lactose were reached in the bioreactor. Feeding of inducer solutions was started at the end of the batch phase triggered by the DO signal. Constant glucose feeding was started in parallel but with on-off settings triggered by DO signal. DO and glucose feed were each measured for two biological replicates during fed-batch fermentation and samples were taken for CDW measurement in technical triplicates and HPLC analysis of sugars. Cell samples were harvested after 23 h for purification of GFP1-10 detector protein. Modified from [89]

is stopped below 10% and started again above 35% DO. This leads to a characteristic fluctuation pattern of DO (Fig. 3.2a, d). Analysis of supernatant samples showed glucose concentrations close to or at limiting conditions throughout the fed-batch phase (Fig. 3.2c, f), leading to a final CDW around 25 g L^{-1} independent of the induction with IPTG or lactose for each of the two biological replicate cultivations (Fig. 3.2b, e). In case of lactose as an inducer, the analysis of supernatant samples shows a lactose increase during the first 3.5 h after start of induction in the fed-batch phase followed by rapid decrease until depletion after approximately 4 h for both biological replicates (Fig. 3.2f). Although the CDW growth profile of both replicates with lactose induction are almost identical, the DO shows a difference. For STR 2 a slight overfeeding in the first 2.5 h of the fed-batch is observed resulting in an intermediary glucose accumulation of approximately 7 g L^{-1}. After 13.5 h of cultivation the DO-triggered feed was initiated. However, the DO concentration decreased to 14–16% only, so that the glucose feed remained active, which resulted to non-limiting glucose levels during the first 2.5 h. This effect was not present for the STR 1 cultivation and could have resulted from a deviation of the DO sensor signal. Consequently, characteristic oscillating DO profile due to intermittent glucose dosing was observed after glucose and lactose depletion approximately 4 h after feed start.

Cells from all cultivations were disrupted by French press and GFP1-10 was purified from the inclusion body fractions following the preparation protocol. Refolded GFP1-10 was applied for split GFP assay with a reference supernatant containing cutinase-GFP11 from *C. glutamicum* pPBEx2-NprE-Cutinase-GFP11 (Fig. 3.3). Saturation in fluorescence intensity of approximately 650 a.u. was reached after 6.5 h for detector protein solutions from both STRs induced with lactose as well as from STR 2 induced with IPTG. Strikingly, the GFP1-10 detector protein response from STR 1 induced with IPTG showed slower fluorescence increase and lower maximum fluorescence intensity of about 500 a.u. after 13.5 h. Since cultivation data of the biological duplicates induced with IPTG are very similar, the difference in quality of the detector protein solution could have also originated from the multi-step purification protocol.

To conclude, the developed fed-batch process with DO-triggered glucose feeding strategy is a suitable way to increase biomass concentration in order to increase total detector protein formation. Moreover, both induction variants, either by IPTG or lactose, led to satisfactory results in terms of detector protein response in the split

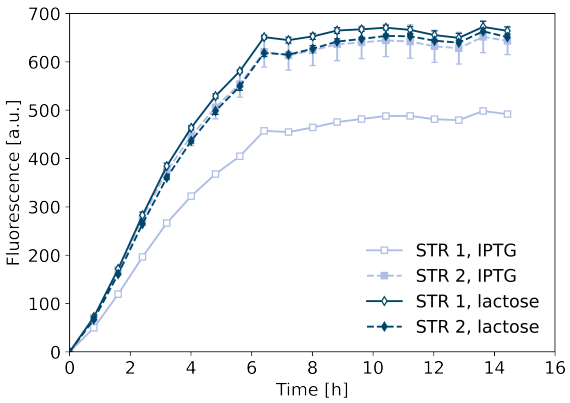

Fig. 3.3. Split GFP assay with GFP1-10 from fed-batch fermentation. Samples of cells containing intracellular GFP1-10 were taken after 23 h of fed-batch fermentation with IPTG or lactose for induction. $OD_{580\,nm}$ were adjusted to 20 and cells were disrupted with a French press. GFP1-10 was purified from the inclusion body fraction and used for detection of cutinase-GFP11 in *C. glutamicum* pPBEx2-NprE-Cutinase-GFP11 supernatant by split GFP assay [89]

GFP assay and could be used for fed-batch production processes. From one fed-batch bioreactor cultivation a total amount of final GFP1-10 detector solution can be obtained sufficient to handle up to 385 screenings in 96-well MTPs.

Since the total amount of inclusion body formation and detector protein quality could be dependent on the harvest time point of the cultivation, this was investigated in a fed-batch bioreactor cultivation with IPTG induction (Fig. 3.4). Samples for GFP1-10 purification were taken 8, 9, 10 and 11 h after the feed start of IPTG. The process and CDW data were very comparable to the previous experiment (Fig. 3.2b), indicating good reproducibility of the fed-batch process (Fig. 3.4a). At all sampling times for GFP1-10 purification, microscopic images show inclusion body formation in the cells (data not shown). GFP1-10 was purified from the inclusion body fraction and used for split GFP assay with supernatant containing cutinase-GFP11 which was obtained from secretory production using *C. glutamicum* pPBEx2-NprE-Cutinase-GFP11 (Fig. 3.4b).

Fluorescence signal profiles were very similar for all harvest time points, except for the detector solution derived 8 h after induction. Here, the maximum fluorescence intensity was about 10% higher. Generally, the harvest time seems to show no critical influence in the overall process and all harvesting times tested are suitable for purification of the GFP1-10 from the inclusion body fraction. Since total biomass concentration is the highest after 10 h, this latest harvesting time point is preferred.

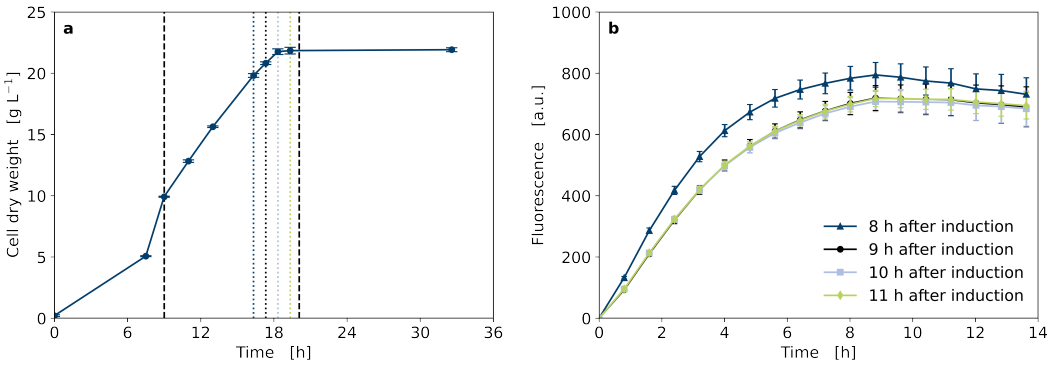

Fig. 3.4. Impact of harvest time in fed-batch GFP1-10 production in DeLisa defined medium on quality of GFP1-10 detector solution. GFP1-10 expression in *E. coli* BL21(DE3) pET22b-sfGFP1-10 was induced with IPTG and samples for preparation of GFP1-10 detector solution were taken 8, 9, 10 and 11 h after induction. (a) CDW during fermentation with dashed black lines indicating start and end of feed-phase and dotted lines indicating sampling times. (b) Split GFP assay with detector solutions derived from fermentation samples 8, 9, 10 and 11 h after induction. Supernatant containing cutinase-GFP11 was mixed with the respective detector solutions and holo-GFP formation was measured at 25 °C. Data is shown as mean of eight technical replicates with standard deviation. Modified from [89]

It is very likely, that fed-batch phase could be prolonged in order to achieve even higher detector protein yield, but this is not covered by experimental data so far.

3.1.3. Storage stability of GFP1-10

By scaling production of GFP1-10 from a shake flask batch to laboratory-scale STR fed-batch process, substantial amounts of detector solution could be obtained from a single bioreactor run sufficient for split assays in approximately 385 96-well MTPs for high-throughput screenings. To test the shelf-life of purified GFP1-10 detector solution, refolded GFP1-10 was stored at –20 °C for 7 months before application in the split GFP assay. This is compared to freshly produced and purified detector solution for detection of cutinase-GFP11 in supernatant of *C. glutamicum* pPBEx2-NprE-Cutinase-GFP11 (Fig. 3.5).

Strikingly, even after 7 months of storage at –20 °C, the GFP1-10 detector solution resulted in fluorescence signals only slightly lower (approximately 10%) than with freshly prepared detector solution. This enables production of a larger stock of GFP1-10 solution with subsequent storage at –20 °C until use for at least 7 months. It is likely, that this period could be extended, but this is not covered by the results obtained so far. In a typical screening application, a set of samples from the same

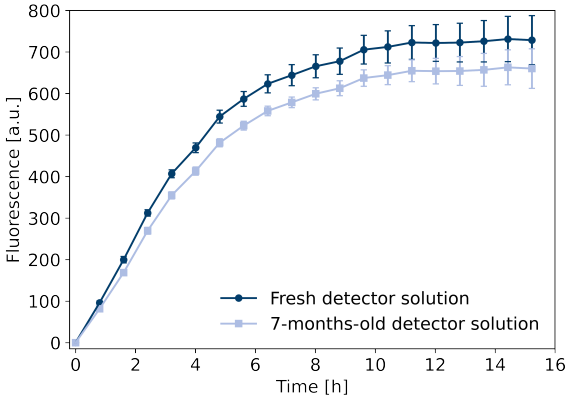

Fig. 3.5. Split GFP assay with stored compared to freshly prepared detector solution. GFP1-10 detector solution was stored for 7 months at –20 °C and used for detection of cutinase-GFP11 in *C. glutamicum* pPBEx2-NprE-Cutinase-GFP11 supernatant. Another detector solution was freshly produced in shake flasks, purified and used as comparison. The split GFP assay was conducted at 25 °C incubation temperature. Modified from [89]

screening run are directly compared, making variances in the detector quality over time negligible. Nevertheless, potential differences in the performance of the detector protein solution in terms of the absolute maximum fluorescence signal of the split GFP assay can be compensated. This could be done by correlation of GFP signal with data from activity assay in form of a calibration function to deduce absolute quantitative information.

3.1.4. Characterization of split GFP assay

The split GFP assay can be used for screening of GFP11-tagged target proteins secreted by *C. glutamicum*. For this, effects of incubation conditions as well as potential influences of supernatant composition must be characterized.

The split GFP assay was performed with culture supernatant of the cutinase-GFP11 secretion strain *C. glutamicum* pPBEx2-NprE-Cutinase-GFP11 and GFP1-10 detector solution in MTPs without shaking for 16 h at different temperatures with eight replicates each (Fig. 3.6). The highest fluorescence signals were measured at 20 °C while incubation at 4 °C resulted in almost half of the fluorescence. It can be speculated that the lower temperature hampered proper assembly of the 11th β-sheet to form the GFP chromophore and that maximum fluorescence seems not be reached after 16 h. Besides, folding and stability of the target protein could also have an

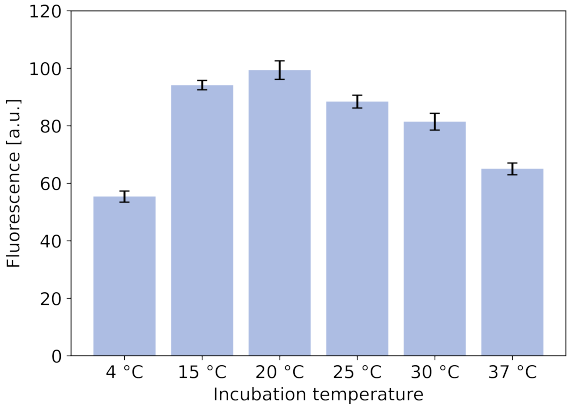

Fig. 3.6. Impact of incubation temperature on holo-GFP formation in split GFP assay. Identical detector solution was mixed with supernatant from *C. glutamicum* pPBEx2-NprE-Cutinase-GFP11 cultivation in shake flask with 6 h of cutinase-GFP11 expression. Fluorescence of eight replicates each were measured after 16 h of incubation at different temperatures without shaking and standard deviations were calculated [89]

impact on the maturation of the chromophore. Temperatures higher than 20 °C also show signal decrease. Nevertheless, for further experiments an assay temperature of 25 °C was chosen, which is slightly above typical laboratory temperature. This shall avoid conflicts with incubation devices that do not have cooling options.

Assay robustness against variations in the composition of *C. glutamicum* supernatant was tested. The pH of *C. glutamicum* pPBEx2-NprE-Cutinase-GFP11 supernatant after cutinase-GFP11 secretion was changed from 7.5 to 7.1–7.8 by adding 10 M HCl or 8 M NaOH before split GFP assay. Moreover, the impact of additional 0–250 mM succinate, lactate, glutamate, ketoglutarate and acetate was investigated. Such compounds comprise typical by-product metabolites in microbial cultivations. Neither for the change of pH value, nor the addition of the metabolites a negative impact on the development of GFP split assay fluorescence signal was observed (Fig. A.2 and Fig. A.3).

To ensure that the split GFP assay is a reliable alternative to enzymatic activity measurements, *C. glutamicum* pPBEx2-NprE-Cutinase-GFP11 supernatant containing cutinase-GFP11 was used to generate a dilution series which was measured by both, split GFP and cutinase activity assay (Fig. 3.7).

Data show very good comparability between the two assays. This supports the findings with *B. subtilis* as host for secretion, where the split GFP assay was also proven

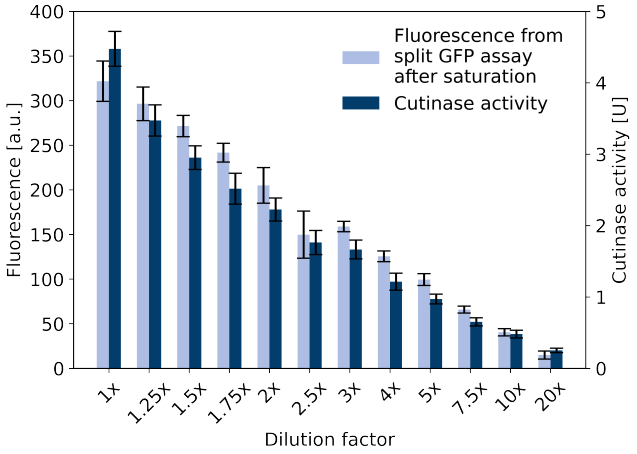

Fig. 3.7. Correlation of split GFP assay and cutinase-GFP11 activity. *C. glutamicum* pPBEx2-NprE-Cutinase-GFP11 supernatant was diluted with different factors and cutinase-GFP11 was detected by split GFP and cutinase activity assay with eight replicates. The fluorescence signal of the split GFP assay was measured when saturation was reached after 10.5 h of incubation at 25 °C [89]

to be a good alternative to activity measurements for the detection of homologous and heterologous target proteins [88].

3.1.5. Application in screening

To demonstrate the applicability of the improved fed-batch production process for generation and application of detector protein, two *C. glutamicum* strains secreting cutinase-GFP11 with *B. subtilis* signal peptides NprE or Pel were used. *C. glutamicum* pPBEx2-NprE-Cutinase-GFP11 and pPBEx2-Pel-Cutinase-GFP11 were cultivated with 24 biological replicates in a BioLector® Pro microscale cultivation device with backscatter-triggered induction of cutinase-GFP11 expression. The amount of secreted cutinase-GFP11 in supernatant samples was determined by split GFP and cutinase activity assay (Fig. 3.8).

All replicate cultivations of both strains showed very similar growth profiles and cutinase-GFP11 expression was induced by IPTG at the same time in the mid exponential phase. However, with respect to the achieved cutinase activity in the supernatant both strains showed very different cutinase-GFP11 formation. While the strain with NprE signal peptide showed much higher split GFP assay response and measured cutinase activity in the range of 300 a.u. and 2.1 U, the strain harboring

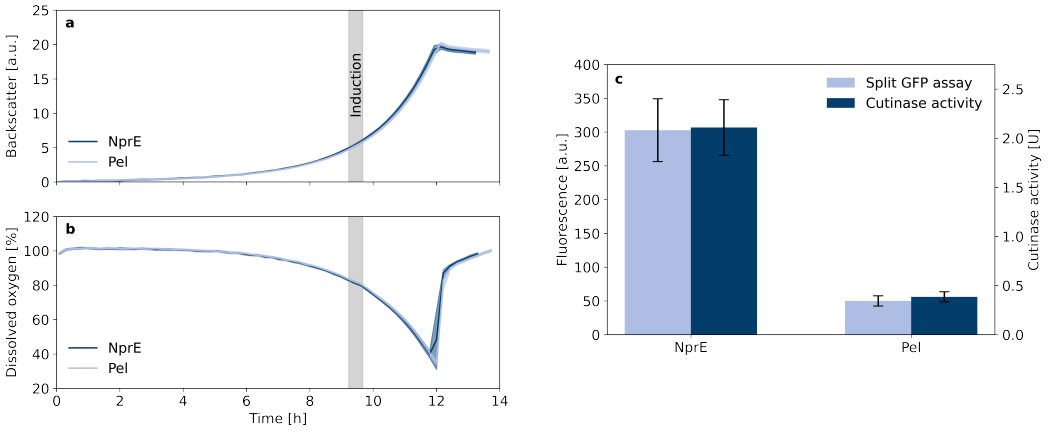

Fig. 3.8. Application of split GFP assay in screening of cutinase-GFP11 secretion. Growth of *C. glutamicum* pPBEx2-NprE-Cutinase-GFP11 and pPBEx2-Pel-Cutinase-GFP11 was monitored from 24 biological replicates by backscattered light (a) and DO (b). Each replicate was individually induced with IPTG as soon as a certain backscatter threshold was reached. The cultivation period in which all samples were induced is highlighted in gray. Cells were harvested after 4 h of target gene expression and cutinase-GFP11 in supernatant was detected by split GFP and cutinase activity assay (c). Error bars deviated from technical duplicates per 24 biological replicates. Fluorescence signal of split GFP assay was measured after 16 h incubation [89]

Pel signal peptide showed around 6x lower values in the range of 50 a.u. and 0.4 U, respectively. The large performance difference was expected and has been confirmed for similar *C. glutamicum* strains for secretory cutinase formation with NprE and Pel signal peptides [72]. With respect to the comparison between activity measurement and split GFP assay, the values were highly comparable in terms of the absolute values as well as the standard error. This gives rise to the conclusion that the developed fed-batch process for GFP1-10 detector protein production is well suited to produce a larger stock of detector protein solution, which can be stored up to seven months with minor loss of fluorescence response in the range of 10% only.

3.1.6. Conclusion of 3.1.

The production of detector protein GFP1-10 could be successfully scaled from a shake flask batch to a laboratory-scale STR fed-batch process. By fed-batch fermentation with intermittent glucose feed triggered by DO, detector solution for up to

385 screenings in 96-well MTPs could be obtained. GFP1-10 detector solution could be stored at –20 °C for at least seven months with very little performance loss.

Applicability of split GFP assay in high-throughput secretion screening of cutinase-GFP11 with *C. glutamicum* as host was verified. The split GFP assay can be easily automated as no appropriate sample dilution is needed and only the detector solution needs to be provided. In addition, the split GFP assay offers excellent opportunities for data normalization to reliably compare secretion performance within a screening round or after correlation with enzyme activity data measured for absolute calibration as this is demonstrated in the correlation of split GFP fluorescence versus cutinase in the application study.

The biggest advantage of the split GFP assay is that it can be easily adapted to other target proteins. As long as the GFP11-tag is accessible, nothing needs to be changed in the screening workflow. Even proteins without enzymatic activity or without an established activity assay can be detected without elaborate alternatives like enzyme-linked immunosorbent assay (ELISA).

Since sufficient GFP1-10 detector solution for high-throughput screening can now be produced in one production run and a correlation of the split GFP to the activity assay has been shown for heterologous cutinase-GFP11 secretion, the next step would be an automated signal peptide screening. For this, *C. glutamicum* strains need to be prepared that differ in the *B. subtilis* signal peptide. The robotic screening workflow needs to be further optimized to avoid manual handling of pre-cultures, which is particularly laborious when comparing many different strains.

3.2. Screening of cutinase secretion by *C. glutamicum*

This chapter focuses on automated workflows for targeted construction of *C. glutamicum* strains for cutinase-GFP11 secretion based on the newly created pCMEx-based plasmids. A *C. glutamicum* strain with inducible and tightly controlled GFP secretion was prepared for testing automated cultivation workflows with online product monitoring. An automated screening workflow starting from cryo-conserved cultures to detection of cutinase-GFP11 via activity and split GFP assay was developed and secretion performance was investigated. Varying RBS spacer lengths between Shine-Dalgarno sequence and start codon of the *B. subtilis* signal peptides were tested and results were compared to those with *B. subtilis* as host. Secretion stress was assessed using the *C. glutamicum* K9 biosensor strain. Secretion performance of microscale batch and fed-batch cultivation was compared for cutinase-GFP11 secretion with *C. glutamicum* K9 in an alternative semi-rational approach of signal peptide sequence optimization. Cutinase secretion mediated by the NprE signal peptide was compared for pPBEx2- and pCMEx8-based expression, and the effect of different RBS sequences in pCMEx8 on secretion was tested. Parts of this chapter were based on data from student projects I, V & VI and work was presented at conferences with poster III & IV and talks I–III and partly published in publications II & IV.

Author's contributions:
C. Müller supervised the student projects and did the molecular cloning and testing of GFP-secreting *C. glutamicum* strains. C. Müller, V. Waffenschmidt and L. Pohlen constructed pCMEx-based plasmids and *C. glutamicum* ATCC 13032 secretion strains and V. Waffenschmidt automated molecular biological workflows. C. Müller, V. Waffenschmidt and L. M. Helleckes contributed to the automation of the screening workflow. V. Waffenschmidt and C. Müller screened for cutinase-GFP11 secretion with *C. glutamicum* ATCC 13032 and C. Müller compared pCMEx-based to pPBEx2-based secretion. P. J. Bakkes prepared *C. glutamicum* K9 strains for pCMEx-based cutinase-GFP11 secretion, analyzed their biosensor response and secretion performance, and contributed to the writing of the results and the discussion about the biosensor. P. Lenz provided plasmids and protocols for the split GFP assay and investigated the impact of the RBS spacer on cutinase secretion in *B. subtilis*. M. Oldiges, A. Knapp, R. Freudl, K.-E. Jaeger and W. Wiechert contributed to the study design, review and editing of publication II. C. Müller wrote the publication II with parts of the methods provided by P. J. Bakkes and P. Lenz. For publication IV, P. Bakkes did the conceptualization, implemented the split GFP assay, did the library construction and screening, as well as data analysis and visualization and wrote the manuscript. P. Lenz and A. Knapp contributed to the initial study design, provided plasmids and protocols for establishing the split GFP assay and contributed to the writing of the manuscript. C. Müller performed

fed-batch cultivations and contributed to the writing of the manuscript. A. Bida constructed site-directed mutants and performed cutinase activity assays. D. Dohmen-Olma did bacterial transformations and SDS-PAGE. M. Oldiges, K.-E. Jaeger and R. Freudl contributed to the study design and the writing of the manuscript of publication IV.

Secretion of bacterial proteins into the culture medium simplifies downstream processing by avoiding cell disruption for target protein purification. However, a suitable signal peptide for efficient secretion needs to be identified and currently, there are no tools available to predict optimal combinations of signal peptides and target proteins. The selection of such a combination is influenced by several factors, including protein biosynthesis efficiency and cultivation conditions, which both can have a significant impact on secretion performance. As a result, a large number of combinations must be tested. Here, the detection of secreted proteins can be done not only by activity, but also with the split GFP assay if the target protein is covalently linked to a GFP11-tag.

3.2.1. Strain construction and automation

In this study, various combinations of *B. subtilis* signal peptides and RBS spacer sequences ranging from 4–12 nt between the Shine-Dalgarno sequence and the start codon were tested for secretion of *F. solani* f. sp. *pisi* cutinase in *C. glutamicum*. For accelerated plasmid construction by automation, traditional cloning cannot be used. Here, the DNA fragments are usually purified by gel extraction between restriction digestion and ligation, which is difficult to automate. Golden Gate assembly as an alternative uses type IIS restriction enzymes such as BsaI that cut outside their recognition site. Since the target plasmid no longer contains the recognition sequence, it is not further digested, unlike other plasmids in the reaction mix. Thus, restriction and ligation can be performed in one-pot setup without gel extraction in between [194].

To create a suitable plasmid backbone for Golden Gate assembly, the NdeI restriction site in plasmid pPBEx2 [8] was removed and the insert of the synthetic pUC57-Insert-Amp was integrated via CPEC. This insert has an altered sequence between the tac promoter and the terminator that consists of a 12 nt RBS spacer, *B. subtilis yncM* signal peptide sequence, *A. equina blue chromoprotein aeCP597* under the control of the constitutive EM7 promoter and a GFP11-tag sequence that is not in

frame with *aeCP597*. The resulting plasmid pCMEx12 (GenBank accession number OM801558, plasmid map in Fig. A.4a) allows for exchange of spacer and signal peptide sequence by cassette mutagenesis with restriction enzymes PstI/NdeI and NdeI/EcoRI, respectively. The constitutively expressed reporter gene *aeCP597* can be exchanged with the gene of interest by Golden Gate assembly. After a successful exchange, *E. coli* colonies have lost their blue color and the cutinase gene is cloned in frame with the signal peptide and GFP11-tag sequence under the control of the tac promoter (Fig. A.4b). The workflow of the sequence exchanges from the starting plasmid pCMEx12 to the secretion screening is shown in Fig. A.5.

The exchange of the gene of interest was automated using the Opentrons OT-2 robot with a Thermocycler and Magnetic Module. Unit operations were the Golden Gate assembly, heat-shock transformation of *E. coli*, magnetic beads based plasmid purification and restriction digestion as a control for successful Golden Gate assembly in addition to the colony color. Restriction enzymes would cut once before and twice after the successful integration of the target gene by Golden Gate assembly and DNA fragments were subsequently analyzed by capillary electrophoresis. If only one DNA fragment was visible, either new transformants were picked for plasmid purification or the Golden Gate assembly was repeated. Python scripts can be found online in the JuBiotech Git repository [186].

Comparison of the time required for manual or automated treatment of 96 samples showed an overall reduction of process time to about 58% of the time needed for the manual process (Fig. 3.9). However, the time savings varied among unit operations. For Golden Gate assembly, both options took about the same time since they do not differ in the automatically running thermocycler protocol. Automated test digestion even took slightly longer, albeit the manual work was reduced compared to manual test digestion. In contrast, automation of heat-shock transformation reduced the overall time to about 75% with only 25 min of manual work left to prepare the robot. The manually laborious plasmid purification by hand took about 6 h, assuming that only 24 samples can be handled in parallel using the NucleoVac 24 Vacuum Manifold. Thus, automation slightly reduced the total time to 4.25 h, but importantly the majority of this process is fully automated and does not require operator supervision.

As proposed by Tenhaef et al. [123], the Opentrons OT-2 system with additional Thermocycler and Magnetic Module is suitable for plasmid construction, which can

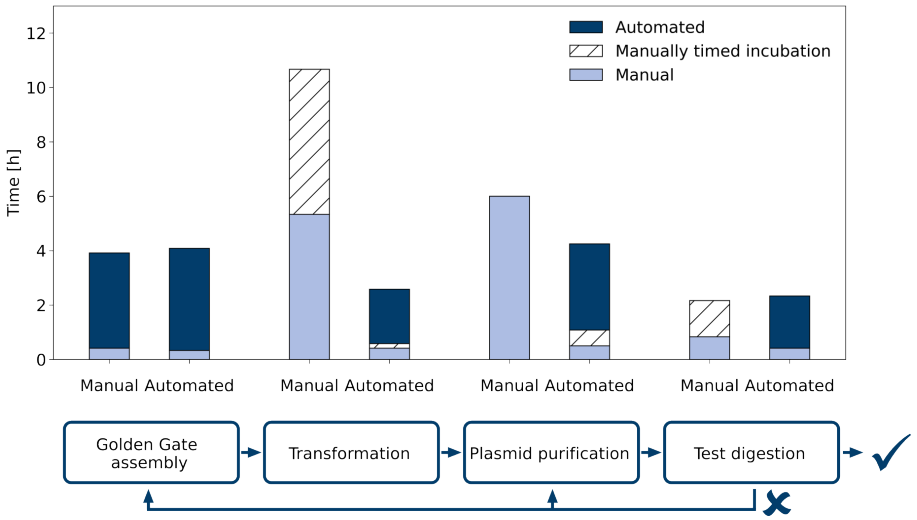

Fig. 3.9. Comparison of automated and manual construction of 96 plasmids. The plasmid construction can be separated into four unit operations: (1) Golden Gate assembly of plasmid carrying the gene of interest and a backbone with the desired spacer and signal peptide combination, (2) heat-shock transformation of *E. coli* with Golden Gate assembly samples, (3) magnetic beads based plasmid purification from *E. coli* and (4) restriction digestion of the purified plasmids for additional control. For Golden Gate assembly, either the plasmids with 96 different inserts or backbones were already appropriately diluted in a 96-well plate. 96 samples were handled in parallel in automated plasmid construction workflows. For manual transformation, usually up to 12 samples can be handled in parallel and a second batch can start when the first batch is in the regeneration phase. For plasmid purification, only the steps from cell harvest to plasmid elution were considered and 24 samples at a time were handled manually using the NucleoVac 24 Vacuum Manifold. Analysis of test digestion samples via capillary electrophoresis is not included. More detailed time tables of the unit operations can be found in Tabs. A.1 to A.3 [175]

be modularized and consecutively processed. The user can profit from the simple operation and customizable open source software for tailor-made plasmid assembly and strain construction workflows. However, this robotic system would not be sufficient to handle more complex microbial cultivation and screening processes which require more robotic functionality and precisely timed liquid handling manipulations. In such a case, more advanced liquid handling laboratory robotics is required, such as the Tecan Freedom EVO® 200 with integrated BioLector® Pro, centrifuge and microplate reader (see subsection 2.1.4). This system allows to execute more complex protocols and workflows with autonomous decision making during the process [141, 162], adding a further level of complexity.

Additionally, such script programming and workflow optimization for automated plasmid construction needs to be justified by a correspondingly large number of samples and iterations. Justification is given by the screening for cutinase secretion appli-

cation example presented here, and by the possibility to assemble combinations of spacer and signal peptide sequences for any given protein, thereby providing a rapid strain library prototyping for alternative target proteins besides the cutinase. In addition, the individual unit operations can also be used separately for completely different molecular biological objectives, since *E. coli* shuttle vectors and methods such as heat-shock transformation, plasmid purification and restriction digestions are widely used and small script adaptations can be easily made.

3.2.2. Testing automated cultivation workflows

For testing and optimization of cultivation workflows, the *C. glutamicum* with the pPBEx2-based plasmid pCGPhoD^{Cg}-GFP (later referred to as pEKEx2-PhoD^{Cg}-GFP) is often used [141, 146]. The capability of Tat-dependent secretion of GFP_{uv} with the homologous signal peptide PhoD allows for online product monitoring via fluorescence measurement in BioLector® cultivations. Target protein secretion is controlled by the *tacI* promoter and the *lac* repressor allele *lacI^q* and thus it is IPTG-inducible. Bakkes et al. [8] discovered that pEKEx2-based plasmids lack stability due to intraplasmid duplicate sequences. Furthermore, a modified carboxyl-terminus of the *lac* repressor leads to gene expression even in the absence of inducer. These findings resulted in the construction of the improved pPBEx2-based expression vector pPBEx2 with tight gene expression and improved plasmid stability [8].

To also enable tight control of GFP secretion, *phoD^{Cg}-gfp$_{uv}$* was amplified from pEKEx2-PhoD^{Cg}-GFP, digested with KpnI and SbfI and ligated into likewise digested pPBEx2. After the sequence of pPBEx-PhoD^{Cg}-GFP was verified, *C. glutamicum* was transformed by electroporation. Pre-cultures of *C. glutamicum* pEKEx2-PhoDCg-GFP and pPBEx2-PhoDCg-GFP in flasks were harvested in the late exponential phase and used to inoculate 24 wells of a FlowerPlate®, respectively. Tightly controlled expression was verified by backscatter-triggered induction with 0–1 000 µM IPTG and results were compared to those with *C. glutamicum* pEKEx2-PhoD^{Cg}-GFP (Fig. 3.10).

Growth phenotypes were overall comparable for the respective replicates of the strains, but the stationary phase was reached 0.6 h earlier with the pEKEx2-based strain and final backscatter values were on average around 6.4% lower. With the *C. glutamicum* pEKEx2-PhoD^{Cg}-GFP, almost no GFP secretion performance was

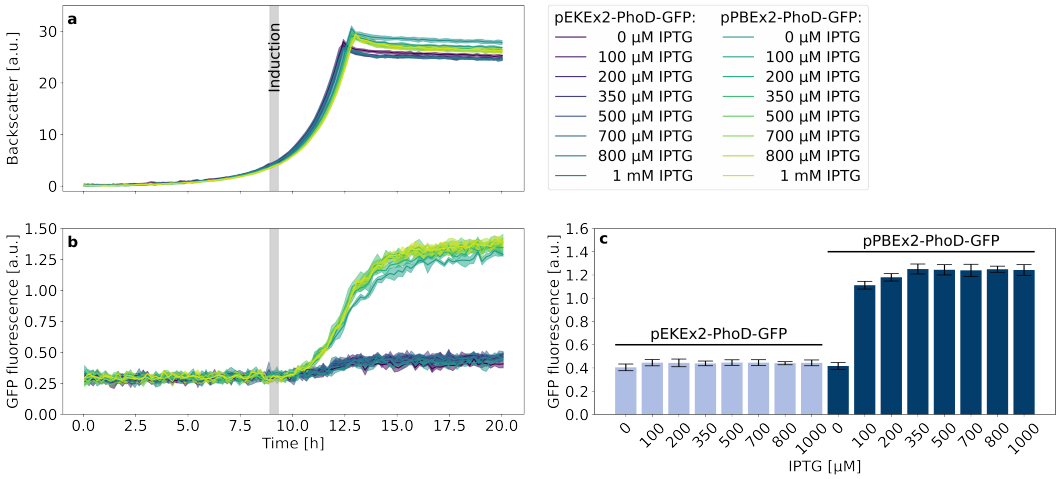

Fig. 3.10. Tat-dependent GFP secretion with *C. glutamicum*. (a) Backscatter. (b) GFP fluorescence (c) Fluorescence average and standard deviation of cycles 71–75 (14.06–14.86 h).Three replicates per strain and IPTG concentration were measured

detected (Fig. 3.10b and c). This indicates that no GFP gene is present due to intraplasmid recombination, explaining the different growth phenotype and highlighting the need for an optimized strain. In contrast, different fluorescence levels were measured depending on the amount of IPTG added to the cultivation media of the pPBEx2-based strain. Without inducer, average fluorescence levels between 14.06–14.86 h were below 0.45 a.u. and thus comparable to those of *C. glutamicum* pEKEx2-PhoD^{Cg}-GFP. By adding 100 µM IPTG, a steep increase to 1.11 a.u. average fluorescence was measured. Further increase in IPTG concentration above 350 µM did not lead to higher fluorescence levels than 1.25 a.u. but most likely to higher stress as the final backscatter signal was higher without any IPTG. This is also supported by literature, as reduced growth has already been shown for IPTG concentrations above 50 µM for over-expression of sigma factor genes in *C. glutamicum* [195].

3.2.3. Automated screening workflow for cutinase-GFP11 secretion

Screening of heterologous cutinase secretion was automated using a microcultivation robotic platform with Tecan Freedom EVO® 200, BioLector® Pro, centrifuge and microplate reader (schematic in Fig. 2.2 in subsection 2.1.4). The workflow described in subsection 3.1.5 and published in [89] was extended to automated pre-

cultures in the BioLector® to avoid laborious pre-cultures in flasks and to enable more standardized autonomous handling of pre- and main cultures (Fig. 2.4a).

In this workflow, main cultures are performed in triplicates, showing low deviation and a high degree of growth comparability (see Fig. 3.11a and b). The 12 pre-cultures are inoculated from cryo cultures placed on deck of the robotic system into the wells in the outer columns. Inoculation of three main cultures per pre-culture as well as induction of main cultures with IPTG are triggered individually by the backscatter signal of the cultivation that correlates with the cell density. The three wells next to the pre-culture wells are used for main cultures, i.e., 20 µL of the pre-cultures were transferred from column 1 and 8 to main cultures in column 2–4 and 5–7, respectively. Harvesting is triggered 4 h after induction and cutinase-GFP11 is detected in supernatants after all cultivations are finished by split GFP and cutinase activity assay. Using this workflow, the manual work is minimized and no operator supervision is required after providing cryo cultures and media on the robotic deck. One disadvantage, however, is the reduced throughput as only 48 cultivation wells are available. Here, with integrated pre-culture and main cultivation performed in triplicates the throughput is reduced to 12 strains per cultivation run.

3.2.4. Impact of the RBS spacer on the secretion performance

The accelerated plasmid construction workflow followed by the automated robotic cultivation and screening workflow was employed for investigating the impact of the RBS spacer sequences between the Shine-Dalgarno sequence and the start codon. The pPBEx2 plasmid which is the scaffold for pCMEx-based plasmids contains an 8 nt spacer. In total, 9 spacer sequences ranging from 4–12 nt were compared using the *B. subtilis* signal peptide of the protease NprE for cutinase-GFP11 secretion in *C. glutamicum* (Fig. 3.11). Although the lag-phases and resulting growth phenotypes of nine different strains varied in the pre-cultures, all main cultures grew comparably with a net cultivation time between 11.6–12.3 h from inoculation to harvest in the stationary phase. Such differences in the pre-culture growth were likely to be expected, due to potential deviations in the individual cell viability in the cryo cultures and inoculation density. Such deviation was effectively corrected by the individual inoculation strategy of the main cultures using a backscatter trigger enabling an autonomous inoculation of the main cultures. This led to growth phenotypes with high

similarity between the replicates of the 9 individual strains in terms of backscatter biomass signal (Fig. 3.11a) as well as DO profile (Fig. 3.11b).

The same applied for the secretion performance data, showing good comparability for the replicate data, but with considerably different secretion performance for the different spacer lengths (Fig. 3.11c). The secretion performance was evaluated based on direct measurement of cutinase activity and fluorescence data from split GFP assay. The assembly of holo-GFP and the formation of chromophores was similar to previous experiments (Section 3.1 and [89]). Results from the split GFP and cutinase activity assays showed standard deviations in the range of 10% and below, and the corresponding data are in good agreement, ranging from around 1 074–7 124 a.u. and 0.7–2.8 U mL^{-1}, respectively. The spacer length of 8 nt was already among the top performance values with the highest values for the 11 nt spacer. Strikingly, for 7–12 nt a considerable plateau region of high secretion performance was observed and no decrease at a spacer length beyond the 8 nt was found. The opposite was observed for smaller spacer lengths, with a clear negative effect of approx. 75% decrease in cutinase activity for a 4 nt RBS spacer. It seems that the reduction of the spacer length has a more severe effect on secretory production than its extension, which had a minor effect only.

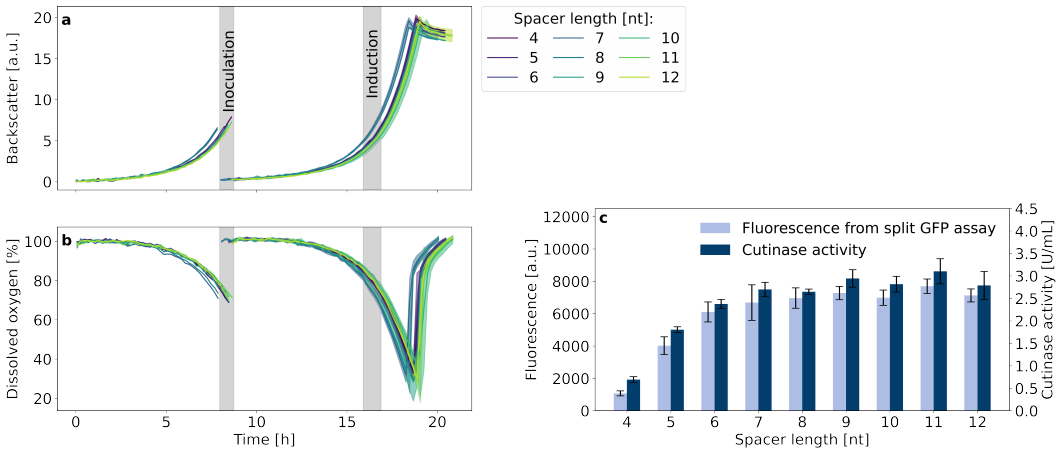

Fig. 3.11. Cutinase-GFP11 secretion with RBS spacer lengths from 4–12 nt. Backscatter (a) and DO (b) were measured during cultivation of *C. glutamicum* pCMEx[4-12]-NprE-Cutinase. Precultures inoculated from cryo cultures were used to inoculate three main cultures, which are shown as mean with standard deviation in confidence tubes. Inoculation and induction of main cultures with IPTG to a final concentration of 200 µM were triggered by backscatter signals. Cells were harvested 4 h after induction, and cutinase-GFP11 in the supernatant was detected via the split GFP and cutinase activity assays (c) in analytical duplicates of the respective three main cultures. For comparison with the cutinase activity, the maximum holo-GFP fluorescence after saturation was used [175]

Next, the automated screening of clones harboring plasmids with 4–12 nt spacer lengths was repeated with *B. subtilis* signal peptides Pel, Epr and Bsn for cutinase-GFP11 secretion in *C. glutamicum*. The growth phenotypes of the respective variants were similar to those of NprE (Figs. A.7 to A.9). To facilitate comparison, the cutinase activity and split GFP fluorescence data for all signal peptides including NprE were each normalized to x-fold change relative to the strain with the 4 nt spacer, as this strain was expected to show the lowest secretion performance (Fig. 3.12). Results were compared to those with *B. subtilis* as host (Fig. 3.12e–h), where data marked with an asterisk are from Volkenborn et al. [78] (Creative Commons CC BY license). In general, the data for cutinase activity and split GFP assay were comparable for the two strains and the 4–12 nt spacers used provided a clear picture of the effects with slightly higher x-fold changes for the split GFP data. For the four signal peptides in *C. glutamicum* a very similar response to changes of the spacer length was observed, showing the lowest values for the 4 nt RBS spacer and highest for 8–10 nt spacers with a gradual increase in between. This seems to confirm the initial results for the NprE signal peptide and may indicate a universal response to spacer length variation.

For *B. subtilis* the picture seems to be more heterogeneous. Again, a small 4 nt spacer length showed lowest performance and spacer lengths of 7 nt and longer were superior. The overall highest x-fold changes were measured for the signal peptide NprE with an 8 nt RBS spacer with an increase of about 20-fold in activity and 26-fold in split GFP fluorescence compared with the shortest spacer length (Fig. 3.12e). However, the individual response to nucleotide elongation was different for the four signal peptides. For the signal peptide NprE, a stepwise increase to high activity was observed going from 5 to 6 nt (Fig. 3.12e). For signal peptides Pel and Bsn, a gradual increase similar as in *C. glutamicum* was found (Fig. 3.12f* and h*). Although a gradual increase was also observed for the Epr signal peptide, this positive effect of spacer elongation required at least 8 nt to show increased formation of cutinase activity (Fig. 3.12g*). For this signal peptide, a significantly longer spacer led to optimized secretion performance. Overall, the secretion performance was lowest with the 4 nt spacer and was gradually increased by elongation with one or more nucleotides with 8–10 nt being necessary to obtain close to optimal cutinase activity. This is similar to the poor cutinase secretion with short spacer lengths of 4–5 nt that was observed in *B. subtilis* secretion studies in which identical combinations of RBS spacer, signal peptide and target protein were used [78]. These

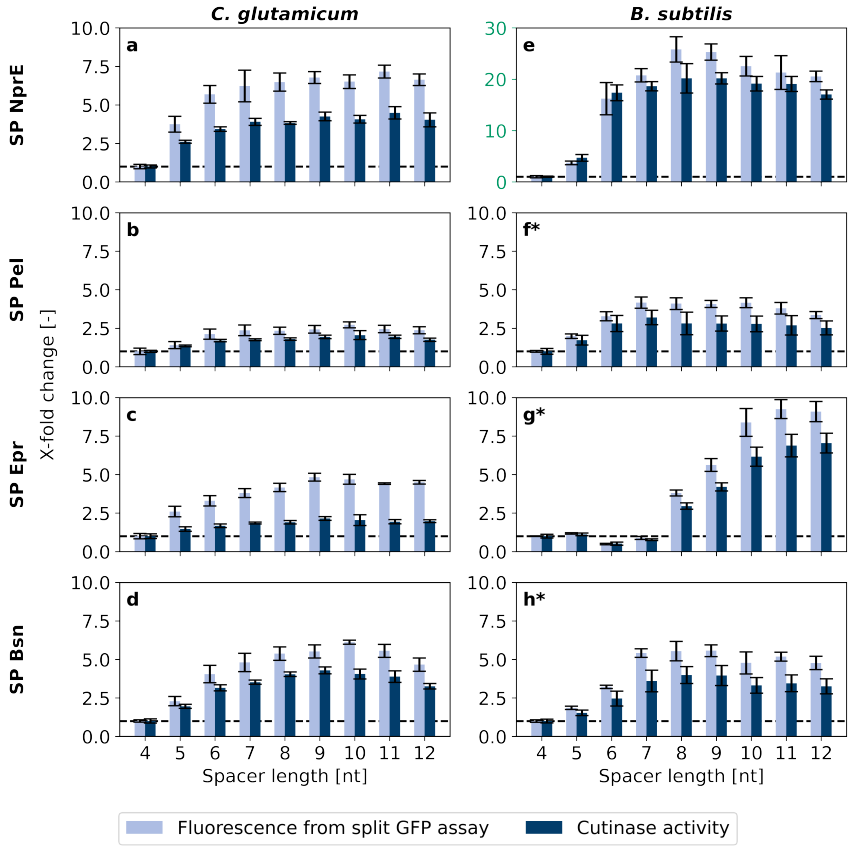

Fig. 3.12. Impact of spacer length on cutinase-GFP11 secretion with *B. subtilis* signal peptides NprE, Pel, Epr and Bsn. *C. glutamicum* (a—d) or *B. subtilis* (e—h) were used as secretion hosts. Cutinase-GFP11 was detected in supernatant samples of *C. glutamicum* by cutinase activity and split GFP assay in analytical duplicates of three cultivation supernatants, respectively. Cutinase-GFP11 in *B. subtilis* cultivation supernatants was detected in triplicates. Enzymatic activity and holo-GFP fluorescence after saturation were normalized to x-fold changes relative to the respective strain with a 4 nt RBS spacer (dashed line). The Y-axis scaling for subfigure 4e differs from the others and is highlighted in green. *data from [78], Creative Commons CC BY license [175]

results are also consistent with reports on intracellular ornithine transcarbamoylase production in *C. glutamicum*. Herein, enzyme activities were decreased by reducing the RBS spacer from 8 nt to 5 nt [196].

Interestingly, secretion performance was much less sensitive to longer RBS spacers than for those being shorter than 8 nt. Longer spacer sequences could lead to suboptimal translation initiation, but at the same time perhaps relieve bottlenecks in other steps of the secretion process. This may result in more secreted proteins being correctly folded, which could explain the secretion performance plateau for spacers of 8–12 nt [78].

3.2.5. Signal peptide screening

A *B. subtilis* signal peptide screening for cutinase-GFP11 secretion by *C. glutamicum* was performed based on plasmid pCMEx8 which harbors an 8 nt spacer sequence (Fig. 3.13). An extended set of signal peptide sequences that were all previously tested for cutinase secretion with *B. subtilis* [67] with high (YncM, Epr) medium (PhoB, LipA, YoaW) or low (Mpr, NprE, YpjP) secretion performance was used. Other signal peptide sequences were already used for cutinase secretion by *C. glutamicum* (NprE, Pel, YwmC, YpjP) as described elsewhere [72, 76, 89, 147]. Two additional signal peptides have been applied for high secretion of other target proteins, i.e., the signal peptide sequences of PhoB [197] and NprB [198]. Growth phenotypes of these *C. glutamicum* strain variants were very similar to those observed in Fig. 3.11 and Figs. A.7 to A.9, exhibiting a duration of the main cultures of 12–12.8 h (Fig. 3.13a and b).

For the signal peptides YncM and YpjP, a more linear than exponential growth was observed with lower final backscatter values. These results may indicate a potential metabolic burden or cellular stress due to cutinase-GFP11 secretion. This becomes particularly clear when IPTG is already added to the main culture of *C. glutamicum* secreting cutinase-GFP11 mediated by the YncM signal peptide sequence at the beginning of the cultivation as shown in Fig. A.6.

Cutinase-GFP11 activity in the supernatant showed substantial differences for the extended set of signal peptides used. The highest activities were measured for signal peptides NprE and YncM with approximately 3 U mL^{-1}, while only very low activities were detected with signal peptides YwmC, Epr and PelB.

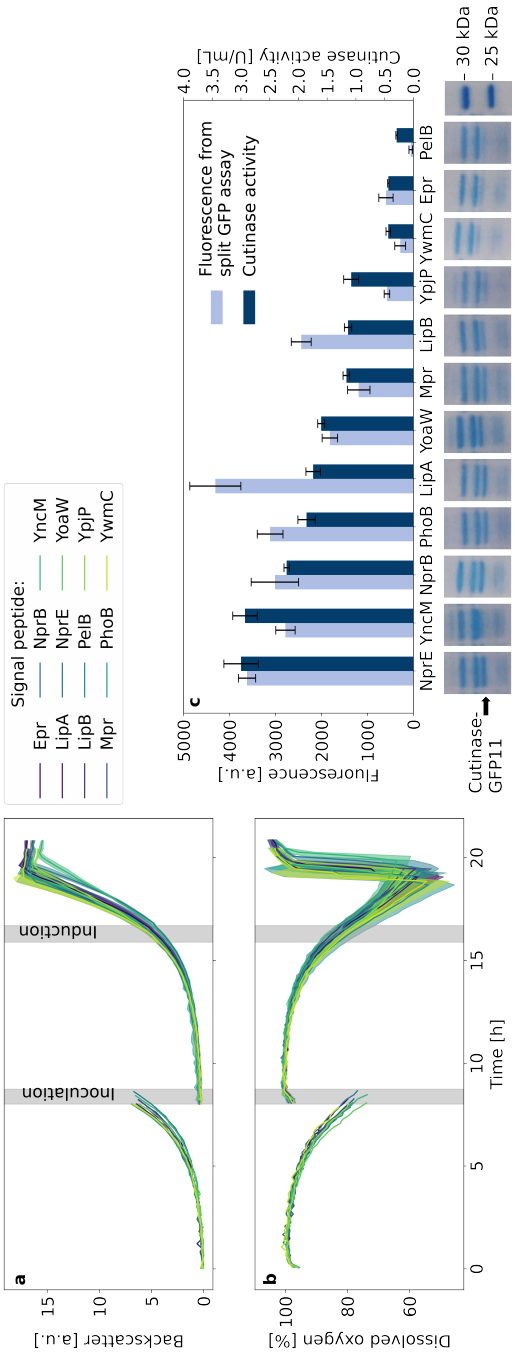

Fig. 3.13. Cutinase-GFP11 secretion with different signal peptides and a 8 nt RBS spacer. *C. glutamicum* pCMEx8-[SP]-Cutinase online cultivation data of backscatter (a) and DO (b) were measured. Pre-cultures were inoculated from cryo cultures. Triggered by the backscatter signal in the early exponential phase, pre-cultures were used to inoculate three main cultures that are shown as mean with standard deviation in confidence tubes. Induction of main cultures with IPTG to a final concentration of 200 µM was triggered by backscatter signals in the exponential phase and cells were harvested 4 h later. Cutinase-GFP11 in the supernatant was detected via SDS-PAGE, split GFP and cutinase activity measurements (c). Assays were conducted in analytical duplicates of the respective three main cultures with determination of fluorescence after saturation of self-assembled GFP. Supernatants of the same strain were pooled and proteins were precipitated with TCA before SDS-PAGE [175]

Strikingly, based on the split GFP assay, the highest amount of cutinase-GFP11 was detected with signal peptide LipA. Higher fluorescence than expected based on the activity results was also measured for the signal peptide LipB. It should be noted that the split GFP assay basically determines the amount of cutinase-GFP11 protein and does not directly report on the cutinase activity. This indicates that a lot of inactive protein is secreted with the signal peptide LipA. It could be that some of the secreted cutinase molecules were incompletely folded, misfolded or partially degraded and thus enzymatically inactive, whereas the GFP11-tag is still accessible and allows for holo-GFP assembly. This does not seem to be the case with the signal peptide NprE, for example. However, the five signal peptides facilitating the highest extracellular cutinase activities, i.e., NprE, YncM, NprB, PhoB and LipA, were identified as top performers in both assays. In all supernatants, at least small amounts of cutinase-GFP11 could be identified with TCA precipitation followed by SDS-PAGE at the expected molecular weight of 25.1 kDa.

3.2.6. Secretion stress measured by *C. glutamicum* K9

Previous studies on *C. glutamicum* have indicated that high-level production of secretory proteins is typically accompanied by secretion stress at the cellular envelope [75, 76, 199]. To assess the impact of the spacer length and signal peptide on cutinase secretion and the accompanying secretion stress, plasmids were transferred to the *C. glutamicum* K9 secretion stress biosensor strain. In this strain the secretion-stress responsive gene *htrA*, which codes for the periplasmic housekeeping protease HtrA is replaced by an *eyfp* gene that is under control of the htrA promoter. The resulting biosensor strain enables the monitoring of the Sec-dependent protein secretion stress by means of intracellular eYFP fluorescence [76]. In a proof of concept, *C. glutamicum* K9 pCMEx[4–12]-NprE-Cutinase were cultivated with online eYFP measurement, while cutinase-GFP11 in the supernatant at the end of the cultivation was detected manually with the split GFP and cutinase activity assays (Fig. 3.14).

The secretion performance of cutinase-GFP11 mediated by NprE in dependence of the spacer length in the biosensor strain showed trends similar to those observed in the wild type strain (compare Fig. 3.14 to Fig. 3.11c). However, absolute values with the *C. glutamicum* K9 biosensor strain were different due to differences in cultivation conditions, such as less glucose and 20 h of target gene expression as well as in

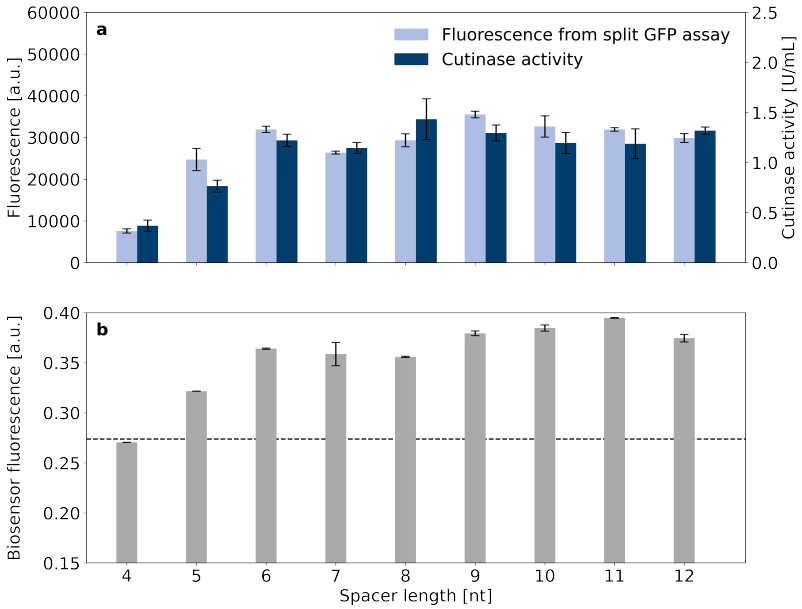

Fig. 3.14. Secretion performance and secretion stress associated with cutinase-GFP11 secretion using the signal peptide NprE in combination with RBS spacers of different lengths (4–12 nt). Two independent clones of *C. glutamicum* K9 pCMEx[4–12]-NprE-Cutinase were cultivated and secreted cutinase-GFP11 was detected via split GFP and cutinase activity measurements in analytical duplicates (a). At the end of the cultivation, the cell-specific eYFP fluorescence was determined of two independent clones and the average is shown with standard deviation (b). The dashed line indicates the normal background fluorescence associated with secretion stress in the absence of cutinase expression [175]

assay conduction, such as a reduced cutinase assay volume and microplate reader settings. Importantly, the biosensor fluorescence output at the end of the cultivation correlated with the secretion performance. High absolute cutinase-GFP11 secretion was accompanied by high biosensor fluorescence, indicating increased secretion stress. Herein, the secretion stress reached a plateau for RBS spacers with 6–12 nt length (Fig. 3.14b), which largely coincided with the secretion performance plateau (Fig. 3.14a). In earlier work it was demonstrated that biosensor cells which carry the empty vector typically exhibit a biosensor fluorescence of around 0.27 a.u. at the end of the cultivation, which represents the normal background secretion stress in the absence of cutinase expression [75]. Therefore, this value was set as a threshold for the biosensor output (Fig. 3.15b, dashed line). With pCMEx4-NprE-Cutinase (Fig. 3.14b) and for instance pCMEx8-Pel-Cutinase (Fig. 3.15b), the biosensor fluorescence did not exceed 0.27 a.u., which indicates that the corresponding low-level cutinase secretion with typically less than 0.4 U mL^{-1} does not impose significant secretion stress to the cells.

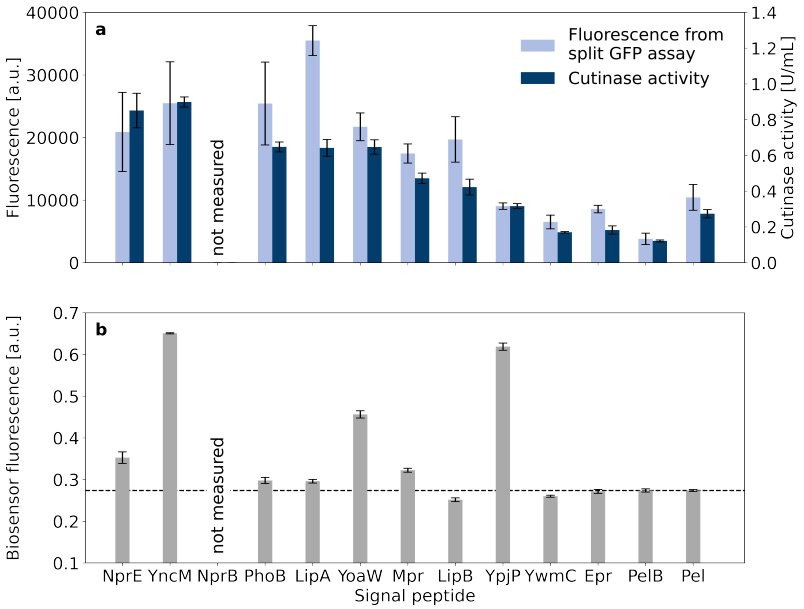

Fig. 3.15. Secretion performance and secretion stress associated with cutinase-GFP11 secretion using different signal peptides in combination with an 8 nt RBS spacer. Secreted cutinase-GFP11 from *C. glutamicum* K9 pCMEx8-[SP]-Cutinase was detected via split GFP and cutinase activity measurements that were performed manually (a). At the end of the cultivation, the cell-specific eYFP fluorescence was determined of two independent clones and the average is shown with standard deviation (b). The dashed line indicates the normal background fluorescence associated with secretion stress in the absence of cutinase expression [175]

In addition, the impact of different signal peptides on the cutinase secretion and the accompanying secretion stress was assessed. For this purpose, the indicated constructs all carrying an 8 nt RBS spacer were transferred to the *C. glutamicum* K9 biosensor strain (Fig. 3.15a). Importantly, the secretion performance of the different signal peptides in the biosensor strain showed trends similar to those observed in the wild type strain (compare Fig. 3.15a and Fig. 3.13c). Interestingly, also in the biosensor strain a disproportionally high split GFP fluorescence in comparison to the cutinase activity is noted in case of the LipA and LipB signal peptides (Fig. 3.15a). Strikingly, cutinase export via either of these signal peptides did not lead to a substantial increase in secretion-associated stress, as evidenced by the low biosensor fluorescence output. On the other hand, the highest biosensor response was observed for cutinase-GFP11 secretion mediated by the signal peptides YncM and YpjP.

It is important to note that the secretion biosensor responds to the extent of stress caused by the accumulation of incorrectly folded target protein at the trans-side of

the cytoplasmic membrane upon Sec-dependent protein translocation, but not to the biologically active secreted target protein. Nevertheless, a general dose-dependent effect was observed between the secretion performance of an individual signal peptide and the secretion stress in dependence of the spacer length, similar to the dependence on IPTG concentrations [76]. However, when comparing a large set of different signal peptides, it must be considered, that the signal peptides may have distinct influences on the number and quality of exported cutinase molecules, e.g. by altering the synthesis, export efficiency, processing or folding of the target protein [52]. Because the biosensor responses for YncM- and YpjP-mediated cutinase secretion were similarly high, whereas the secretion performance with YpjP was threefold lower, the signal peptide YpjP seems to have a stronger negative effect on the cutinase quality. For both signal peptides, there appears to be a correlation to impaired growth, as expression of the respective constructs in the wild-type strain already resulted in a slightly impaired growth phenotype. This gives rise to the conclusion that the cutinase export mediated by signal peptides YncM and YpjP is accompanied by considerable secretion stress, showing also an impact on growth (Figs. 3.13, 3.15 and A.6). Taken together, the data suggest that signal peptide specific effects may occur at later stages of Sec-dependent secretion, upon signal peptide removal or possibly even upon protein folding. The results indicate that the biosensor strain has its limitations in applications where the screening of a large number of signal peptides that are structurally very distinct is desired.

3.2.7. Cutinase-GFP11 secretion in fed-batch

While batch cultivations are mainly used for screenings, fed-batch processes are dominant in production. This is particularly challenging because it has been shown that batch conditions for screening are not fully transferable to fed-batch processes, and variants that show better secretion performance under batch cultivation conditions may underperform in fed-batch experiments [66].

To investigate this in relation to cutinase-GFP11 secretion, *C. glutamicum* K9 strains were cultivated in microliter-scale under batch and fed-batch conditions and secretion performance was compared. In contrast to the previous sections, these secretion strains do not differ in signal peptides themselves, but variants of the *B. subtilis* signal peptide Pel were prepared in an untargeted approach using error-prone PCR

by P. J. Bakkes. Fluorescence-activated cell sorting was used to isolate cells with increased eYFP fluorescence in response to increased secretion stress. Five isolated Pel variants (mutants F11I and P16S, double mutant F11I/P16S and triple mutant F11I/G13A/P16S) as well as *C. glutamicum* K9 pPBEx2-NprE-cutinase-GFP11 and pPBEx2-Pel-cutinase-GFP11 were cultivated in fed-batch (Fig. 3.16). Only slow and almost linear growth was recorded in the fed-batch cultivation. This could be due to omitted urea in the medium and perhaps too high pH during the cultivation. After a drop in the pH value at the beginning of the experiment due to the interference of the optical measurement by PCA in the medium [146], the online pH was measured around the target value of 6.8. However, the PCA content in the media may still have shifted the online pH to lower values than would have actually been measured offline, resulting in deteriorated growth.

Secretion performance of the five Pel variants was compared to the cutinase-GFP11 secretion with signal peptides NprE and Pel by P. J. Bakkes with data normalized to those with signal peptide Pel (Fig. 3.17). As in batch experiments (see Fig. 3.8), a significantly higher cutinase-GFP11 secretion was measured with the *B. subtilis* signal peptide NprE, here about 450% of the secretion performance with the Pel signal peptide. The standard error for the fed-batch data showed good reproducibility for all variants. Regarding activities, the secretion ranking of the different signal peptide variants followed the order Pel < F11I < P16S < F11I/P16S < NprE < F11I/G13A/P16S. This confirms the results from the batch experiments [75], although there the secretion with the Pel variant F11I/P16S was even closer to that with signal peptide NprE than 0.9x in the fed-batch cultivation. It seems as if with the triple mutant, the secretion performance with signal peptide NprE could even be exceeded by around 1.1x regarding activity. Interestingly, the corresponding fluorescence from split GFP assay was substantially lower with around 250% of the secretion performance with the Pel signal peptide. A similar effect has already been observed in batch cultivations [75] as well as in the pCMEx8-based signal peptide screening for some strains (Fig. 3.13). These results indicate that the signal peptide sequence itself as well as only mutations in three amino acid positions of a signal peptide might affect the holo-GFP assembly in split GFP assay. Possible explanations are changes in the signal peptide processing by signal peptidases and/or protein folding after secretion.

The successful transfer of the optimized signal peptide variants from batch to fed-batch cultivation demonstrates that the signal peptide screening approach can de-

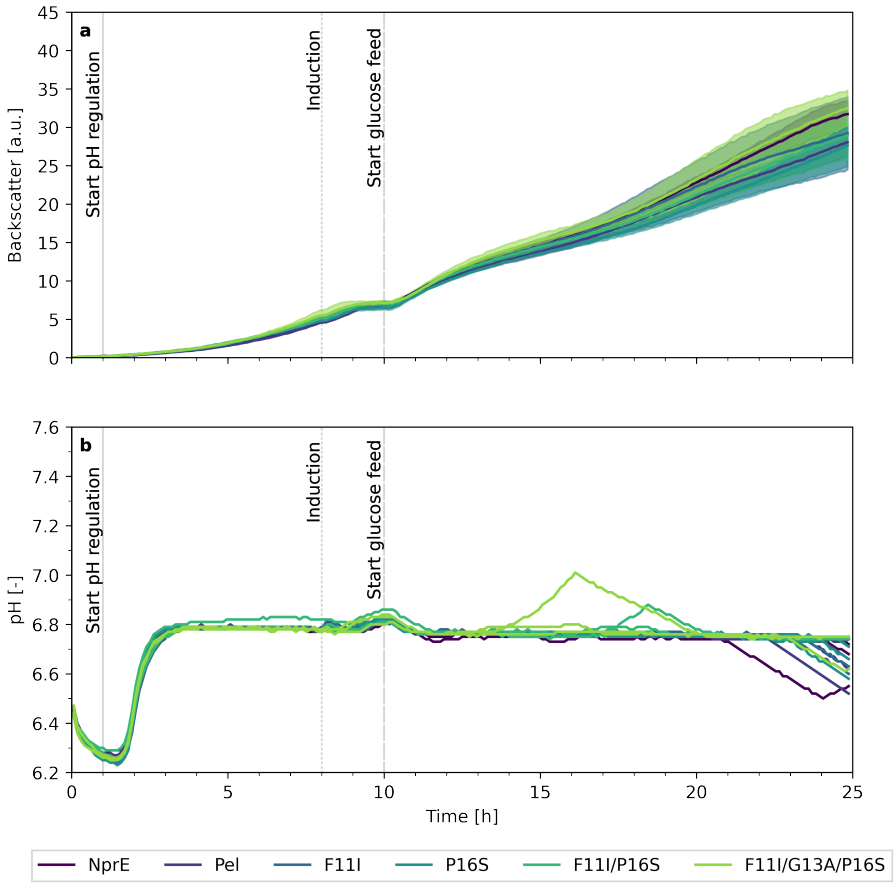

Fig. 3.16. Fed-batch of *C. glutamicum* K9 for secretory production of cutinase-GFP11. Biosensor cells carrying plasmids pPBEx2-NprE-cutinase-GFP11 (NprE), pPBEx2-Pel-cutinase-GFP11 (Pel) or the Pel variants F11I, P16S, F11I/P16S or F11I/G13A/P16S were cultivated in CGXII medium with an initial glucose concentration of 5 g L^{-1} inoculated to an $OD_{600\,nm}$ of 0.5 from the respective pre-cultures. The fed-batch cultivation was conducted in a BioLector® Pro under standard conditions but with ≥30% headspace oxygen. Biomass (a) and pH (b) were measured with error tubes in biomass measurement originating from at least three replicates. After 10 h, glucose was fed with a constant rate of 5.22 µL h^{-1} (equals 2.09 mg h^{-1} glucose). The pH was adjusted to 6.8 with 3 M KOH beginning after 1 h. Cutinase-GFP11 expression was induced with 250 µm IPTG (final concentration at the time of induction) after 8 h. The supernatants were taken after about 25 h and used for split GFP and cutinase activity assay. Modified from [75]

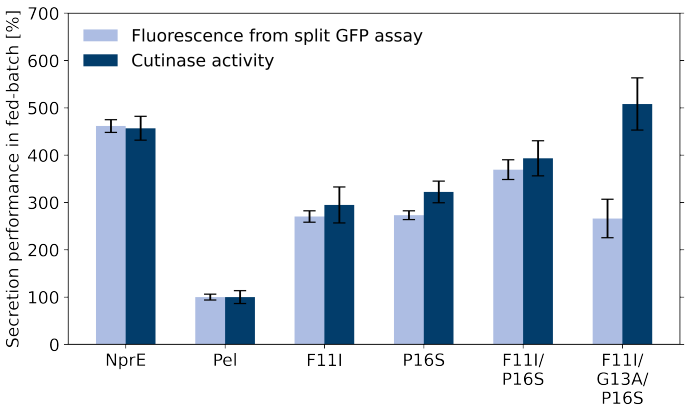

Fig. 3.17. Secretion performance of *C. glutamicum* K9 cultivated in fed-batch. Cutinase-GFP11 in supernatant samples were detected via cutinase activity and split GFP assay. Modified from [75]

liver high performing strains not only under batch screening, but also under fed-batch conditions relevant for further development stages.

3.2.8. Differences in pCMEx8- and pPBEx2-based expression

With pCMEx8-based expression of cutinase-GFP11 with the NprE signal peptide, activities in the *C. glutamicum* supernatant were substantially lower compared to pPBEx2-based expression. This could be attributed to differences in plasmid sequence, such as in the 5'-untranslated region or the linker between signal peptide and gene of interest. Some of these sequence changes were necessary to enable automated cloning and to investigate the influence of spacer length between the Shine-Dalgarno sequence and the start codon of the signal peptide on secretion performance. Between the promoter and the gene of interest, an additional incomplete Shine-Dalgarno sequence is present in the pPBEx2 plasmid, as well as additional start codons, some of which are in frame with the target gene. Since *C. glutamicum* has around 33% leaderless transcripts [200], these had to be removed by single point mutations in pCMEx8 to thoroughly investigate the impact of spacer lengths without a possible effect of leaderless transcription. To compare results to those from *B. subtilis*, the 8 nt spacer sequence itself was slightly changed from 5'-atatagat-3' in pPBEx2 to 5'-aaaaacat-3' in pCMEx8. A BbsI recognition site was inserted upstream of the Shine-Dalgarno sequence defined by Pfeifer-Sancar et al. [200] with the core sequence 5'-aggag-3' to allow a backbone exchange via

Golden Gate assembly. Additionally to the 5'-untranslated region, changes in the linker sequence between the signal peptide and the protein of interest were made. By Golden Gate assembly of the gene of interest with BsaI, the linker was shortened from four amino acids (Ala-Glu-Phe-Ala) in pPBEx2-based plasmids to two amino acids (Glu-Phe) in pCMEx8-based plasmids.

These differences in secretion performance with the pPBEx2 and pCMEx8 backbones were examined with a focus on the effect of RBS. Sequence replacements in the RBS of pCMEx8-NprE-Cutinase can easily be made by cassette mutagenesis likewise to the exchange of the spacer sequence. The plasmid pCMEx8-NprE-Cutinase was digested with restriction enzymes PstI/NdeI, purified by gel extraction and ligated with respectively hybridized RBS oligonucleotides, which have correspondingly suitable overhangs for directional cloning. The plasmids pCMEx8a–d were prepared using this approach to represent four intermediates of the RBS of pPBEx2 and pCMEx8 as shown in Tab. 3.1. After plasmid sequence verification and preparation of *C. glutamicum* strains, cutinase-GFP11 secretion of these variants was compared to pCMEx8-NprE-Cutinase and pPBEx2-NprE-Cutinase-GFP11. The growth phenotypes in BioLector® cultivation with automated pre-culture were highly similar (see Fig. A.10).

Tab. 3.1. RBS variants and their 5'→ 3' DNA sequence from the PstI restriction site (5'-ctgcag-3') to the spacer. SD: Shine-Dalgarno sequence (bold sequence), BbsI: BbsI recognition site (underlined sequence)

Plasmid	**Description**	**5'→ 3' DNA sequence**
pCMEx8a-NprE-Cutinase	SD_{pPBEx2}, $spacer_{pPBEx2}$	ctgca**gaaggag**atatagat
pCMEx8b-NprE-Cutinase	SD_{pPBEx2}, $spacer_{pCMEx8}$	ctgca**gaaggag**aaaaacat
pCMEx8c-NprE-Cutinase	BbsI, SD_{pPBEx2}, $spacer_{pCMEx8}$	ctgcagagaagac**gaaggag**aaaaacat
pCMEx8d-NprE-Cutinase	BbsI, SD_{pPBEx2}, $spacer_{pPBEx2}$	ctgcagaagac**gaaggag**atatacat
Comparison to:		
pCMEx8-NprE-Cutinase		ctgcagagaagac**aggag**aaaaacat
pPBEx2-NprE-Cutinase-GFP11		ctgcag**gaaggag**atatagat

As shown in Fig. 3.18, the activities differ with the highest activity measured in *C. glutamicum* pPBEx2-NprE-Cutinase-GFP11 supernatant with 7.3 U mL^{-1}. Cutinase-GFP11 activities in the supernatant were increased with all new RBS variants compared to the initial pCMEx8-NprE-Cutinase plasmid with around 3 U mL^{-1}, although

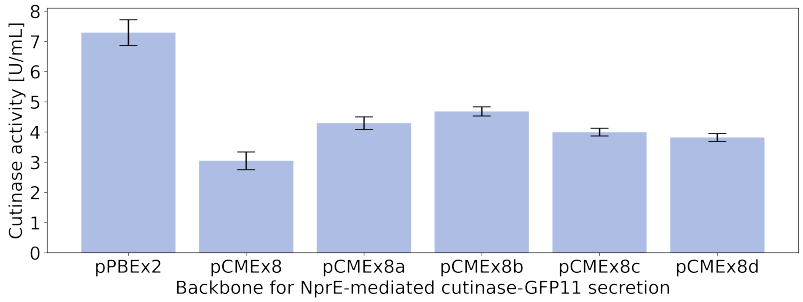

Fig. 3.18. Cutinase-GFP11 activities from NprE-mediated secretion with different RBS

only to a maximum of 4.7 U mL^{-1} with *C. glutamicum* pCMEx8b-NprE-Cutinase. Strikingly, expression with the pCMEx8d-NprE-Cutinase plasmid that has the pPBEx2 RBS with an inserted BbsI recognition site resulted in the second lowest cutinase-GFP11 activity. The best pCMEx8-based plasmid variants, b and a, have both no BbsI recognition site. This indicates that the Shine-Dalgarno sequence is not restricted to 5'-aggag-3', but beyond in the 5' direction. Recently, a consensus sequence of 5'-gaaaggagg-3' for *C. glutamicum* was proposed [201] , which differs from that of pPBEx2 only by an additional adenine. For the pCMEx8 plasmid, it is most likely the insertion of a BbsI recognition site associated with the pyrimidine cytosine that interferes with ribosome binding to the by default purine-rich Shine-Dalgarno sequence [202]. Also the DNA sequence of the spacer has an impact on overall cutinase-GFP11 secretion performance, as the best pCMEx8 variants pCMEx8a-NprE-Cutinase and pCMEx8b-NprE-Cutinase differ in this sequence only. The spacer sequence 5'-aaaaacat-3' of pCMEx8b-NprE-Cutinase led to significantly ($p < 0.05$) better cutinase-GFP11 secretion, although it might lead to mRNA secondary structures that would decrease the translation initiation rate. It is possible that this nevertheless has a positive effect on overall protein secretion performance by slowing down translation to reduce bottlenecks in other secretion steps such as translocation through the SecYEG pore.

Since no activities comparable to those with pPBEx2 as backbone were measured by changing the RBS sequences, the RBS seems to be not the only factor for reduced cutinase-GFP11 secretion with pCMEx8-based plasmids. It has already been shown in the literature that the +1 amino acid adjacent to the signal peptidase recognition site impacts cleavage and thus also secretion [69, 79]. It could be that the cleavage site is more accessible due to the adjacent small hydrophobic amino acid alanine in pPBEx2-NprE-Cutinase-GFP11. However, it was observed for *C. gluta-*

micum R that +1 glutamine residues adjacent to the signal peptidase cleavage site have a positive effect on amylase secretion and a change to the smaller residue alanine reduced secretion performance [69]. Watanabe et al. [69] hypothesized that the +1 amino acid affects the state of the pre-secretory proteins in the SecYEG pore. This might not only be affected by the size of a residue, but also the properties. Glutamine is significantly larger than the hydrophobic alanine, but polar and uncharged. On the other hand, glutamic acid adjacent to the cleavage site in pCMEx8-based plasmids is negatively charged, which may have a negative effect on the translocation itself and signal peptidase cleavage. Of particular interest would be how an additional +1 alanine next to the signal peptidase recognition site in pCMEx8-based plasmids (peptide linker Ala-Glu-Phe) affects secretion and whether this can bring secretion efficiency to the level of pPBEx2.

In addition to the linker sequence, although less likely, removal of the additional incomplete Shine-Dalgarno sequence as well as additional start codons, some of which are in frame with the target gene, may be a factor. This possibly decreases the likelihood of ribosome binding that is known to increase mRNA stability [203]. To study this effect on secretion, these sequence changes could be restored step by step and activities could be compared to pPBEx2-based secretion.

The differences in secretion performance depending on the backbone used demonstrate that there is great potential for optimization here as well. In the best case, a backbone for secretion screening should combine strong secretion as in pPBEx2 plasmids with the possibility for automatable high-throughput cloning methods as in pCMEx8.

3.2.9. Conclusion of 3.2.

This section highlights the benefits of laboratory automation for optimization of strain construction, protein secretion and performance evaluation. Depending on the application, low cost robotics can be used, e.g., for plasmid construction, and push the throughput far beyond the level of manual procedures. For handling of more complex workflows such as microbial cultivation and screening processes, multi-purpose high performance laboratory automation is required that allows autonomous decision making during the process [141, 162]. Automated secretion screening including pre-cultures enabled high comparability between strains due to autonomous in-

oculation and induction events for individual cultures triggered by online biomass monitoring. This is a great step towards standardization of experimental procedures providing improved reliability and reproducibility of cultivation data while minimizing the manual work and operator supervision. One disadvantage, however, is the reduced throughput as only 48 cultivation wells are available. Here, with integrated pre-culture and main cultivation performed in triplicates the throughput is reduced to 12 strains. Nevertheless, replicate data of the main cultures were very comparable in terms of growth phenotype and activity of secreted cutinase, paving the way to modify the workflow to run pre- and main cultures in unicates. Thus, up to 24 different strains could be tested in one run in future screenings.

To test automated cultivation workflows such as for secretion screenings, a *C. glutamicum* model strain with tightly controlled induction of Tat-dependent GFP secretion was successfully prepared. The *C. glutamicum* pPBEx2-PhoD^{Cg}-GFP can be used for all applications where tight control and online monitoring of product formation is desired.

Results obtained from automated screening using different RBS spacer lengths for cutinase-GFP11 secretion combined with the *B. subtilis* signal peptides NprE, Pel, Bsn and Epr in *C. glutamicum* revealed that in the range of the 4–12 nt spacers, the use of at least 8 nt is advised and only poor secretion was observed with the shortest spacer lengths of 4–5 nt. While shorter than 8 nt RBS spacers led to substantial performance loss, the results with 8–12 nt spacers were comparable. These results indicate that the transcriptional machinery is more sensitive to shorter than to longer RBS spacers and that at least an 8 nt spacer should be used for secretion screenings.

Since there was no generally more suitable spacer length for the signal peptides tested for cutinase-GFP11 secretion, an automated signal peptide screening was done with the 8 nt spacer. As expected from [72], secretion varies according to the signal peptide used, with NprE being the best signal peptide for cutinase secretion in *C. glutamicum*. In some cases, the signal peptide sequence itself as well as mutations in as few as three amino acid positions of a signal peptide appear to affect holo-GFP assembly in the split-GFP assay, resulting in divergent results from activity and fluorescence. However, since the same best 5 signal peptides for cutinase-GFP11 secretion were identified with both the split GFP and the cutinase activity assay, the easily automatable split GFP assay proved to be a valuable tool for rapid

strain pre-selection exhibiting high cutinase secretion. Moreover, the automated split GFP assay would be particularly useful for the detection of target proteins for which no suitable activity assay is available or in cases where the assay is strongly error-prone. For this, it must first be generally verified by other methods such as western blots that the GFP11-tag bound to the target protein is accessible. After a pre-selection of strains, false positive hits could subsequently be discarded by manual or more elaborate methods.

Taken together, the *C. glutamicum* K9 biosensor strain provides an overall dose-dependent response for approaches with structurally similar signal peptides, as was the case for testing of different spacer lengths for cutinase-GFP11 secretion mediated by the NprE signal peptide or the approach with the error-prone PCR of the Pel sequence. For the latter, screening results were successfully transferred from batch to fed-batch cultivation. The results from the signal peptide screening for cutinase-GFP11 secretion, however, indicate limitations when comparing structurally distinct signal peptides for target protein secretion. Apart from this, the biosensor responses suggest that the signal peptide affects secretion at the last steps of the Sec pathway, after signal peptidase cleavage or possibly even during the protein folding step.

For optimized plasmid-based secretion, not only the signal peptide sequence is important, but also the 5'-untranslated region including the RBS spacer or (if present) the amino acids between the signal peptide and the target protein. The aim is to optimize the plasmid to enable advanced methods for automatable cloning in combination with strong secretion.

3.3. A model-based screening strategy for PETase secretion by *C. glutamicum*

The focus of this chapter lies in the evaluation of PETase secretion by *C. glutamicum* mediated by *B. subtilis* signal peptides. The screening workflow described in Section 3.2 was further optimized. The cutinase activity assay was used for detection of secreted target proteins. A Bayesian process model was developed and applied in screenings to take batch effects and biological errors into account and to qualify the uncertainty. As a decision policy, a Thompson sampling algorithm was implemented to detect the combination of signal peptide and PETase with the highest secretion performance with a high degree of statistical certainty and without wasting resources. Results were compared to a standard evaluation approach. Furthermore, scalability of PETase secretion from cultivation in a microbioreactor to a liter-scale stirred bioreactor was shown. This chapter is based on data from student projects VI and VII, conference talks I–III and publication III.

Author's contributions:
C. Müller did the supervision of the student project VI and C. Müller and L. M. Helleckes jointly supervised the student project VII. The publication was written and revised by C. Müller and L. M. Helleckes. While the focus of C. Müller was on the experimental side and interpretation from a biological point of view, the focus of L. M. Helleckes was on the development and optimization of the process model and on the interpretation of the model results. C. Müller, T. Griesbach and V. Waffenschmidt prepared *C. glutamicum* PETase secretion strains. Screening workflows were automated by C. Müller, T. Griesbach, V. Waffenschmidt and L. M. Helleckes. T. Griesbach did PETase secretion screenings in microliter-scale. Laboratory-scale bioreactor cultivations and PETase activity measurements with the respective samples were conducted by M. Moch. L. M. Helleckes build the process model, analyzed data and implemented Thompson sampling. M. Osthege contributed to building the process model and M. Oldiges and W. Wiechert to the study design, review and editing of publication III.

Extracellular production of target proteins simplifies downstream processing due to obsolete cell disruption. However, optimal combinations of a heterologous protein, suitable signal peptide and secretion host can currently not be predicted, resulting in large strain libraries that need to be tested (see Section 3.2). On the experimental side, this challenge can be tackled by miniaturization, parallelization and automation, which provide high-throughput screening data. These data need to be condensed

into a candidate ranking for decision making to focus bioprocess development on the most promising candidates.

The application example in this section is the Sec secretion of two PETases, LCC and PE-H mutants, by *C. glutamicum* mediated by different *B. subtilis* signal peptides. Besides the use of a fully automated screening process, an accompanying modeling framework was developed and applied in screenings for highest enzyme activity by L. M. Helleckes (Forschungszentrum Jülich GmbH). In contrast to classical evaluation methods, batch effects and biological errors are taken into account and their uncertainty is quantified. Within only two rounds of screening, the most suitable signal peptide was identified for each PETase. Results from LCC secretion in microliter-scale cultivation were shown to be scalable to laboratory-scale bioreactors.

3.3.1. Preliminary PETase screening

After the successful strain construction of the *C. glutamicum* variants secreting the PETases PE-H mutant Y250S and LCC mutant ICCG mediated by 24 different *B. subtilis* signal peptides, secretion performance was examined by the split GFP assay and by enzyme activity once before building the process model (see Fig. 3.19).

It has to be noted here that enzymatic activities are determined as 4NPP hydrolytic activities rather than PET degradation. Nevertheless, the degradation of 4NPP is a valid measure to compare the secretion performance between different signal peptides for the secretion of the same enzyme. However, secretion performance cannot be compared in absolute values regarding PET hydrolysis. This is due to the structural differences of the LCC and the PE-H [107, 108], which is why they can presumably convert the 4NPP substrate to different extents. Moreover, for method development, which is the actual focus of this section, it is helpful to use an already established and automated activity assay for the detection of secreted target proteins.

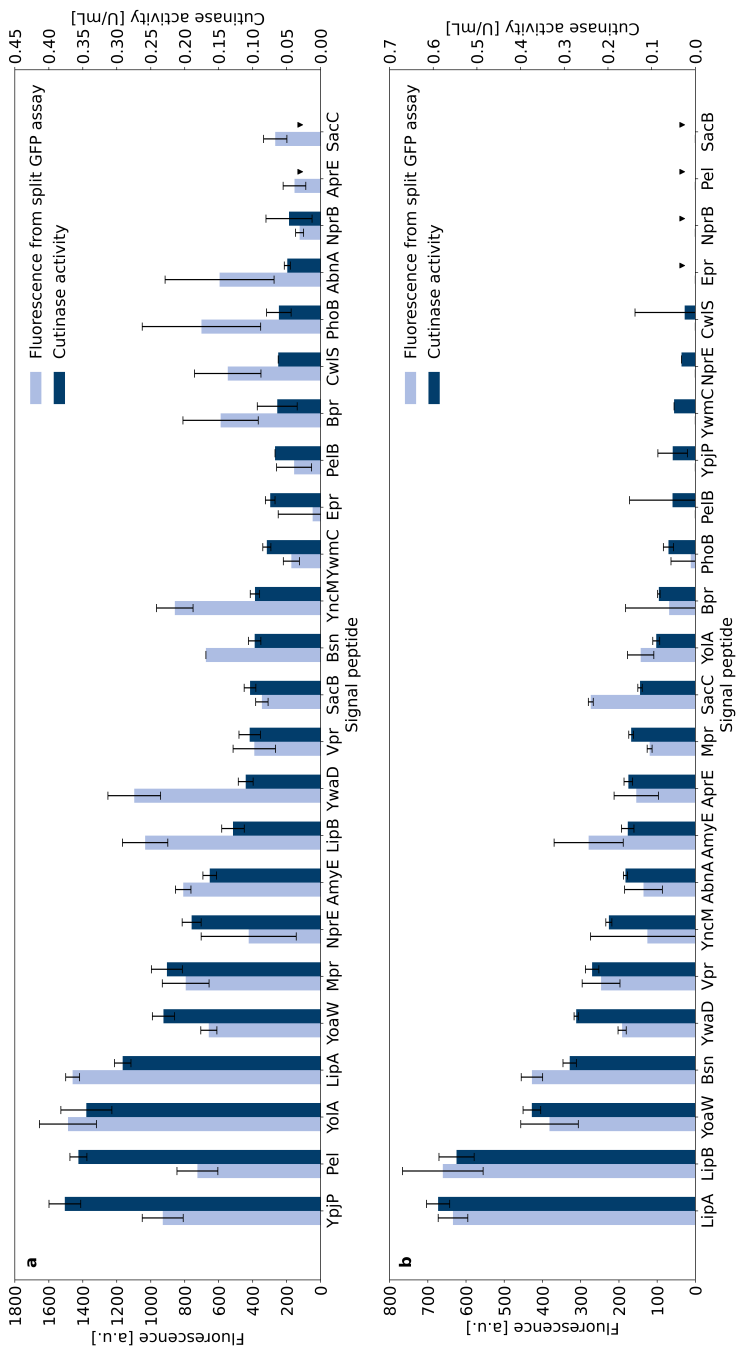

Fig. 3.19. Detection of PETase secreted by *C. glutamicum*. Supernatants from *C. glutamicum* pCMEx8-[SP]-PE-H (a) and pCMEx8-[SP]-LCC (b) were analyzed by cutinase activity and split GFP assay in technical duplicates of two main cultures from different batch cultivations. The fluorescence was determined after saturation of self-assembled GFP. Error bars show the 95% confidence intervals calculated with t values from replicates. Activities with a coefficient of determination of less than 0.99 are not considered (▾)

For all heterologous target proteins, the heterologous *F. solani* f. sp. *pisi* cutinase (refer to Section 3.2 and [175]) or the PETases PE-H (Fig. 3.19a) and LCC (Fig. 3.19b), different *B. subtilis* signal peptide sequences resulted in the best secretion performances. The signal peptide sequences of YpjP, Pel and YolA led to highest extracellular PE-H activities around 0.34 U mL^{-1}, while only low cutinase-GFP11 secretion performance was measured with the Pel signal peptide. Highest extracellular activities were measured for the LCC with the LipA and LipB signal peptides around 0.6 U mL^{-1} and almost no target protein was detected with the signal peptide NprE, which is known to lead to a high cutinase secretion by *C. glutamicum* [66, 175].

The split GFP assay results indicated a generally higher secretion of the PE-H than of the LCC, with maximum fluorescence values around 1 500 a.u. compared to 650 a.u. However, the correlation of the split GFP assay and the enzyme activity is not given for every PETase secretion strain. Out of the five strains with the highest secretion performance ranked by activity, only four LCC secreting strains were also identified using the split GFP assay. For PE-H secretion, only three of the best performing strains in the activity assay were under the five strains with the highest split GFP assay response. Although ranked only 9th and 10th based on their activities, PE-H secretion with LipB and YwaD signal peptides yielded a higher holo-GFP fluorescence than secretion with the signal peptide YpjP, the strain with the highest extracellular activity. This indicates that the signal peptides LipB and YwaD result in secretion of a lot of inactive PE-H. It could be that due to incomplete folding, misfolding, or partial protein degradation, the PETase is inactive, but the GFP11 tag is still accessible and functional. For strains with high extracellular activity and only low split GFP-assay fluorescence, such as the *C. glutamicum* pCMEx8-YpjP-PE-H, it is possible that the GFP11-tag of the secreted PETase is only partially accessible or susceptible to degradation.

Because the correlation between the split GFP assay and enzyme activities is not given for each PETase secretion strain, the split GFP assay was not used in further PETase secretion screenings and only the activity assay was included as a detection method in the process model for PETase secretion. The process model should also enable the identification of the most suitable strain, even if it cannot be distinguished from other strains using classical evaluation methods, such as for LCC secretion with signal peptides LipA and LipB.

3.3.2. Model building and experimental learning

An essential part of the screening workflow is the Bayesian process model described in Subsection 2.5.5. Before applying the process model to the LCC and PE-H secretion strain libraries, the influence of different experimental effects was investigated and an iterative cycle of model building and experimental improvements was performed. In the following, two findings of this workflow improvement are highlighted: first, the choice of the reaction kinetics is explained, second, a bias in the detected activities caused by the position of samples in the assay MTP is detailed.

In previous studies [128, 175] and Sections 3.1 and 3.2, the slope of absorption in the cutinase activity assay has been used to calculate enzymatic activities. Therefore, a process model assuming linear reaction kinetics was constructed first (see Fig. 3.20a and c).

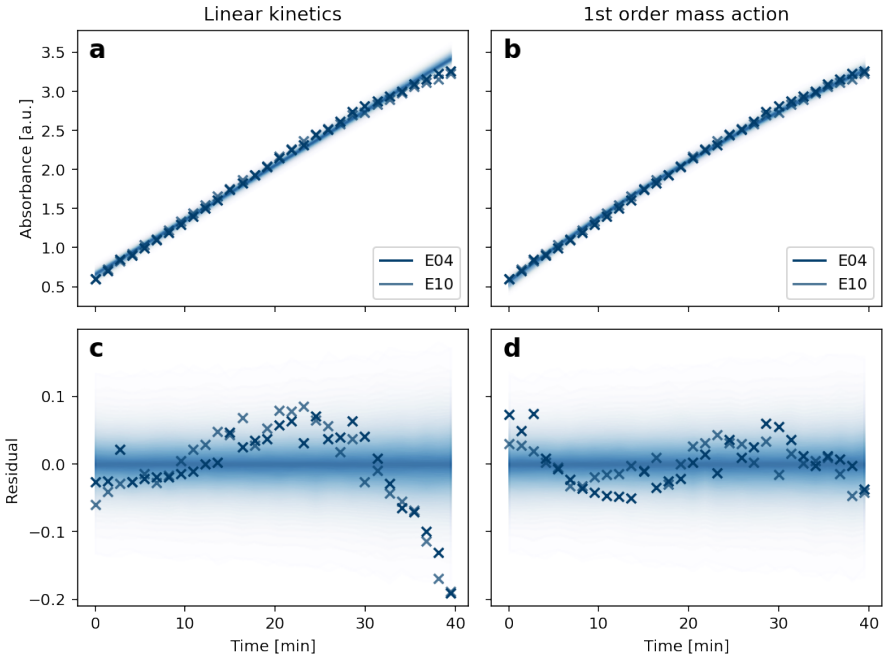

Fig. 3.20. Comparison of linear (a, c) and exponential (b, d) model for reaction kinetics in wells E04 and E10 of PE-H screening in round 1. Plots c and d show the residuals between data and model fit. The density bands visualize the distribution of predicted absorbance by the model [181]

Fig. 3.20a shows the trajectory of absorbance value over the incubation time of 40 min for the LCC combined with LipB as a signal peptide, a variant with a com-

parably high activity (see Fig. 3.25). After 35 min assay reaction time, the model significantly deviates from the measurements, which is also evident from the lack-of-fit indicated in the residual plot (Fig. 3.20a and c). The trajectory indicates that the lower substrate concentration seems to limit the reaction rate towards the end of measurement. Therefore, the kinetics was changed to a first order mass action law (Fig. 3.20b and d). This exponential trajectory describes the kinetics with a lower lack-of-fit (Fig. 3.20d). The first order kinetics were thus chosen in the final process model.

As part of model building, the influence of pipetting errors, batch effects and positional effects was investigated within the different MTPs of the automated screening workflow (Subsection 2.4.3). Fig. 3.21 shows one finding, namely a positional effect, where all 8 wells in the first column of the 96-well MTP show a systematically lower activity of the PETases (Subsection 2.5.5). The plot includes the median (white dot)

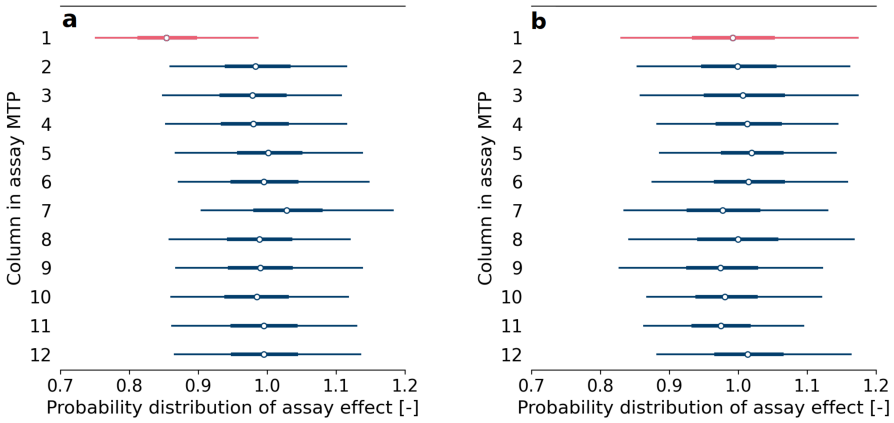

Fig. 3.21. Influence of position in assay MTP before (a) and after (b) experimental optimization of the assay. The probability distributions of the assay effect for each column is shown. An assay effect of 1 indicates that the position has no influence while smaller and higher values indicate a negative and positive influence on the activity, respectively [181]

as well as intervals of 94% probability (whiskers) for the parameter `assay effect` in all 12 columns of the assay MTP. A value of 1 indicates that the respective column has no influence on the activity, values smaller and greater than 1 correspond to lower and higher activities caused by the position in the MTP. The probability distributions are deduced from replicate data of the same signal peptide which lie in different columns. Fig. 3.21a shows the assay effect before experimental optimization. Here, it can be seen that wells in the first column show systematically lower activities with a median of around 0.85. However, the probability distribution inter-

val of the first column is similar to all other columns, indicating that all wells of this column are affected in the same manner. With this feedback from the model, the experimental workflow of the cutinase activity assay was re-examined.

The robotic liquid handler uses fixed tips, which distribute the substrate solution column-wise. The substrate solution dispense step of the last column is followed by a washing step with water to clean the needles and to prevent a carry-over of the substrate. However, dispense of the substrate in the first column was done with needles that were not conditioned with the organic substrate solution. Since the pipettes were not wetted initially, the first column contained slightly less substrate. Wetting of the PTFE-coated stainless steel tips with the organic substrate 4NPP diminished the positional effect of the first column. The experimental procedure was thus changed to include a step of tip wetting before the substrate is distributed into the assay MTP. The improved result can be seen in Fig. 3.21b.

After optimization, the positional effect of the first column was resolved and the posterior probabilities of the parameter `assay effect` are now similar for all columns. The prior for the assay effect is $f_{\text{assay effect}} \sim \text{LogNormal}(\mu = 0, \sigma = 0.1)$, which was chosen to allow for fluctuation of the activity around 20%. The highest density interval containing 94% of the prior probability mass is approximately $[0.83, 1.21]$. Overall, the distributions for all columns fluctuate in a similar range, with the median close to 1. This shows that the remaining certainty in the parameter `assay effect` is now reflecting random noise, rather than the systematic bias that was previously seen due to the positional effect. This shows that the assay effect was strongly reduced by the improvements of the pipetting operation and it can be neglected in the process model for future experiments.

To conclude, the examples show that the Bayesian process parameters are easy to interpret, since they mimic experimental errors. The width of their probability distributions can give an insight on how well the respective effect is characterized by the observed data. The analysis can also point out experimental sources of error and targets for workflow improvements, as it was demonstrated for the parameter `assay effect`. It was thus shown how the process model can guide experimental developments in an iterative cycle, where experimental improvements can simplify the required process model. An additional influential factor, namely a batch effect between different cultivation rounds, is discussed in section Subsection 3.3.4.

3.3.3. Signal peptide screening for PE-H secretion

Firstly, the process model was applied to the strain library of 24 signal peptides combined with the PE-H mutant Y250S. In order to facilitate the process of model building and assess model parameters such as the batch effect, the first round of screening consisted of two batch cultivations as described in Subsection 2.4.3. In each batch cultivation, all 24 variants were cultivated, resulting in 24 main cultures which were automatically inoculated from the respective 24 pre-cultures, induced with IPTG and harvested. The supernatant of each culture was subjected to the cutinase activity assay in duplicates (Subsection 2.5.4). Accordingly, the two batch cultivations led to four replicates for activity measurements per variant, which were simultaneously analyzed with the process model (Subsection 2.5.5). In the following, the combined analysis of these two batch cultivations is always referred to as round 1.

As a KPI for finding the most suitable signal peptide for PE-H secretion, the rate constant k of the first order reaction kinetics (Subsection 2.5.5) was chosen. The more active enzyme is present in the supernatant, the higher the rate constant k of the variant. The resulting probability of the KPI for round 1 is depicted in Fig. 3.22a. The

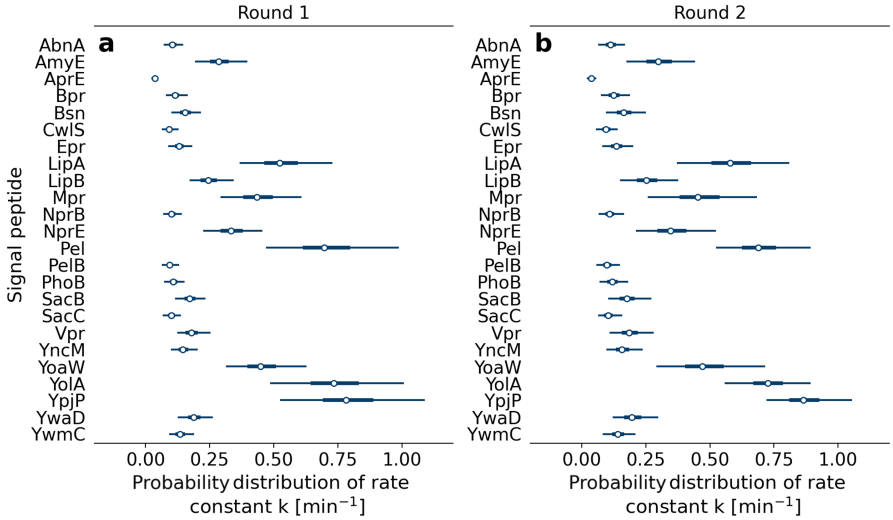

Fig. 3.22. Posterior probability distributions of rate constant k for each signal peptide variant of PE-H after round 1 (a) and round 2 (b). Modified from [181]

plot reveals that more than half of the signal peptides lead to a low rate constant, indicating that little active enzyme was present in the supernatant. This can be the

consequence of either low overall secretion or misfolding and thus inactive enzyme. Strikingly, four technical replicates are enough to distinguish these unpromising candidates from the remaining top 6 *B. subtilis* signal peptides, namely YpjP, YolA, Pel, LipA, YoaW and Mpr. Biological as well as technical errors such as the pipetting, which are taken into account by the model, cause uncertainty in the estimation, which is reflected by the broad distributions for k for the best signal peptides. For example, the 94% probability range (highest density interval) of the rate constant k for variant YpjP lies between $[0.53, 1.09]$ min^{-1}. The distributions shown here are the basis for the Thompson sampling algorithm to draw variants for the next cultivation round. To understand this process, the probability for each variant to be the best signal peptide so far was calculated as described in Subsection 2.5.5. The results are shown in Fig. 3.23a. After the first round of two biological replicates per variant

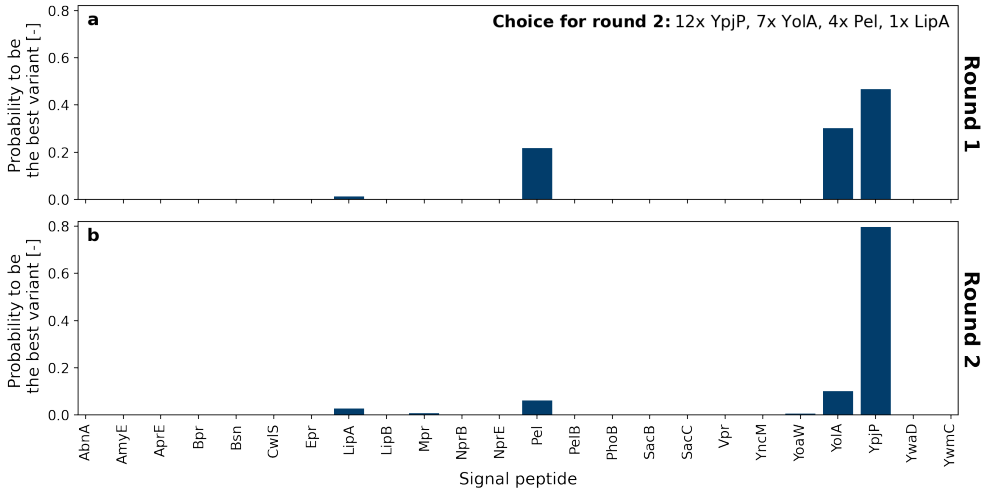

Fig. 3.23. Probability for each signal peptide to be the best variant for PE-H secretion after first and second round of screening [181]

with four technical replicates of the assay, only four signal peptides have a probability significantly greater than zero to be the best performing one. This demonstrates the exploitation part of Thompson sampling. Since the process model can clearly distinguish low performing variants from the top ones, they have no chance to be chosen for the next rounds. However, exploration is still necessary to distinguish the top four variants. Within these, YpjP has the highest probability of being the best signal peptide at around 46%. It is followed by YolA with around 30%, Pel with around 22% and LipA with less than 2%. For comparison, using *C. glutamicum* and the same plasmid expression system for secretion of a heterologous cutinase re-

sulted in very poor secretion performance for the *B. subtilis* signal peptides from Pel and YpjP (see Section 3.2 and [175]). These results confirm that the selection of an appropriate signal peptide is heavily dependent on the target protein.

As indicated by the text in subplot a, the choice for the next round reflects the probabilities of a signal peptide being the best, while small deviations in the ratio are caused by the small batch size of only 24 main culture wells. The whole screening workflow was conducted a second time with the respective replicates. Fig. 3.23b shows the results after the second screening round. With overall 28 replicates from three batch cultivations, YpjP shows the highest probability of around 80% to be the best signal peptide, while YolA, Pel, LipA and Mpr show significantly lower probabilities smaller than 10%. The resulting probability distributions for the KPIs can be seen in Figure Fig. 3.23b. For comparison, in a strategy with equal numbers of replicates per signal peptide, it would have taken 14 rounds of cultivation and thus more than four times longer to obtain the same certainty about the KPI for the most suitable signal peptide YpjP for PE-H secretion. This shows the efficiency of combined process model and Thompson sampling algorithm.

3.3.4. Signal peptide screening for LCC secretion

For signal peptide screening for secretion of the LCC mutant ICCG, the same strategy was used as for the successful screening with the secretory PE-H target protein. The first round comprised four technical replicates per variant accordingly, while the second was composed of suggestions from Thompson sampling. The resulting rankings after each round concerning the rate constant k are shown in Fig. 3.24.

Again, compared to the heterologous secretion of the *F. solani* f. sp. *pisi* cutinase (refer to Section 3.2 and [175]) or to the PE-H, two other signal peptide sequences, namely those of LipA and LipB, led to the highest extracellular LCC activities. All other signal peptides showed significantly less activity in the enzyme assay, more precisely less than half the rate constant. These results highlight the need to determine an appropriate signal peptide sequence for each target protein and thus the potential for combining automation and process models with Thompson sampling for accelerated screening. Moreover, it can be seen for round 1 (Fig. 3.24a) that the activities after secretion mediated with signal peptides LipA and LipB were very sim-

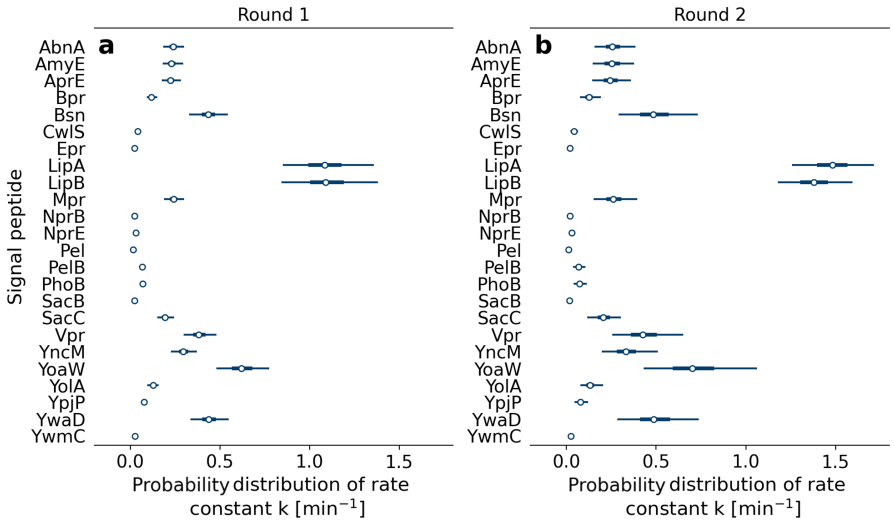

Fig. 3.24. Probability distributions of rate constant k for each signal peptide variant of LCC after round 1 (a) and round 2 (b). Modified from [181]

ilar when taking measurement uncertainties into account, where the median (white dot) of LipB is slightly higher.

For round 2 (Fig. 3.24b), Thompson sampling selected to an equal amount of replicates accordingly. With these data, the variants can be separated to a higher extend, where LipA shows a higher median in the probability distribution for k. Moreover, the higher number of replicates lead to narrower intervals of 95% probability (whiskers) compared to round 1. Although the variants other than LipA and LipB were not measured in round 2, their distributions are wider than before. This is caused by the the parameter `batch effect` of the process model (Subsection 2.5.5), which assumes an experimental error between different biological replicates in different rounds. Between round 1 and round 2, it could be observed that the activities increased for both LipA and LipB (compare Fig. 3.27 in section Subsection 3.3.6) due to an apparent batch effect. After only one round, no such effect could be assumed and the width of distributions is thus mainly influenced by deviation between technical replicates in the assay. However, with the information gained from LipA and LipB in both rounds, the process model can now account for the batch effect. Since the other variants were only measured in round 1, but uncertainty is added by the batch effect, the posterior distributions in Fig. 3.24b are wider. The batch effect will be further discussed in section Subsection 3.3.6.

Taking the probability distributions for k from Fig. 3.24, the question which signal peptide has the highest probability to be the best variant can be answered (Fig. 3.25). As for the ranking, Fig. 3.25a illustrates that LipA and LipB were very

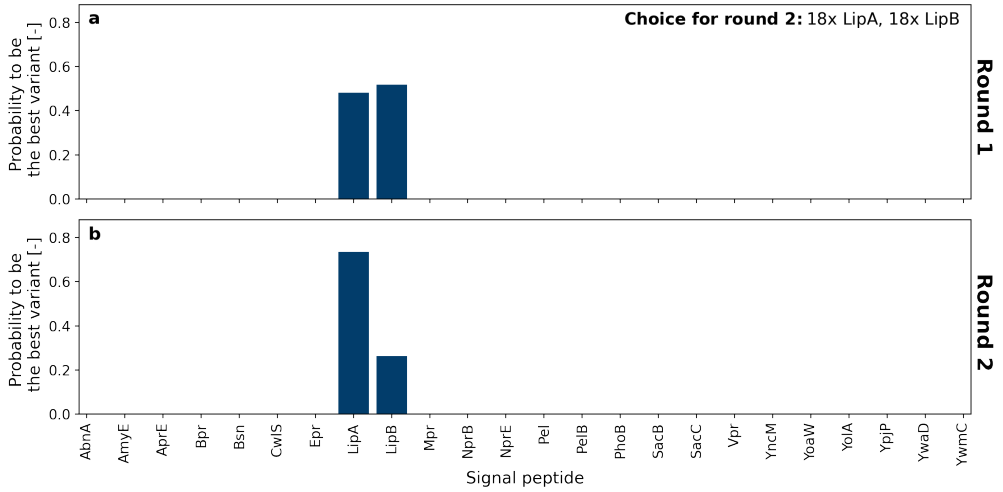

Fig. 3.25. Probability for each signal peptide to be the best variant for LCC secretion after first (a) and second (b) round of screening [181]

close after round 1, with LipB having a slightly higher probability to be advantageous concerning secretion. In Thompson sampling, the candidates for the next round are drawn randomly according to their probability of being optimal based on the available data. Here, probabilities of LipA and LipB are close to 50%, which results in 18 main cultures of each variant being suggested for round 2.

Fig. 3.25b shows the results after analysis of all 22 technical replicates of LipA and LipB after two rounds. Although the measurements were very similar for both variants (see classical statistical analysis in Subsection 3.3.6), the pairwise comparison of posterior samples results in a probability of around 75% that LipA is the best signal peptide. This shows the advantages of the process model, as no distinction between LipA and LipB could be seen in the classical statistical analysis. Importantly, the previously discussed positional effects and the batch effect between round 1 and 2 are taken into account, assuring that the rate constant k of the secreted enzyme is the dominant factor in the ranking. To investigate whether the screening is representative for pre-selection of variants, both LipA and LipB, as well as the third-best variant YoaW, were chosen for a scale-up application.

3.3.5. Comparison to batch fermentation in liter-scale bioreactors

In order to examine the scalability of the microcultivation process and to validate the results, *C. glutamicum* was cultivated in laboratory-scale STRs with 1 L working volume. LCC secretion mediated by the best *B. subtilis* signal peptides from microcultivation in the BioLector®, i.e., LipA, LipB and YoaW, were compared with laboratory-scale cultivation data depicted in the supplementary information (see Figs. A.12 and A.13). Maximum oxygen transfer rates of almost 100 mmol L^{-1} h^{-1} were reached after approximately 12 h and the final cell dry weights were around 9.1–9.6 g L^{-1}. The probability distributions of the rate constant k between the microliter- and liter-scale are compared in Fig. 3.26.

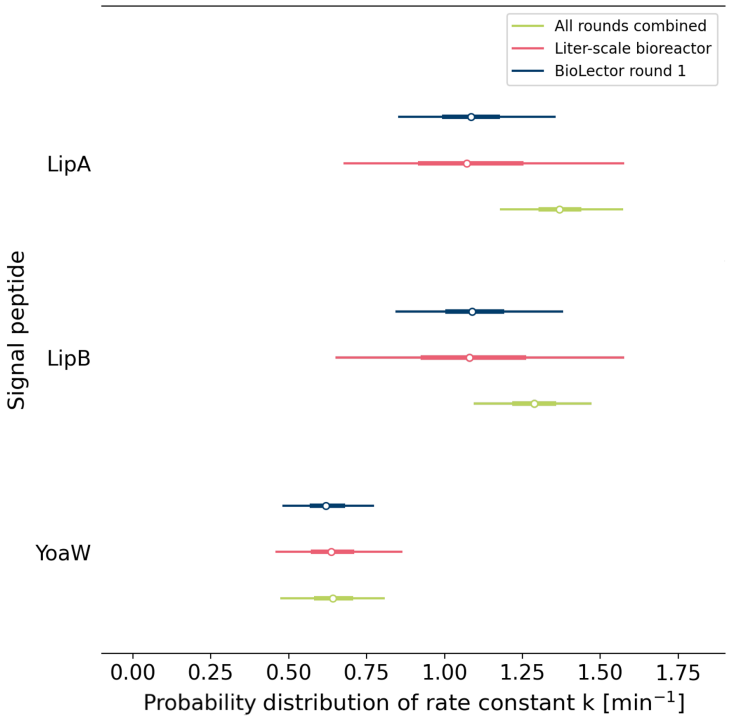

Fig. 3.26. Comparison of LCC rankings after microliter-scale BioLector® cultivation round 1, fermentation in liter-scale bioreactors and the combined analysis of all BioLector® and 1 L STR runs. Modified from [181]

The laboratory bioreactor data (red) show a similar ranking for the LipA and LipB signal peptides with YoaW approximately 40% behind. In comparison to the first BioLector® run (blue), the laboratory-scale bioreactor data shows a very similar performance ranking. Thus, protein production with *C. glutamicum* could be transferred

from the shaken cultivation in the BioLector® in microliter-scale to the 1 L STR in the liter-scale, as demonstrated elsewhere for cutinase secretion by *C. glutamicum* [71]. However, uncertainties are higher for LipA and LipB in the liter-scale bioreactor despite the equal number of biological replicates ($n = 2$). The higher uncertainty is likely to be caused by the different scheme of sampling. While all BioLector® experiments were sampled 4 h after induction, which corresponds to the early stationary phase, the fermentation was sampled at six different time points before and after induction. Due to different growth behaviors at the two scales, samples cannot be compared at the exact same process time. However, it is possible to take samples in identical growth phases. Accordingly, all available time points in the stationary phase were used for analysis of liter-scale bioreactor data. In case of LipA and LipB, these correspond to 22, 25 and 26 h process time (Figs. A.12 and A.13). The combination of three different sampling points with slightly different activities is likely to account for the higher uncertainty in the estimated rate constant k of LipA and LipB.

For the YoaW signal peptide, which was measured with four biological replicates in the bioreactor, the uncertainties are more similar to those of BioLector® replicates. Moreover, only one time point lied within the stationary phase, which was after 23.5 h process time. This also suggests that the different time points have an influence on the uncertainty. In the future, a time-dependent analysis for the activity could be conducted for both scales. However, the obtained results for the rate constant k are in good accordance for different scales. This demonstrate the advantage of the high-throughput approach, which is representing the larger scale well.

The probabilities in Fig. 3.26 shown in green are the results of combining round 1 of microliter-scale cultivation and the liter-scale bioreactor data with BioLector® round 2, where additional 18 biological replicates of LipA and LipB were measured. In contrast to the other probabilities, rate constants k for LipA and LipB can be better distinguished in the combined case. Moreover, a batch effect becomes evident, which can be detected from the higher overall median in the combined case. This is caused by overall higher activities in BioLector® round 2, which are further discussed later.

Overall, the scale-up shows that a large number of replicates is necessary to see differences of strain variants with a very similar secretion performance. This is often not feasible in laboratory-scale cultivations due to the higher costs and efforts. For this purpose, microliter-scale cultivations are beneficial as they allow for a large number of replicates and thus a better resolution of very similar variants.

3.3.6. Comparison to linear regression analysis

As a final validation of the method, a classical statistical analysis by linear regression of the absorbance measurements was conducted as described in Subsection 2.5.4 (Fig. 3.27). After the first round, LipA (dark blue) and LipB (light blue) cannot be dis-

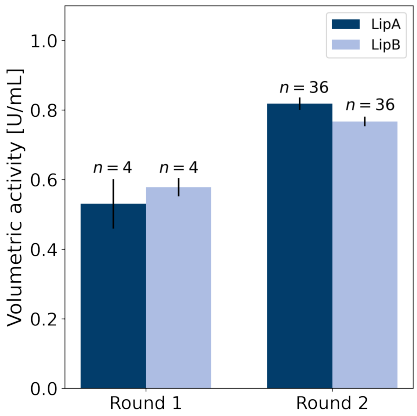

Fig. 3.27. Results for LipA (dark blue) and LipB (light blue) for two rounds of screening with classical data analysis by linear regression. Error bars represent the 95% confidence intervals. The number of replicates refers to the technical replicates [181]

tinguished, which can be seen by the overlapping 95% confidence intervals between the variants. While the activities are still similar between the variants in the second round, the higher number of replicates leads to smaller confidence intervals and indicates that LipA is the better signal peptide. However, the large batch effect between round 1 and round 2 for both variants makes it difficult to combine the results of both rounds in a purely statistical analysis. A main challenge is that technical and biological error could not be separated if all data are pooled for the linear regression, leading to large confidence intervals that do not allow to distinguish the variants. This is important though to exclude that LipA is favored by positional or batch effect in the second round. Batch effects most likely result from the activity assay and not from the cultivation, since differences in cryo culture viability are compensated by backscatter-triggered individual inoculation of the main cultures and induction of target protein expression and secretion (Section 3.2 and [175]). In the activity assay, the reaction mix has a limited stability only [128]. Although directly prepared before each assay, the reaction mix could impact enzymatic 4NPP degradation due to minor deviations in the composition and the poor solubility of the organic substrate. Here, the process model proves advantageous, since the uncertainty can be

assigned to several experimental and biological effects and the data from different rounds can inform the probability of both, batch effects and pipetting errors. Using the process model we determined a probability of around 75% for LipA being the best signal peptide (see Fig. 3.25). Overall, this demonstrates how the approach sampling can lead to more insight and faster screening and is thus promising for large libraries.

3.3.7. Conclusion of 3.3.

Heterologous Sec-dependent secretion of the PETases mutants LCC ICCG and PE-H Y250S could be shown for the first time with *C. glutamicum* as a secretion host. The best suited out of 24 *B. subtilis* Sec-type signal peptides was found using the automated procedures for high-throughput screening using the cutinase activity assay and the accompanying modeling in just two rounds of screening. As expected from previous studies on the secretion of heterologous proteins, the best signal peptide was different for the cutinase, LCC, and PE-H, implying that a suitable signal peptide must be found for each heterologous target protein. Even strain variants that were indistinguishable with classical methods due to batch effects could be resolved by the process model. The successful transfer from shaken cultivation in the BioLector® to 1 L STRs demonstrates the scalability of the secretion screening results.

Combined with the automated workflows for high-throughput cloning, this paves the way for screening of hundreds of strains or different process conditions in the Design-Build-Test-Learn cycle. Especially for application examples with much increased design space, where screening of all variants in multiple replicates becomes infeasible due to restrictions of resources in terms of both time and cost, model-based decision making as presented in this study is a valuable addition to the experimental high-throughput platforms. In the future, the process model could be further extended by process conditions such as the temperature or media composition. By solving these complex optimization problems such as strain and process conditions simultaneously, our modeling approach can become an even more powerful tool to tackle the exploration–exploitation dilemma even in expanded design spaces in the future.

4. Conclusion and outlook

To date, it is not possible to predict which combination of signal peptide and heterologous target protein is suitable for strong secretion with a particular host. In addition, other factors such as the 5'-untranslated region affect the secretion performance. In this work, different aspects of bacterial protein secretion were thoroughly investigated. Methods and automated workflows were established to test different combinations for heterologous protein secretion in a targeted approach in microliter-scale.

4.1. Automated plasmid construction

To enable automated workflows for plasmid construction and thus accelerated strain generation, a new pPBEx2-based *E. coli*/*C. glutamicum* shuttle vector was developed. The pCMEx-based plasmids enable the exchange of the RBS spacer and signal peptide sequence via cassette mutagenesis and the exchange of a constitutively expressed blue chromoprotein with the gene of interest via Golden Gate assembly. The insertion of the gene of interest and the corresponding unit operations Golden Gate assembly, *E. coli* heat-shock transformation, plasmid preparation based on magnetic beads and a restriction digestion as a control step for successful Golden Gate assembly were successfully automated. For this purpose, the Opentrons OT-2 liquid handling robot with integrated Thermocycler and Magnetic Module was used, which is characterized by relatively low costs, a simple operation and open source software. The overall and hands-on time for processing of 96 samples was greatly reduced to about 58% of that for the manual handling.

With automated workflows, targeted strain generation is likely no longer a limiting factor when generating and comparing different variants, such as combinations of signal peptide and target protein. Protocols for other cloning methods, such as Gibson assembly or phosphorothioate-based ligase-independent gene cloning

(PLICing), can also be established on the liquid handling robot in the future. Using more complex robotic platforms for molecular cloning steps, it would also be possible to integrate colony pickers to further reduce hands-on time. Integration of a suitable image recognition software could allow the colony picker to distinguish between blue and white colonies indicating unsuccessful and successful Golden Gate assembly, respectively, based on the blue chromoprotein expression. The scope of this work was the automated and accelerated plasmid generation only, not the overall strain generation. The host transformation method used here, electroporation, cannot really be automated with the equipment currently on the market. Automated workflows for conjugation as an alternative transformation method for *C. glutamicum* in contrast were developed by Tenhaef et al. [123]. With appropriate adjustments in the plasmid backbone, this approach would also be possible using pCMEx-based plasmids. In addition, the generation of cryo-conserved cultures could be automated using a robotic platform equipped for cultivation.

4.2. Automated cultivation and screening workflow

Automated workflows for cultivation and screening were established on a Tecan Freedom EVO® 200 with integrated BioLector® Pro for cultivation in microliter-scale, centrifuge, cooled sample storage and MTP reader. By integrating the pre-culture handling into the robotic workflow, the hands-on time was reduced significantly. Autonomous decision making based on the individual backscatter-signals or triggered by defined time periods resulted in a high degree of standardization and comparability of growth phenotypes. By using the workflow for one main culture per pre-culture, up to 24 *C. glutamicum* secretion strains can be compared in one experiment within approximately 1.5 days from cultivation to detection of the target protein in the supernatant by cutinase activity and split GFP assay, and even less than 24 h without the split GFP assay. Human interaction is only needed before starting the cultivation and to provide assay reagents with a limited stability, such as the reaction mix of the cutinase activity assay. The 48 wells of a FlowerPlate® for cultivation in the BioLector®, that cannot be exchanged by the robotic platform, are still a limiting factor. By integrating a freezer for storage of cryo-conserved cultures and a recycling strategy for the FlowerPlate®, more cultivation rounds would be possible in one experiment. Depending on the target proteins for future investigations, further assays for detection

of secreted target proteins could be automated using the robotic platform, e.g, for activity measurements or ELISA. This is necessary in cases were the split GFP assay is not suitable for screening approaches, e.g., if the GFP11-tag is not accessible. For testing of new cultivation workflows, the *C. glutamicum* pPBEx2-PhoD^{Cg}-GFP can be used as a model strain, enabling the online monitoring of product formation with tightly controlled induction of Tat-dependent GFP secretion.

4.3. GFP1-10 production and split GFP assay

It was shown that the split GFP assay can be applied for screening of cutinase-GFP11 secreted by *C. glutamicum*, and that the fluorescence of self-assembled GFP correlates with cutinase activity. The split GFP assay can easily be automated and adapted to other target proteins, making it suitable for use in high-throughput protein secretion screenings. This first requires verification by other methods such as Western blots that the GFP11-tag of the target protein is accessible. For high-throughput screenings using the split GFP assay, high amounts of detector protein GFP1-10 are needed. In this work, the intracellular GFP1-10 production by *E. coli* in inclusion bodies was scaled from shake flasks to laboratory-scale bioreactors. An intermittent glucose feed triggered by the DO signal was used to produce detector solution for up to 385 screenings in 96-well MTPs in one fed-batch fermentation. Storage of this detector solution was possible for at least seven months at –20 °C with only little performance loss. However, holo-GFP assembly seems to be affected by the signal peptide sequence and even mutations in only three amino acid positions of a signal peptide. This leads to divergent results for activity and fluorescence, with the number of outliers appearing to depend on the target protein. For cutinase-GFP11 secretion, the five best performing signal peptides were identified with both the split GFP and the cutinase activity assay, making the split GFP assay a valuable tool for rapid strain pre-selection. Still, the results must be verified by other methods, such as the activity or ELISA. For some of the PETase secretion strains, no correlation between the split GFP and cutinase activity assay was found and therefore, the split GFP assay was not used for signal peptide screening and not included in the accompanying process model.

It remains unknown why the correlation of activity and split GFP assay is not given for every combination of signal peptide and target protein. It could be investigated,

how the signal peptide sequence affects folding of the secreted protein and thus the accessibility of the GFP11-tag and enzymatic activity. Furthermore, pre-maturation of GFP1-10 could accelerate the holo-GFP formation and thus fluorescence measurement. However, this would slow down the preparation of the detector solution [120, 121].

4.4. Cutinase secretion by *C. glutamicum*

Besides the signal peptide sequence, the 5'-untranslated region affects protein secretion including the RBS. This also seems to be partly responsible for the approximately 2.5x poorer NprE-cutinase-GFP11 secretion with the pCMEx8 plasmid compared to pPBEx2. RBS spacer lengths from 4–12 nt were tested for cutinase-GFP11 secretion combined with the *B. subtilis* signal peptides NprE, Pel, Bsn and Epr in *C. glutamicum*. It was shown that the shortest spacers resulted in poor secretion only and a RBS spacer length of at least 8 nt should be used. An 8 nt spacer was used for an automated signal peptide screening and consistent with previous studies such as by Hemmerich et al. [72], with NprE being the most suitable signal peptide for cutinase-GFP11 secretion in *C. glutamicum*. In addition to the *C. glutamicum* ATCC 13032, the biosensor strain K9 was also used for screening. The *C. glutamicum* K9 has its limitations in screening structurally distinct signal peptides by the biosensor output as indicated by the cutinase-GFP11 screening. Nevertheless, it can be utilized for comparing structurally similar signal peptides. An overall dose-dependent response was measured when comparing different spacer lengths for NprE-cutinase-GFP11 secretion mediated by the NprE signal peptide or the approach with the error-prone PCR of the Pel sequence. For the latter screening approach, results were successfully transferred from batch to fed-batch cultivation in microliter-scale.

If amino acids are present between the signal peptide and the target protein, they may influence secretion. This could also be partly responsible for the poorer secretion with pCMEx8-based compared to pPBEx2-based plasmids, since the linker sequence between signal peptide and cutinase gene is different in the two plasmids. How this manifests itself and whether there is an optimal amino acid sequence for the linker between the signal peptide sequence and the target gene in pCMEx8 could be investigated in further studies.

4.5. Model-based PETase secretion screening

In addition to the cutinase, Sec-dependent secretion of the heterologous PETases LCC mutant ICCG and PE-H mutant Y250S was investigated and could be shown for the first time using *C. glutamicum* as a secretion host. To identify the best out of 24 *B. subtilis* signal peptides, automated workflows were used for high-throughput screening, and in a collaborative project, an accompanying modeling approach was used for evaluation of secretion performance. As a result, the most suitable Sec-dependent signal peptide was identified with a probability of 80% for the PE-H and 75% for the LCC after only three batch cultivations. Due to the modeling approach, batch effects could be taken into account and the differentiation of the two strains *C. glutamicum* pCMEx8-LipA-LCC and pCMEx8-LipB-LCC with very comparable secretion was possible, which was not accomplished with classical evaluation. A successful scale-up from shaken microliter-scale cultivation in the BioLector® to stirred tank reactors with 1 L working volume was demonstrated.

The process model could be adapted to other target proteins and thus detection methods in the future. A continued model development could lead to further process conditions such as the temperature being taken into account.

In this work, the focus was on the investigation of Sec-dependent secretion with *C. glutamicum* by combining 9 different RBS spacers with 24 *B. subtilis* signal peptides and 3 target proteins under comparable cultivation conditions. However, many other effects could additionally play a role, such as the substrate uptake, transcription rate, extracellular protein folding, and the expression system itself. Thus, the design space can and needs to be further expanded to eventually fully understand protein secretion and the structure-function relationship of signal peptides and target proteins. In the best case, it will eventually be possible to predict which combinations are suitable for the successful secretion of a particular target protein. Here, laboratory automation and versatile detection methods besides the split GFP assay, e.g., the NanoLuc luciferase-based assay [204], combined with the process modeling approach can be a valuable tool to find possible patterns. This also shows that interdisciplinary collaborations offer enormous potential for solving complex biological problems in the future and certainly not only with regard to this example of heterologous protein secretion.

References

[1] S. Kinoshita, S. Udaka, and M. Shimono. “Studies on the amino acid fermentation”. In: *J Gen Appl Microbiol* 3.3 (1957), pp. 193–205. DOI: 10.2323/jgam.3.193.

[2] H. Yukawa and M. Inui, eds. *Microbiology Monographs. Corynebacterium glutamicum. Biology and Biotechnology*. Springer Berlin Heidelberg, 2013. 416 pp. ISBN: 978-3-642-29857-8. DOI: 10.1007/978-3-642-29857-8.

[3] N. Bayan, C. Houssin, M. Chami, and G. Leblon. “Mycomembrane and S-layer: two important structures of *Corynebacterium glutamicum* cell envelope with promising biotechnology applications”. In: *J Biotechnol* 104.1 (2003), pp. 55–67. ISSN: 0168-1656. DOI: 10.1016/S0168-1656(03)00163-9.

[4] J. Kalinowski, B. Bathe, D. Bartels, N. Bischoff, M. Bott, A. Burkovski, N. Dusch, L. Eggeling, B. J. Eikmanns, L. Gaigalat, A. Goesmann, M. Hartmann, K. Huthmacher, R. Krämer, B. Linke, A. C. McHardy, F. Meyer, B. Möckel, W. Pfefferle, A. Pühler, D. A. Rey, C. Rückert, O. Rupp, H. Sahm, V. F. Wendisch, I. Wiegräbe, and A. Tauch. “The complete *Corynebacterium glutamicum* ATCC 13032 genome sequence and its impact on the production of l-aspartate-derived amino acids and vitamins”. In: *J Biotechnol* 104.1-3 (2003), pp. 5–25. DOI: 10.1016/s0168-1656(03)00154-8.

[5] M. Ikeda and S. Nakagawa. “The *Corynebacterium glutamicum* genome: features and impacts on biotechnological processes”. In: *Appl Microbiol Biotechnol* 62.2-3 (2003), pp. 99–109. DOI: 10.1007/s00253-003-1328-1.

[6] M. Jakoby, C.-E. Ngouoto-Nkili, and A. Burkovski. “Construction and application of new *Corynebacterium glutamicum* vectors”. In: *Biotechnol Tech* 13.6 (1999), pp. 437–441. DOI: 10.1023/a:1008968419217.

[7] R. Gauttam, C. Desiderato, L. Jung, A. Shah, and B. J. Eikmanns. “A step forward: compatible and dual-inducible expression vectors for gene co-expression in *Corynebacterium glutamicum*”. In: *Plasmid* 101 (2019), pp. 20–27. DOI: 10.1016/j.plasmid.2018.12.004.

[8] P. J. Bakkes, P. Ramp, A. Bida, D. Dohmen-Olma, M. Bott, and R. Freudl. “Improved pEKEx2-derived expression vectors for tightly controlled production of recombinant proteins in *Corynebacterium glutamicum*”. In: *Plasmid* 112 (2020), p. 102540. DOI: 10.1016/j.plasmid.2020.102540.

[9] M. Chai, C. Deng, Q. Chen, W. Lu, Y. Liu, J. Li, G. Du, X. Lv, and L. Liu. “Synthetic biology toolkits and metabolic engineering applied in *Corynebacterium glutamicum* for biomanufacturing”. In: *ACS Synth Biol* (2021). DOI: 10.1021/acssynbio.1c00355.

[10] L. Eggeling and M. Bott, eds. *Handbook of Corynebacterium glutamicum*. CRC Press, 2005. 632 pp. DOI: 10.1201/9781420039696.

[11] T. Hermann. “Industrial production of amino acids by coryneform bacteria”. In: *J Biotechnol* 104.1-3 (2003), pp. 155–172. DOI: 10.1016/s0168-1656(03)00149-4.

[12] W. Leuchtenberger, K. Huthmacher, and K. Drauz. “Biotechnological production of amino acids and derivatives: current status and prospects”. In: *Appl Microbiol Biotechnol* 69.1 (2005), pp. 1–8. DOI: 10.1007/s00253-005-0155-y.

[13] X.-X. Liu, Y. Li, and Z.-H. Bai. “*Corynebacterium glutamicum* as a robust microbial factory for production of value-added proteins and small molecules: fundamentals and applications”. In: *Microbial Cell Factories Engineering for Production of Biomolecules*. Ed. by V. Singh. Academic Press, 2021, pp. 235–263. ISBN: 978-0-12-821477-0. DOI: 10.1016/b978-0-12-821477-0.00006-4.

[14] S. Okino, M. Inui, and H. Yukawa. “Production of organic acids by *Corynebacterium glutamicum* under oxygen deprivation”. In: *Appl Microbiol Biotechnol* 68.4 (2005), pp. 475–480. DOI: 10.1007/s00253-005-1900-y.

[15] M. Inui, H. Kawaguchi, S. Murakami, A. A. Vertès, and H. Yukawa. “Metabolic engineering of *Corynebacterium glutamicum* for fuel ethanol production under oxygen-deprivation conditions”. In: *J Mol Microbiol Biotechnol* 8.4 (2004), pp. 243–254. DOI: 10.1159/000086705.

[16] B. Litsanov, A. Kabus, M. Brocker, and M. Bott. “Efficient aerobic succinate production from glucose in minimal medium with *Corynebacterium glutamicum*”. In: *Microb Biotechnol* 5.1 (2011), pp. 116–128. DOI: 10.1111/j.1751-7915.2011.00310.x.

[17] A. Zahoor, S. N. Lindner, and V. F. Wendisch. “Metabolic engineering of *Corynebacterium glutamicum* aimed at alternative carbon sources and new products”. In: *Comput Struct Biotechnol J* 3.4 (2012), e201210004. DOI: 10.5936/csbj.201210004.

[18] J.-Y. Lee, Y.-A. Na, E. Kim, H.-S. Lee, and P. Kim. “The actinobacterium *Corynebacterium glutamicum*, an industrial workhorse”. In: *J Microbiol Biotechnol* 26.5 (2016), pp. 807–822. DOI: 10.4014/jmb.1601.01053.

[19] A. A. Vertès. “Protein secretion systems of *Corynebacterium glutamicum*”. In: *Corynebacterium glutamicum: Biology and Biotechnology*. Ed. by H. Yukawa and M. Inui. Berlin, Heidelberg: Springer Berlin Heidelberg, 2013, pp. 351–389. ISBN: 978-3-642-29857-8. DOI: 10.1007/978-3-642-29857-8_13.

[20] R. Freudl. “Beyond amino acids: use of the *Corynebacterium glutamicum* cell factory for the secretion of heterologous proteins”. In: *J Biotechnol* 258 (2017), pp. 101–109. DOI: 10.1016/j.jbiotec.2017.02.023.

[21] M. J. Lee and P. Kim. “Recombinant protein expression system in *Corynebacterium glutamicum* and its application”. In: *Front Microbiol* 9 (2018). DOI: 10.3389/fmicb.2018.02523.

[22] G. Georgiou and P. Valax. “Expression of correctly folded proteins in *Escherichia coli*”. In: *Curr Opin Biotechnol* 7.2 (1996), pp. 190–197. DOI: 10.1016/s0958-1669(96)80012-7.

[23] A. Villaverde and M. M. Carrió. “Protein aggregation in recombinant bacteria: biological role of inclusion bodies”. In: *Biotechnol Lett* 25.17 (2003), pp. 1385–1395. DOI: 10.1023/a:1025024104862.

[24] E. García-Fruitós, N. González-Montalbán, M. Morell, A. Vera, R. M. Ferraz, A. Arís, S. Ventura, and A. Villaverde. “Aggregation as bacterial inclusion bodies does not imply inactivation of enzymes and fluorescent proteins”. In: *Microb Cell Factories* 4.1 (2005). DOI: 10.1186/1475-2859-4-27.

[25] V. D. Jäger, R. Lamm, K. Küsters, G. Ölcücü, M. Oldiges, K.-E. Jaeger, J. Büchs, and U. Krauss. “Catalytically-active inclusion bodies for biotechnology—general concepts, optimization, and application”. In: *Appl Microbiol Biotechnol* 104.17 (2020), pp. 7313–7329. DOI: 10.1007/s00253-020-10760-3.

[26] B. Eggenreich, M. Willim, D. J. Wurm, C. Herwig, and O. Spadiut. “Production strategies for active heme-containing peroxidases from *E. coli* inclusion bodies – a review”. In: *Biotechnol Rep* 10 (2016), pp. 75–83. DOI: 10.1016/j.btre.2016.03.005.

[27] D. Humer and O. Spadiut. “Wanted: more monitoring and control during inclusion body processing”. In: *World J Microbiol Biotechnol* 34.11 (2018). DOI: 10.1007/s11274-018-2541-5.

[28] Y. Wang, C. Ling, Y. Chen, X. Jiang, and G.-Q. Chen. “Microbial engineering for easy downstream processing”. In: *Biotechnol Adv* 37.6 (2019), p. 107365. DOI: 10.1016/j.biotechadv.2019.03.004.

[29] M. Schallmey, A. Singh, and O. P. Ward. “Developments in the use of *Bacillus* species for industrial production”. In: *Can J Microbiol* 50.1 (2004), pp. 1–17. DOI: 10.1139/w03-076.

[30] J. M. van Dijl and M. Hecker. “*Bacillus subtilis*: from soil bacterium to super-secreting cell factory”. In: *Microb Cell Factories* 12.1 (2013), p. 3. DOI: 10.1186/1475-2859-12-3.

[31] X. C. Wu, W. Lee, L. Tran, and S. L. Wong. “Engineering a *Bacillus subtilis* expression-secretion system with a strain deficient in six extracellular proteases”. In: *J Bacteriol* 173.16 (1991), pp. 4952–4958. DOI: 10.1128/jb.173.16.4952-4958.1991.

[32] K. Murashima, C.-L. Chen, A. Kosugi, Y. Tamaru, R. H. Doi, and S.-L. Wong. “Heterologous production of *Clostridium cellulovorans* engB, using protease-deficient *Bacillus subtilis*, and preparation of active recombinant cellulosomes”. In: *J Bacteriol* 184.1 (2002), pp. 76–81. DOI: 10.1128/jb.184.1.76-81.2002.

[33] H. Nguyen, T. Phan, and W. Schumann. “Analysis and application of *Bacillus subtilis* sortases to anchor recombinant proteins on the cell wall”. In: *AMB Expr* 1.1 (2011), p. 22. DOI: 10.1186/2191-0855-1-22.

[34] P. Natale, T. Brüser, and A. J. M. Driessen. “Sec- and Tat-mediated protein secretion across the bacterial cytoplasmic membrane—distinct translocases and mechanisms”. In: *Biochim Biophys Acta - Biomembr* 1778.9 (2008), pp. 1735–1756. DOI: 10.1016/j.bbamem.2007.07.015.

[35] R. Freudl. “Leaving home ain’t easy: protein export systems in Gram-positive bacteria”. In: *Res Microbiol* 164.6 (2013), pp. 664–674. DOI: 10.1016/j.resmic.2013.03.014.

[36] J. Luirink, S. High, H. Wood, A. Giner, D. Tollervey, and B. Dobberstein. “Signal-sequence recognition by an *Escherichia coli* ribonucleoprotein complex”. In: *Nature* 359.6397 (1992), pp. 741–743. DOI: 10.1038/359741a0.

[37] K. Shen, S. Arslan, D. Akopian, T. Ha, and S.-o. Shan. “Activated GTPase movement on an RNA scaffold drives co-translational protein targeting”. In: *Nature* 492.7428 (2012), pp. 271–275. DOI: 10.1038/nature11726.

[38] K. Denks, A. Vogt, I. Sachelaru, N.-A. Petriman, R. Kudva, and H.-G. Koch. “The Sec translocon mediated protein transport in prokaryotes and eukaryotes”. In: *Mol Membr Biol* 31.2-3 (2014), pp. 58–84. DOI: 10.3109/09687688.2014.907455.

[39] D. J. du Plessis, N. Nouwen, and A. J. Driessen. “The Sec translocase”. In: *Biochim Biophys Acta - Biomembr* 1808.3 (2011), pp. 851–865. DOI: 10.1016/j.bbamem.2010.08.016.

[40] U. Swidersky, H. Hoffschulte, and M. Müller. “Determinants of membrane-targeting and transmembrane translocation during bacterial protein export.” In: *EMBO J* 9.6 (1990), pp. 1777–1785. DOI: 10.1002/j.1460-2075.1990.tb08302.x.

[41] J. Wild, P. Rossmeissl, W. A. Walter, and C. A. Gross. “Involvement of the DnaK-DnaJ-GrpE chaperone team in protein secretion in *Escherichia coli*”. In: *J Bacteriol* 178 (1996), pp. 3608–3613. DOI: 10.1128/jb.178.12.3608-3613.1996.

[42] W. R. Lyon, C. M. Gibson, and M. G. Caparon. “A role for Trigger Factor and an Rgg-like regulator in the transcription, secretion and processing of the cysteine proteinase of *Streptococcus pyogenes*”. In: *EMBO J* 17.21 (1998), pp. 6263–6275. DOI: 10.1093/emboj/17.21.6263.

[43] M.-P. Castanié-Cornet, N. Bruel, and P. Genevaux. “Chaperone networking facilitates protein targeting to the bacterial cytoplasmic membrane”. In: *Biochim Biophys Acta - Mol Cell Res* 1843.8 (2014), pp. 1442–1456. DOI: 10.1016/j.bbamcr.2013.11.007.

[44] M. A. Catipovic, B. W. Bauer, J. J. Loparo, and T. A. Rapoport. “Protein translocation by the SecA ATPase occurs by a power-stroke mechanism”. In: *EMBO J* 38.9 (2019). DOI: 10.15252/embj.2018101140.

[45] T. Tsukazaki, H. Mori, Y. Echizen, R. Ishitani, S. Fukai, T. Tanaka, A. Perederina, D. G. Vassylyev, T. Kohno, A. D. Maturana, K. Ito, and O. Nureki. “Structure and function of a membrane component SecDF that enhances protein export”. In: *Nature* 474.7350 (2011), pp. 235–238. DOI: 10.1038/nature09980.

[46] T. Tsukazaki. “Structure-based working model of SecDF, a proton-driven bacterial protein translocation factor”. In: *FEMS Microbiol Lett* 365.12 (2018). DOI: 10.1093/femsle/fny112.

[47] S. L. Rusch and D. A. Kendall. “Interactions that drive Sec-dependent bacterial protein transport”. In: *Biochemistry* 46.34 (2007), pp. 9665–9673. DOI: 10.1021/bi7010064.

[48] T. Palmer and B. C. Berks. “The Twin-arginine translocation (Tat) protein export pathway”. In: *Nat Rev Microbiol* 10.7 (2012), pp. 483–496. DOI: 10.1038/nrmicro2814.

[49] F. Lausberg, S. Fleckenstein, P. Kreutzenbeck, J. Fröbel, P. Rose, M. Müller, and R. Freudl. “Genetic evidence for a tight cooperation of TatB and TatC during productive recognition of Twin-arginine (Tat) signal peptides in *Escherichia coli*”. In: *PLoS One* 7.6 (2012). Ed. by M. Bassilana, e39867. DOI: 10.1371/journal.pone.0039867.

[50] F. Alcock, M. A. B. Baker, N. P. Greene, T. Palmer, M. I. Wallace, and B. C. Berks. “Live cell imaging shows reversible assembly of the TatA component of the twin-arginine protein transport system”. In: *Proc Natl Acad Sci* 110.38 (2013), E3650–E3659. DOI: 10.1073/pnas.1306738110.

[51] Y. Kikuchi, M. Date, H. Itaya, K. Matsui, and L.-F. Wu. “Functional analysis of the twin-arginine translocation pathway in *Corynebacterium glutamicum* ATCC 13869”. In: *Appl Environ Microbiol* 72.11 (2006), pp. 7183–7192. DOI: 10.1128/aem.01528-06.

[52] R. Freudl. “Signal peptides for recombinant protein secretion in bacterial expression systems”. In: *Microb Cell Factories* 17.1 (2018). DOI: 10.1186/s12934-018-0901-3.

[53] G. von Heijne. “How signal sequences maintain cleavage specificity”. In: *J Mol Biol* 173.2 (1984), pp. 243–251. DOI: 10.1016/0022-2836(84)90192-x.

[54] B. C. Berks. “A common export pathway for proteins binding complex redox cofactors?” In: *Mol Microbiol* 22.3 (1996), pp. 393–404. DOI: 10.1046/j.1365-2958.1996.00114.x.

[55] S. Cristobal. “Competition between Sec- and TAT-dependent protein translocation in *Escherichia coli*”. In: *EMBO J* 18.11 (1999), pp. 2982–2990. DOI: 10.1093/emboj/18.11.2982.

[56] N. Blaudeck, P. Kreutzenbeck, R. Freudl, and G. A. Sprenger. “Genetic analysis of pathway specificity during posttranslational protein translocation across the *Escherichia coli* plasma membrane”. In: *J Bacteriol* 185.9 (2003), pp. 2811–2819. DOI: 10.1128/jb.185.9.2811-2819.2003.

[57] W. R. Zückert. “Secretion of bacterial lipoproteins: through the cytoplasmic membrane, the periplasm and beyond”. In: *Biochim Biophys Acta - Mol Cell Res* 1843.8 (2014), pp. 1509–1516. DOI: 10.1016/j.bbamcr.2014.04.022.

[58] C. L. Giltner, Y. Nguyen, and L. L. Burrows. “Type IV pilin proteins: versatile molecular modules”. In: *Microbiol Mol Biol Rev* 76.4 (2012), pp. 740–772. DOI: 10.1128/mmbr.00035-12.

[59] F. Teufel, J. J. A. Armenteros, A. R. Johansen, M. H. Gíslason, S. I. Pihl, K. D. Tsirigos, O. Winther, S. Brunak, G. von Heijne, and H. Nielsen. “SignalP 6.0 predicts all five types of signal peptides using protein language models”. In: *Nat Biotechnol* (2022). DOI: 10.1038/s41587-021-01156-3.

[60] A. Elnaggar, M. Heinzinger, C. Dallago, G. Rehawi, W. Yu, L. Jones, T. Gibbs, T. Feher, C. Angerer, M. Steinegger, D. Bhowmik, and B. Rost. “ProtTrans: towards cracking the language of lifes code through self-supervised deep learning and high performance computing”. In: *IEEE Trans Pattern Anal Mach Intell* (2021), pp. 1–1. DOI: 10.1109/TPAMI.2021.3095381.

[61] C. Peng, Y. Guo, S. Ren, C. Li, F. Liu, and F. Lu. “SPSED: a signal peptide secretion efficiency database”. In: *Front Bioeng Biotechnol* 9 (2022). DOI: 10.3389/fbioe.2021.819789.

[62] P. A. Lee, D. Tullman-Ercek, and G. Georgiou. “The bacterial twin-arginine translocation pathway”. In: *Annu Rev Microbiol* 60.1 (2006), pp. 373–395. DOI: 10.1146/annurev.micro.60.080805.142212.

[63] D. Meissner, A. Vollstedt, J. M. van Dijl, and R. Freudl. “Comparative analysis of twin-arginine (Tat)-dependent protein secretion of a heterologous model protein (GFP) in three different Gram-positive bacteria”. In: *Appl Microbiol Biotechnol* 76.3 (2007), pp. 633–642. DOI: 10.1007/s00253-007-0934-8.

[64] Y. Song, G. Fu, H. Dong, J. Li, Y. Du, and D. Zhang. “High-efficiency secretion of β-mannanase in *Bacillus subtilis* through protein synthesis and secretion optimization”. In: *J Agric Food Chem* 65.12 (2017), pp. 2540–2548. DOI: 10.1021/acs.jafc.6b05528.

[65] Y. Kikuchi, H. Itaya, M. Date, K. Matsui, and L.-F. Wu. “TatABC overexpression improves *Corynebacterium glutamicum* Tat-dependent protein secretion”. In: *Appl Environ Microbiol* 75.3 (2009), pp. 603–607. DOI: 10.1128/aem.01874-08.

[66] J. Hemmerich, M. Moch, S. Jurischka, W. Wiechert, R. Freudl, and M. Oldiges. “Combinatorial impact of sec signal peptides from *Bacillus subtilis* and bioprocess conditions on heterologous cutinase secretion by *Corynebacterium glutamicum*”. In: *Biotechnol Bioeng* 116.3 (2018), pp. 644–655. DOI: 10.1002/bit.26873.

[67] U. Brockmeier, M. Caspers, R. Freudl, A. Jockwer, T. Noll, and T. Eggert. “Systematic screening of all signal peptides from *Bacillus subtilis*: a powerful strategy in optimizing heterologous protein secretion in gram-positive bacteria”. In: *J Mol Biol* 362.3 (2006), pp. 393–402. DOI: 10.1016/j.jmb.2006.07.034.

[68] G. Fu, J. Liu, J. Li, B. Zhu, and D. Zhang. “Systematic screening of optimal signal peptides for secretory production of heterologous proteins in *Bacillus subtilis*”. In: *J Agric Food Chem* 66.50 (2018), pp. 13141–13151. DOI: 10.1021/acs.jafc.8b04183.

[69] K. Watanabe, Y. Tsuchida, N. Okibe, H. Teramoto, N. Suzuki, M. Inui, and H. Yukawa. “Scanning the *Corynebacterium glutamicum* R genome for high-efficiency secretion signal sequences”. In: *Microbiology* 155.3 (2009), pp. 741–750. DOI: 10.1099/mic.0.024075-0.

[70] C. Degering, T. Eggert, M. Puls, J. Bongaerts, S. Evers, K.-H. Maurer, and K.-E. Jaeger. “Optimization of protease secretion in *Bacillus subtilis* and *Bacillus licheniformis* by screening of homologous and heterologous signal peptides”. In: *Appl Environ Microbiol* 76.19 (2010), pp. 6370–6376. DOI: 10.1128/aem.01146-10.

[71] P. Rohe, D. Venkanna, B. Kleine, R. Freudl, and M. Oldiges. “An automated workflow for enhancing microbial bioprocess optimization on a novel microbioreactor platform”. In: *Microb Cell Factories* 11.1 (2012), p. 144. DOI: 10.1186/1475-2859-11-144.

[72] J. Hemmerich, P. Rohe, B. Kleine, S. Jurischka, W. Wiechert, R. Freudl, and M. Oldiges. “Use of a Sec signal peptide library from *Bacillus subtilis* for the optimization of cutinase secretion in *Corynebacterium glutamicum*”. In: *Microb Cell Factories* 15.1 (2016). DOI: 10.1186/s12934-016-0604-6.

[73] M. Caspers, U. Brockmeier, C. Degering, T. Eggert, and R. Freudl. “Improvement of Sec-dependent secretion of a heterologous model protein in *Bacillus subtilis* by saturation mutagenesis of the N-domain of the AmyE signal peptide”. In: *Appl Microbiol Biotechnol* 86.6 (2010), pp. 1877–1885. DOI: 10.1007/s00253-009-2405-x.

[74] G. Mathiesen, A. Sveen, M. Brurberg, L. Fredriksen, L. Axelsson, and V. G. H. Eijsink. “Genome-wide analysis of signal peptide functionality in *Lactobacillus plantarum* WCFS1”. In: *BMC Genom* 10.1 (2009), p. 425. DOI: 10.1186/1471-2164-10-425.

[75] P. J. Bakkes, P. Lenz, C. Müller, A. Bida, D. Dohmen-Olma, A. Knapp, M. Oldiges, K.-E. Jaeger, and R. Freudl. “Biosensor-based optimization of cutinase secretion by *Corynebacterium glutamicum*”. In: *Front Microbiol* 12 (2021). DOI: 10.3389/fmicb.2021.750150.

[76] S. Jurischka, A. Bida, D. Dohmen-Olma, B. Kleine, J. Potzkei, S. Binder, G. Schaumann, P. J. Bakkes, and R. Freudl. “A secretion biosensor for monitoring Sec-dependent protein export in *Corynebacterium glutamicum*”. In: *Microb Cell Factories* 19.1 (2020). DOI: 10.1186/s12934-019-1273-z.

[77] C. Sauer, E. V. L. van Themaat, L. G. M. Boender, D. Groothuis, R. Cruz, L. W. Hamoen, C. R. Harwood, and T. van Rij. “Exploring the nonconserved sequence space of synthetic expression modules in *Bacillus subtilis*”. In: *ACS Synth Biol* 7.7 (2018), pp. 1773–1784. DOI: 10.1021/acssynbio.8b00110.

[78] K. Volkenborn, L. Kuschmierz, N. Benz, P. Lenz, A. Knapp, and K.-E. Jaeger. “The length of ribosomal binding site spacer sequence controls the production yield for intracellular and secreted proteins by *Bacillus subtilis*”. In: *Microb Cell Factories* 19.1 (2020). DOI: 10.1186/s12934-020-01404-2.

[79] J. E. Musik, Y. M. Zalucki, C. J. Day, and M. P. Jennings. “Efficient function of signal peptidase 1 of *Escherichia coli* is partly determined by residues in the mature N-terminus of exported proteins”. In: *Biochim Biophys Acta - Biomembr* 1861.5 (2019), pp. 1018–1022. DOI: 10.1016/j.bbamem.2019.03.001.

[80] Y. Chen, D. S. Black, and P. J. Reilly. “Carboxylic ester hydrolases: classification and database derived from their primary, secondary, and tertiary structures”. In: *Protein Sci* 25.11 (2016), pp. 1942–1953. DOI: 10.1002/pro.3016.

[81] Nomenclature Committee of the International Union of Biochemistry and Molecular Biology (NC-IUBMB). *EC 3.1.1 Carboxylic Ester Hydrolases*. URL: https://iubmb.qmul.ac.uk/enzyme/EC3/1/1/ (visited on 02/08/2022).

[82] R. E. Purdy and P. E. Kolattukudy. “Hydrolysis of plant cuticle by plant pathogens. Properties of cutinase I, cutinase II, and a nonspecific esterase isolated from *Fusarium solani pisi*”. In: *Biochemistry* 14.13 (1975), pp. 2832–2840. DOI: 10.1021/bi00684a007.

[83] R. E. Purdy and P. E. Kolattukudy. “Depolymerization of a hydroxy fatty acid biopolymer, cutin, by an extracellular enzyme from *Fusarium solani* f. *pisi*: Isolation and some properties of the enzyme”. In: *Arch Biochem Biophys* 159.1 (1973), pp. 61–69. DOI: 10.1016/0003-9861(73)90429-3.

[84] P. Heikinheimo, A. Goldman, C. Jeffries, and D. L. Ollis. “Of barn owls and bankers: a lush variety of α/β hydrolases”. In: *Structure* 7.6 (1999), R141–R146. DOI: 10.1016/s0969-2126(99)80079-3.

[85] M. R. Egmond and J. de Vlieg. “*Fusarium solani pisi* cutinase”. In: *Biochimie* 82.11 (2000). Lipase 2000, pp. 1015–1021. ISSN: 0300-9084. DOI: 10.1016/s0300-9084(00)01183-4.

[86] S. Longhi, M. Czjzek, V. Lamzin, A. Nicolas, and C. Cambillau. “Atomic resolution (1.0 Å) crystal structure of *Fusarium solani* cutinase: stereochemical analysis”. In: *J Mol Biol* 268.4 (1997), pp. 779–799. ISSN: 0022-2836. DOI: 10.1006/jmbi.1997.1000.

[87] C. M. L. Carvalho, M. R. Aires-Barros, and J. M. S. Cabral. “Cutinase: from molecular level to bioprocess development”. In: *Biotechnol Bioeng* 66.1 (1999), pp. 17–34. DOI: 10.1002/(sici)1097-0290(1999)66:1<17::aid-bit2>3.0.co;2-f.

[88] A. Knapp, M. Ripphahn, K. Volkenborn, P. Skoczinski, and K.-E. Jaeger. “Activity-independent screening of secreted proteins using split GFP”. In: *J Biotechnol* 258 (2017), pp. 110–116. DOI: 10.1016/j.jbiotec.2017.05.024.

[89] C. Müller, C. L. Igwe, W. Wiechert, and M. Oldiges. “Scaling production of GFP1-10 detector protein in *E. coli* for secretion screening by split GFP assay”. In: *Microb Cell Factories* 20.1 (2021). DOI: 10.1186/s12934-021-01672-6.

[90] U. K. Winkler and M. Stuckmann. “Glycogen, hyaluronate, and some other polysaccharides greatly enhance the formation of exolipase by *Serratia marcescens*.” In: *J Bacteriol* 138 (3 1979), pp. 663–670. ISSN: 0021-9193. DOI: 10.1128/jb.138.3.663-670.1979.

[91] C. M. L. Carvalho, M. R. Aires-Barros, and J. Cabral. “Cutinase structure, function and biocatalytic applications”. In: *Electron J Biotechn* 1.3 (1998), pp. 28–29. DOI: 10.2225/vol1-issue3-fulltext-8.

[92] S. Chen, L. Su, J. Chen, and J. Wu. “Cutinase: characteristics, preparation, and application”. In: *Biotechnol Adv* 31.8 (2013), pp. 1754–1767. DOI: 10.1016/j.biotechadv.2013.09.005.

[93] A. Nyyssölä. “Which properties of cutinases are important for applications?” In: *Appl Microbiol Biotechnol* 99.12 (2015), pp. 4931–4942. DOI: 10.1007/s00253-015-6596-z.

[94] VCI. *Produktion von Polyethylenterephthalat (PET) in Deutschland in den Jahren von 2013 bis 2020 (in Tonnen)*. German. Statista. 2021. URL: https://de.statista.com/statistik/daten/studie/1285091/umfrage/polyethylenterephthalat-produktion-in-deutschland/ (visited on 03/14/2022).

[95] PlasticsEurope. *Plastics – the facts 2021. An analysis of European plastics production, demand and waste data*. 2022. URL: https://plasticseurope.org/knowledge-hub/plastics-the-facts-2021/ (visited on 03/14/2022).

[96] S. Yoshida, K. Hiraga, T. Takehana, I. Taniguchi, H. Yamaji, Y. Maeda, K. Toyohara, K. Miyamoto, Y. Kimura, and K. Oda. “A bacterium that degrades and assimilates poly(ethylene terephthalate)”. In: *Science* 351.6278 (2016), pp. 1196–1199. DOI: 10.1126/science.aad6359.

[97] I. Taniguchi, S. Yoshida, K. Hiraga, K. Miyamoto, Y. Kimura, and K. Oda. “Biodegradation of PET: current status and application aspects”. In: *ACS Catal* 9.5 (2019), pp. 4089–4105. DOI: 10.1021/acscatal.8b05171.

[98] F. Kawai, T. Kawabata, and M. Oda. “Current knowledge on enzymatic PET degradation and its possible application to waste stream management and other fields”. In: *Appl Microbiol Biotechnol* 103.11 (2019), pp. 4253–4268. DOI: 10.1007/s00253-019-09717-y.

[99] Y. J. Sohn, H. T. Kim, K.-A. Baritugo, S. Y. Jo, H. M. Song, S. Y. Park, S. K. Park, J. Pyo, H. G. Cha, H. Kim, J.-G. Na, C. Park, J.-I. Choi, J. C. Joo, and S. J. Park. “Recent advances in sustainable plastic upcycling and biopolymers”. In: *Biotechnol J* 15.6 (2020), p. 1900489. DOI: 10.1002/biot.201900489.

[100] T. Tiso, T. Narancic, R. Wei, E. Pollet, N. Beagan, K. Schröder, A. Honak, M. Jiang, S. T. Kenny, N. Wierckx, R. Perrin, L. Avérous, W. Zimmermann, K. O’Connor, and L. M. Blank. “Towards bio-upcycling of polyethylene terephthalate”. In: *Metab Eng* (2021). DOI: 10.1016/j.ymben.2021.03.011.

[101] T. Tiso, B. Winter, R. Wei, J. Hee, J. de Witt, N. Wierckx, P. Quicker, U. T. Bornscheuer, A. Bardow, J. Nogales, and L. M. Blank. “The metabolic potential of plastics as biotechnological carbon sources – review and targets for the future”. In: *Metab Eng* (2021). DOI: 10.1016/j.ymben.2021.12.006.

[102] H. P. Austin, M. D. Allen, B. S. Donohoe, N. A. Rorrer, F. L. Kearns, R. L. Silveira, B. C. Pollard, G. Dominick, R. Duman, K. E. Omari, V. Mykhaylyk, A. Wagner, W. E. Michener, A. Amore, M. S. Skaf, M. F. Crowley, A. W. Thorne, C. W. Johnson, H. L. Woodcock, J. E. McGeehan, and G. T. Beckham. "Characterization and engineering of a plastic-degrading aromatic polyesterase". In: *Proc Natl Acad Sci* 115.19 (2018), E4350–E4357. DOI: 10.1073/pnas.1718804115.

[103] S. Joo, I. J. Cho, H. Seo, H. F. Son, H.-Y. Sagong, T. J. Shin, S. Y. Choi, S. Y. Lee, and K.-J. Kim. "Structural insight into molecular mechanism of poly(ethylene terephthalate) degradation". In: *Nat Commun* 9.1 (2018). DOI: 10.1038/s41467-018-02881-1.

[104] M. A. M. E. Vertommen, V. A. Nierstrasz, M. van der Veer, and M. M. C. G. Warmoeskerken. "Enzymatic surface modification of poly(ethylene terephthalate)". In: *J Biotechnol* 120.4 (2005), pp. 376–386. DOI: 10.1016/j.jbiotec.2005.06.015.

[105] V. Tournier, C. M. Topham, A. Gilles, B. David, C. Folgoas, E. Moya-Leclair, E. Kamionka, M.-L. Desrousseaux, H. Texier, S. Gavalda, M. Cot, E. Guémard, M. Dalibey, J. Nomme, G. Cioci, S. Barbe, M. Chateau, I. André, S. Duquesne, and A. Marty. "An engineered PET depolymerase to break down and recycle plastic bottles". In: *Nature* 580.7802 (2020), pp. 216–219. DOI: 10.1038/s41586-020-2149-4.

[106] S. Sulaiman, S. Yamato, E. Kanaya, J.-J. Kim, Y. Koga, K. Takano, and S. Kanaya. "Isolation of a novel cutinase homolog with polyethylene terephthalate-degrading activity from leaf-branch compost by using a metagenomic approach". In: *Appl Environ Microbiol* 78.5 (2012), pp. 1556–1562. DOI: 10.1128/aem.06725-11.

[107] S. Sulaiman, D.-J. You, E. Kanaya, Y. Koga, and S. Kanaya. "Crystal structure and thermodynamic and kinetic stability of metagenome-derived LC-cutinase". In: *Biochemistry* 53.11 (2014), pp. 1858–1869. DOI: 10.1021/bi401561p.

[108] A. Bollinger, S. Thies, E. Knieps-Grünhagen, C. Gertzen, S. Kobus, A. Höppner, M. Ferrer, H. Gohlke, S. H. J. Smits, and K.-E. Jaeger. "A novel polyester hydrolase from the marine bacterium *Pseudomonas aestusnigri* – structural and functional insights". In: *Front Microbiol* 11 (2020). DOI: 10.3389/fmicb.2020.00114.

[109] O. Shimomura, F. H. Johnson, and Y. Saiga. "Extraction, purification and properties of aequorin, a bioluminescent protein from the luminous hydromedusan, *Aequorea*". In: *J Cell Compar Physl* 59.3 (1962), pp. 223–239. DOI: 10.1002/jcp.1030590302.

[110] M. Chalfie, Y. Tu, G. Euskirchen, W. W. Ward, and D. C. Prasher. "Green fluorescent protein as a marker for gene expression". In: *Science* 263.5148 (1994), pp. 802–805. DOI: 10.1126/science.8303295.

[111] R. Y. Tsien. "The green fluorescent protein". In: *Annu Rev Biochem* 67.1 (1998), pp. 509–544. DOI: 10.1146/annurev.biochem.67.1.509.

[112] J.-D. Pédelacq, S. Cabantous, T. Tran, T. C. Terwilliger, and G. S. Waldo. "Engineering and characterization of a superfolder green fluorescent protein". In: *Nat Biotechnol* 24.1 (2005), pp. 79–88. DOI: 10.1038/nbt1172.

[113] S. Cabantous, T. C. Terwilliger, and G. S. Waldo. “Protein tagging and detection with engineered self-assembling fragments of green fluorescent protein”. In: *Nat Biotechnol* 23.1 (2005), pp. 102–107. DOI: 10.1038/nbt1044.

[114] D. P. Barondeau, C. D. Putnam, C. J. Kassmann, J. A. Tainer, and E. D. Getzoff. “Mechanism and energetics of green fluorescent protein chromophore synthesis revealed by trapped intermediate structures”. In: *Proc Natl Acad Sci* 100.21 (2003), pp. 12111–12116. DOI: 10.1073/pnas.2133463100.

[115] D. Kamiyama, S. Sekine, B. Barsi-Rhyne, J. Hu, B. Chen, L. A. Gilbert, H. Ishikawa, M. D. Leonetti, W. F. Marshall, J. S. Weissman, and B. Huang. “Versatile protein tagging in cells with split fluorescent protein”. In: *Nat Commun* 7.1 (2016). DOI: 10.1038/ncomms11046.

[116] S. Feng, S. Sekine, V. Pessino, H. Li, M. D. Leonetti, and B. Huang. “Improved split fluorescent proteins for endogenous protein labeling”. In: *Nat Commun* 8.1 (2017). DOI: 10.1038/s41467-017-00494-8.

[117] J.-D. Pedelacq and S. Cabantous. “Development and applications of superfolder and split fluorescent protein detection systems in biology”. In: *Int J Mol Sci* 20.14 (2019), p. 3479. DOI: 10.3390/ijms20143479.

[118] S. Cabantous and G. S. Waldo. “In vivo and in vitro protein solubility assays using split GFP”. In: *Nat Methods* 3.10 (2006), pp. 845–854. DOI: 10.1038/nmeth932.

[119] J. Santos-Aberturas, M. Dörr, G. S. Waldo, and U. T. Bornscheuer. “In-depth high-throughput screening of protein engineering libraries by split-GFP direct crude cell extract data normalization”. In: *Chem Biol* 22.10 (2015), pp. 1406–1414. DOI: 10.1016/j.chembiol.2015.08.014.

[120] K. P. Kent and S. G. Boxer. “Light-activated reassembly of split green fluorescent protein”. In: *J Am Chem Soc* 133.11 (2011), pp. 4046–4052. DOI: 10.1021/ja110256c.

[121] M. Lundqvist, N. Thalén, A.-L. Volk, H. G. Hansen, E. von Otter, P.-Å. Nygren, M. Uhlen, and J. Rockberg. “Chromophore pre-maturation for improved speed and sensitivity of split-GFP monitoring of protein secretion”. In: *Sci Rep* 9.1 (2019). DOI: 10.1038/s41598-018-36559-x.

[122] A. Knapp, S. Voget, R. Gao, N. Zaburannyi, D. Krysciak, M. Breuer, B. Hauer, W. R. Streit, R. Müller, R. Daniel, and K.-E. Jaeger. “Mutations improving production and secretion of extracellular lipase by *Burkholderia glumae* PG1”. In: *Appl Microbiol Biotechnol* 100.3 (2015), pp. 1265–1273. DOI: 10.1007/s00253-015-7041-z.

[123] N. Tenhaef, R. Stella, J. Frunzke, and S. Noack. “Automated rational strain construction based on high-throughput conjugation”. In: *ACS Synth Biol* 10.3 (2021), pp. 589–599. DOI: 10.1021/acssynbio.0c00599.

[124] N. Olieric, M. Kuchen, S. Wagen, M. Sauter, S. Crone, S. Edmondson, D. Frey, C. Ostermeier, M. O. Steinmetz, and R. Jaussi. “Automated seamless DNA co-transformation cloning with direct expression vectors applying positive or negative insert selection”. In: *BMC Biotechnol* 10.1 (2010), p. 56. DOI: 10.1186/1472-6750-10-56.

[125] R. Bareither and D. Pollard. “A review of advanced small-scale parallel bioreactor technology for accelerated process development: Current state and future need”. In: *Biotechnol Prog* 27.1 (2010), pp. 2–14. DOI: 10.1002/btpr.522.

[126] P. Fernandes, F. Carvalho, and M. P. C. Marques. “Miniaturization in biotechnology: speeding up the development of bioprocesses”. In: *Recent Pat Biotechnol* 5.3 (2011), pp. 160–173. DOI: 10.2174/187220811797579105.

[127] Q. Long, X. Liu, Y. Yang, L. Li, L. Harvey, B. McNeil, and Z. Bai. “The development and application of high throughput cultivation technology in bioprocess development”. In: *J Biotechnol* 192 (2014), pp. 323–338. DOI: 10.1016/j.jbiotec.2014.03.028.

[128] J. Hemmerich, S. Noack, W. Wiechert, and M. Oldiges. “Microbioreactor systems for accelerated bioprocess development”. In: *Biotechnol J* 13.4 (2018), p. 1700141. DOI: 10.1002/biot.201700141.

[129] A. Buchenauer, M. C. Hofmann, M. Funke, J. Büchs, W. Mokwa, and U. Schnakenberg. “Microbioreactors for fed-batch fermentations with integrated online monitoring and microfluidic devices”. In: *Biosens Bioelectron* 24.5 (2009), pp. 1411–1416. DOI: 10.1016/j.bios.2008.08.043.

[130] C. Wittmann, H. M. Kim, G. John, and E. Heinzle. “Characterization and application of an optical sensor for quantification of dissolved O_2 in shake-flasks”. In: *Biotechnol Lett* 25.5 (2003), pp. 377–380. DOI: 10.1023/a:1022402212537.

[131] K. Schneider, V. Schütz, G. T. John, and E. Heinzle. “Optical device for parallel online measurement of dissolved oxygen and pH in shake flask cultures”. In: *Bioprocess Biosyst Eng* 33.5 (2009), pp. 541–547. DOI: 10.1007/s00449-009-0367-0.

[132] M. Scheidle, J. Klinger, and J. Büchs. “Combination of on-line pH and oxygen transfer rate measurement in shake flasks by fiber optical technique and Respiration Activity MOnitoring System (RAMOS)”. In: *Sensors* 7.12 (2007), pp. 3472–3480. DOI: 10.3390/s7123472.

[133] S. Diederichs, A. Korona, A. Staaden, W. Kroutil, K. Honda, H. Ohtake, and J. Büchs. “Phenotyping the quality of complex medium components by simple online-monitored shake flask experiments”. In: *Microb Cell Factories* 13.1 (2014). DOI: 10.1186/s12934-014-0149-5.

[134] G. Munch, A. Schulte, M. Mann, R. Dinger, L. Regestein, L. Rehmann, and J. Büchs. “Online measurement of CO2 and total gas production in parallel anaerobic shake flask cultivations”. In: *Biochem Eng J* 153 (2020), p. 107418. DOI: 10.1016/j.bej.2019.107418.

[135] M. Jeude, B. Dittrich, H. Niederschulte, T. Anderlei, C. Knocke, D. Klee, and J. Büchs. “Fed-batch mode in shake flasks by slow-release technique”. In: *Biotechnol Bioeng* 95.3 (2006), pp. 433–445. DOI: 10.1002/bit.21012.

[136] C. Bähr, B. Leuchtle, C. Lehmann, J. Becker, M. Jeude, F. Peinemann, R. Arbter, and J. Büchs. “Dialysis shake flask for effective screening in fed-batch mode”. In: *Biochem Eng J* 69 (2012), pp. 182–195. DOI: 10.1016/j.bej.2012.08.012.

[137] J. Hemmerich, N. Adelantado, J. M. Barrigón, X. Ponte, A. Hörmann, P. Ferrer, F. Kensy, and F. Valero. “Comprehensive clone screening and evaluation of fed-batch strategies in a microbioreactor and lab scale stirred tank bioreactor system: application on *Pichia pastoris* producing *Rhizopus oryzae* lipase”. In: *Microb Cell Factories* 13.1 (2014). DOI: 10.1186/1475-2859-13-36.

[138] F. Delouvroy, G. L. Reverend, B. Fessler, G. Mathy, M. Harmsen, N. Kochanowski, and L. Malphettes. “Evaluation of the advanced micro-scale bioreactor (ambr™) as a highthroughput tool for cell culture process development”. In: *BMC Proc* 7.S6 (2013). DOI: 10.1186/1753-6561-7-s6-p73.

[139] V. Janakiraman, C. Kwiatkowski, R. Kshirsagar, T. Ryll, and Y.-M. Huang. “Application of high-throughput mini-bioreactor system for systematic scale-down modeling, process characterization, and control strategy development”. In: *Biotechnol Prog* 31.6 (2015), pp. 1623–1632. DOI: 10.1002/btpr.2162.

[140] G. Gebhardt, R. Hortsch, K. Kaufmann, M. Arnold, and D. Weuster-Botz. “A new microfluidic concept for parallel operated milliliter-scale stirred tank bioreactors”. In: *Biotechnol Prog* 27.3 (2011), pp. 684–690. DOI: 10.1002/btpr.570.

[141] R. Jansen, N. Tenhaef, M. Moch, W. Wiechert, S. Noack, and M. Oldiges. “FeedER: a feedback-regulated enzyme-based slow-release system for fed-batch cultivation in microtiter plates”. In: *Bioprocess Biosyst Eng* 42.11 (2019), pp. 1843–1852. DOI: 10.1007/s00449-019-02180-z.

[142] T. Ladner, D. Flitsch, T. Schlepütz, and J. Büchs. “Online monitoring of dissolved oxygen tension in microtiter plates based on infrared fluorescent oxygen-sensitive nanoparticles”. In: *Microb Cell Factories* 14.1 (2015). DOI: 10.1186/s12934-015-0347-9.

[143] S. Teworte, K. Malcı, L. E. Walls, M. Halim, and L. Rios-Solis. “Recent advances in fed-batch microscale bioreactor design”. In: *Biotechnol Adv* 55 (2022), p. 107888. DOI: 10.1016/j.biotechadv.2021.107888.

[144] F. Kensy, C. Engelbrecht, and J. Büchs. “Scale-up from microtiter plate to laboratory fermenter: evaluation by online monitoring techniques of growth and protein expression in *Escherichia coli* and *Hansenula polymorpha* fermentations”. In: *Microb Cell Factories* 8.1 (2009). DOI: 10.1186/1475-2859-8-68.

[145] A. Back, T. Rossignol, F. Krier, J.-M. Nicaud, and P. Dhulster. “High-throughput fermentation screening for the yeast *Yarrowia lipolytica* with real-time monitoring of biomass and lipid production”. In: *Microb Cell Factories* 15.1 (2016). DOI: 10.1186/s12934-016-0546-z.

[146] H. Morschett, R. Jansen, C. Neuendorf, M. Moch, W. Wiechert, and M. Oldiges. “Parallelized microscale fed-batch cultivation in online-monitored microtiter plates: implications of media composition and feed strategies for process design and performance”. In: *J Ind Microbiol Biotechnol* 47.1 (2020), pp. 35–47. DOI: 10.1007/s10295-019-02243-w.

[147] J. Hemmerich, N. Tenhaef, C. Steffens, J. Kappelmann, M. Weiske, S. J. Reich, W. Wiechert, M. Oldiges, and S. Noack. “Less sacrifice, more insight: repeated low-volume sampling of microbioreactor cultivations enables accelerated deep phenotyping of microbial strain libraries”. In: *Biotechnol J* (2018). DOI: 10.1002/biot.201800428.

[148] R. A. Fisher. “Design of experiments”. In: *Brit Med J* 1.3923 (1936), p. 554.

[149] C.-F. Mandenius and A. Brundin. “Bioprocess optimization using design-of-experiments methodology”. In: *Biotechnol Prog* 24.6 (2008), pp. 1191–1203. DOI: 10.1002/btpr.67.

[150] M. W. Lutz, J. A. Menius, T. D. Choi, R. G. Laskody, P. L. Domanico, A. S. Goetz, and D. L. Saussy. “Experimental design for high-throughput screening”. In: *Drug Discov* 1.7 (1996), pp. 277–286. DOI: 10.1016/1359-6446(96)10025-8.

[151] Y.-H. Wang, B. Yang, J. Ren, M.-L. Dong, D. Liang, and A.-L. Xu. “Optimization of medium composition for the production of clavulanic acid by *Streptomyces clavuligerus*”. In: *Process Biochem* 40.3-4 (2005), pp. 1161–1166. DOI: 10.1016/j.procbio.2004.04.010.

[152] Z. Jia, E. Davis, F. J. Muzzio, and M. G. Ierapetritou. “Predictive modeling for pharmaceutical processes using Kriging and response surface”. In: *J Pharm Innov* 4.4 (2009), pp. 174–186. DOI: 10.1007/s12247-009-9070-6.

[153] L. Freier, J. Hemmerich, K. Schöler, W. Wiechert, M. Oldiges, and E. von Lieres. “Framework for Kriging-based iterative experimental analysis and design: optimization of secretory protein production in *Corynebacterium glutamicum*”. In: *Eng Life Sci* 16.6 (2016), pp. 538–549. DOI: 10.1002/elsc.201500171.

[154] L. M. Helleckes. “Bayesian inference in bioprocess development: efficient library screening by Thompson sampling”. Master Thesis. RWTH Aachen University, 2019.

[155] F. Fröhlich, C. Loos, and J. Hasenauer. “Scalable inference of ordinary differential equation models of biochemical processes”. In: *Gene Regulatory Networks: Methods and Protocols*. Ed. by G. Sanguinetti and V. A. Huynh-Thu. New York, NY: Springer New York, 2019, pp. 385–422. ISBN: 978-1-4939-8882-2. DOI: 10.1007/978-1-4939-8882-2_16.

[156] W. R. Thompson. “On the likelihood that one unknown probability exceeds another in view of the evidence of two samples”. In: *Biometrika* 25.3-4 (1933), pp. 285–294. DOI: 10.2307/2332286.

[157] E. M. Schwartz, E. T. Bradlow, and P. S. Fader. “Customer acquisition via display advertising using multi-armed bandit experiments”. In: *Mark Sci* 36.4 (2017), pp. 500–522. DOI: 10.1287/mksc.2016.1023.

[158] K. J. Ferreira, D. Simchi-Levi, and H. Wang. “Online network revenue management using Thompson sampling”. In: *Oper Res* 66.6 (2018), pp. 1586–1602. DOI: 10.1287/opre.2018.1755.

[159] D. J. Russo, B. V. Roy, A. Kazerouni, I. Osband, and Z. Wen. “A tutorial on Thompson sampling”. In: *Found Trends Mach Learn* 11.1 (2018), pp. 1–96. DOI: 10.1561/2200000070.

[160] R. Kumar, C. Carroll, A. Hartikainen, and O. A. Martìn. “ArviZ a unified library for exploratory analysis of Bayesian models in Python”. In: *J open source softw* (2019). DOI: 10.21105/joss.01143.

[161] M. Osthege, N. Tenhaef, R. Zyla, C. Müller, J. Hemmerich, W. Wiechert, S. Noack, and M. Oldiges. “bletl - A Python package for integrating BioLector microcultivation devices in the Design-Build-Test-Learn cycle”. In: *Eng Life Sci* 22.3-4 (2022), pp. 242–259. DOI: 10.1002/elsc.202100108.

[162] M. Osthege, N. Tenhaef, L. M. Helleckes, and C. Müller. *JuBiotech/bletl: v1.1.0*. 2022. DOI: 10.5281/zenodo.6284777.

[163] M. Osthege and L. M. Helleckes. *JuBiotech/calibr8: Toolbox for non-linear calibration modeling*. Version v6.2.1. 2022. DOI: 10.5281/zenodo.5961920.

[164] L. M. Helleckes, M. Osthege, W. Wiechert, E. von Lieres, and M. Oldiges. “Bayesian calibration, process modeling and uncertainty quantification in biotechnology”. In: *PLoS Comput Biol* 18.3 (2022). Ed. by D. Schneidman-Duhovny, e1009223. DOI: 10.1371/journal.pcbi.1009223.

[165] M. Osthege, N. Tenhaef, V. Steier, and A. Reiter. *JuBiotech/detl: v1.0.0*. Version v1.0.0. 2022. DOI: 10.5281/zenodo.6939684.

[166] J. D. Hunter. “Matplotlib: A 2D Graphics Environment”. In: *Comput Sci Eng* 9.3 (2007), pp. 90–95. DOI: 10.1109/mcse.2007.55.

[167] T. A. Caswell, M. Droettboom, A. Lee, E. S. de Andrade, T. Hoffmann, J. Hunter, J. Klymak, E. Firing, D. Stansby, N. Varoquaux, J. H. Nielsen, B. Root, R. May, P. Elson, J. K. Seppänen, D. Dale, J.-J. Lee, D. McDougall, A. Straw, P. Hobson, hannah, C. Gohlke, T. S. Yu, E. Ma, A. F. Vincent, S. Silvester, C. Moad, N. Kniazev, E. Ernest, and P. Ivanov. *matplotlib/matplotlib: REL: v3.4.3*. Version v3.4.3. 2021. DOI: 10.5281/zenodo.5194481.

[168] C. R. Harris, K. J. Millman, S. J. Van Der Walt, R. Gommers, P. Virtanen, D. Cournapeau, E. Wieser, J. Taylor, S. Berg, N. J. Smith, R. Kern, M. Picus, S. Hoyer, M. H. van Kerkwijk, M. Brett, A. Haldane, J. F. del Río, M. Wiebe, P. Peterson, P. Gérard-Marchant, K. Sheppard, T. Reddy, W. Weckesser, H. Abbasi, C. Gohlke, and T. E. Oliphant. “Array programming with NumPy”. In: *Nature* 585.7825 (2020), pp. 357–362. DOI: 10.1038/s41586-020-2649-2.

[169] W. McKinney et al. “Data structures for statistical computing in Python”. In: *Proceedings of the 9th Python in Science Conference*. Vol. 445. 1. Austin, TX. 2010, pp. 51–56. DOI: 10.25080/majora-92bf1922-00a.

[170] J. Reback, jbrockmendel, W. McKinney, J. V. den Bossche, T. Augspurger, P. Cloud, S. Hawkins, gfyoung, M. Roeschke, Sinhrks, A. Klein, T. Petersen, J. Tratner, C. She, W. Ayd, P. Hoefler, S. Naveh, M. Garcia, J. Schendel, A. Hayden, D. Saxton, J. Darbyshire, R. Shadrach, M. E. Gorelli, F. Li, M. Zeitlin, V. Jancauskas, A. McMaster, P. Battiston, and S. Seabold. *pandas-dev/pandas: Pandas 1.3.4*. Version v1.3.4. 2021. DOI: 10.5281/zenodo.5574486.

[171] T. Wiecki, J. Salvatier, A. Patil, M. Kochurov, B. Engels, J. Lao, Colin, O. Martin, R. Vieira, B. T. Willard, and M. Osthege. *pymc-devs/pymc: v4.0.0b2*. Version v4.0.0b2. 2022. DOI: 10.5281/zenodo.5850149.

[172] M. Osthege and L. M. Helleckes. *JuBiotech/robotools: v1.3.0*. 2021. DOI: 10.5281/ZENODO.5745938.

[173] P. Virtanen et al. “SciPy 1.0: fundamental algorithms for scientific computing in Python”. In: *Nat Methods* 17.3 (2020), pp. 261–272. DOI: 10.1038/s41592-019-0686-2.

[174] C. L. Igwe. “Workflow optimization of split GFP assay for automated screening of cutinase secretion in *Corynebacterium glutamicum*”. Master thesis. RWTH Aachen University, 2020.

[175] C. Müller, P. J. Bakkes, P. Lenz, V. Waffenschmidt, L. M. Helleckes, K.-E. Jaeger, W. Wiechert, A. Knapp, R. Freudl, and M. Oldiges. “Accelerated strain construction and characterization of *C. glutamicum* protein secretion by laboratory automation”. In: *Appl Microbiol Biotechnol* 106.12 (2022), pp. 4481–4497. DOI: 10.1007/s00253-022-12017-7.

[176] M. Osthege. “Accelerated bioprocess research by autonomous experimentation and Bayesian modeling”. PhD thesis. RWTH Aachen University, 2022.

[177] T. Eggert, U. Brockmeier, M. J. Dröge, W. J. Quax, and K.-E. Jaeger. “Extracellular lipases from *Bacillus subtilis*: regulation of gene expression and enzyme activity by amino acid supply and external pH”. In: *FEMS Microbiol Lett* 225.2 (2003), pp. 319–324. DOI: 10.1016/s0378-1097(03)00536-6.

[178] H. Jeong, V. Barbe, C. H. Lee, D. Vallenet, D. S. Yu, S.-H. Choi, A. Couloux, S.-W. Lee, S. H. Yoon, L. Cattolico, C.-G. Hur, H.-S. Park, B. Ségurens, S. C. Kim, T. K. Oh, R. E. Lenski, F. W. Studier, P. Daegelen, and J. F. Kim. "Genome sequences of *Escherichia coli* B strains REL606 and BL21(DE3)". In: *J Mol Biol* 394.4 (2009), pp. 644–652. DOI: 10.1016/j.jmb.2009.09.052.

[179] J. Chen, Y. Li, K. Zhang, and H. Wang. "Whole-genome sequence of phage-resistant strain *Escherichia coli* DH5α". In: *Genome Announc* 6.10 (2018). DOI: 10.1128/genomea.00097-18.

[180] U. Brockmeier, M. Wendorff, and T. Eggert. "Versatile expression and secretion vectors for *Bacillus subtilis*". In: *Curr Microbiol* 52.2 (2006), pp. 143–148. DOI: 10.1007/s00284-005-0231-7.

[181] L. M. Helleckes, C. Müller, T. Griesbach, M. Moch, M. Osthege, W. Wiechert, and M. Oldiges. "Explore or exploit? A novel screening strategy for PETase secretion by *Corynebacterium glutamicum*". In: *Biotechnol Bioeng* 120.1 (2023), pp. 139–153. DOI: 10.1002/bit.28261.

[182] B. J. Eikmanns, N. Thum-Schmitz, L. Eggeling, K.-U. Ludtke, and H. Sahm. "Nucleotide sequence, expression and transcriptional analysis of the *Corynebacterium glutamicum gltA* gene encoding citrate synthase". In: *Microbiology* 140.8 (1994), pp. 1817–1828. DOI: 10.1099/13500872-140-8-1817.

[183] J. Miller. *Experiments in molecular genetics*. Cold Spring Harbor, N.Y.: Cold Spring Harbor Laboratory, 1972. ISBN: 0879691069.

[184] M. P. DeLisa, J. Li, G. Rao, W. A. Weigand, and W. E. Bentley. "Monitoring GFP-operon fusion protein expression during high cell density cultivation of *Escherichia coli* using an on-line optical sensor". In: *Biotechnol Bioeng* 65.1 (1999), pp. 54–64. DOI: 10.1002/(SICI)1097-0290(19991005)65:1<54::AID-BIT7>3.0.CO;2-R.

[185] S. Unthan, A. Grünberger, J. van Ooyen, J. Gätgens, J. Heinrich, N. Paczia, W. Wiechert, D. Kohlheyer, and S. Noack. "Beyond growth rate 0.6: what drives *Corynebacterium glutamicum* to higher growth rates in defined medium". In: *Biotechnol Bioeng* 111.2 (2014), pp. 359–371. DOI: 10.1002/bit.25103.

[186] C. Müller and L. M. Helleckes. *JuBiotech/OT-2-autoclone*. Version v1.0.1. 2022. DOI: 10.5281/zenodo.6393652.

[187] M. E. van der Rest, C. Lange, and D. Molenaar. "A heat shock following electroporation induces highly efficient transformation of *Corynebacterium glutamicum* with xenogeneic plasmid DNA". In: *Appl Microbiol Biotechnol* 52.4 (1999), pp. 541–545. DOI: 10.1007/s002530051557.

[188] C. Guan, W. Cui, J. Cheng, L. Zhou, J. Guo, X. Hu, G. Xiao, and Z. Zhou. "Construction and development of an auto-regulatory gene expression system in *Bacillus subtilis*". In: *Microb Cell Factories* 14.1 (2015), pp. 1–15.

[189] L. Helleckes and M. Osthege. *JuBiotech/petase-ts-paper: 2022-07-26*. Version 2022-07-26. 2022. DOI: 10.5281/zenodo.6908129.

[190] M. D. Hoffman and A. Gelman. "The No-U-Turn sampler: adaptively setting path lengths in Hamiltonian Monte Carlo". In: *J Mach Learn Res* 15.1 (2014), pp. 1593–1623.

[191] K. Kandasamy, G. Dasarathy, J. Schneider, and B. Póczos. "Multi-fidelity bayesian optimisation with continuous approximations". In: *International Conference on Machine Learning*. PMLR. 2017, pp. 1799–1808.

[192] M. Osthege and K. Felton. *michaelosthege/pyrff: v2.0.1*. Version v2.0.1. 2020. DOI: 10.5281/zenodo.4317685.

[193] D. J. Wurm, J. Quehenberger, J. Mildner, B. Eggenreich, C. Slouka, A. Schwaighofer, K. Wieland, B. Lendl, V. Rajamanickam, C. Herwig, and O. Spadiut. "Teaching an old pET new tricks: tuning of inclusion body formation and properties by a mixed feed system in *E. coli*". In: *Appl Microbiol Biotechnol* 102.2 (2017), pp. 667–676. DOI: 10.1007/s00253-017-8641-6.

[194] C. Engler, R. Kandzia, and S. Marillonnet. "A one pot, one step, precision cloning method with high throughput capability". In: *PLoS One* 3.11 (2008). Ed. by H. A. El-Shemy, e3647. DOI: 10.1371/journal.pone.0003647.

[195] H. Taniguchi and V. F. Wendisch. "Exploring the role of sigma factor gene expression on production by *Corynebacterium glutamicum*: sigma factor H and FMN as example". In: *Front Microbiol* 6 (2015). DOI: 10.3389/fmicb.2015.00740.

[196] J. Schneider, D. Eberhardt, and V. F. Wendisch. "Improving putrescine production by *Corynebacterium glutamicum* by fine-tuning ornithine transcarbamoylase activity using a plasmid addiction system". In: *Appl Microbiol Biotechnol* 95.1 (2012), pp. 169–178. DOI: 10.1007/s00253-012-3956-9.

[197] W. Zhang, M. Yang, Y. Yang, J. Zhan, Y. Zhou, and X. Zhao. "Optimal secretion of alkali-tolerant xylanase in *Bacillus subtilis* by signal peptide screening". In: *Appl Microbiol Biotechnol* 100.20 (2016), pp. 8745–8756. DOI: 10.1007/s00253-016-7615-4.

[198] X.-Z. Zhang, Z.-L. Cui, Q. Hong, and S.-P. Li. "High-level expression and secretion of methyl parathion hydrolase in *Bacillus subtilis* WB800". In: *Appl Environ Microbiol* 71 (2005), pp. 4101–4103. DOI: 10.1128/aem.71.7.4101-4103.2005.

[199] B. Kleine, A. Chattopadhyay, T. Polen, D. Pinto, T. Mascher, M. Bott, M. Brocker, and R. Freudl. "The three-component system EsrISR regulates a cell envelope stress response in *Corynebacterium glutamicum*". In: *Mol Microbiol* 106.5 (2017), pp. 719–741. DOI: 10.1111/mmi.13839.

[200] K. Pfeifer-Sancar, A. Mentz, C. Rückert, and J. Kalinowski. "Comprehensive analysis of the *Corynebacterium glutamicum* transcriptome using an improved RNAseq technique". In: *BMC Genom* 14.1 (2013), p. 888. DOI: 10.1186/1471-2164-14-888.

[201] N. A. Henke, I. Krahn, and V. F. Wendisch. "Improved plasmid-based inducible and constitutive gene expression in *Corynebacterium glutamicum*". In: *Microorganisms* 9.1 (2021), p. 204. DOI: 10.3390/microorganisms9010204.

[202] J. Shine and L. Dalgarno. "The 3′-terminal sequence of *Escherichia coli* 16S ribosomal RNA: complementarity to nonsense triplets and ribosome binding sites". In: *Proc Natl Acad Sci* 71.4 (1974), pp. 1342–1346. DOI: 10.1073/pnas.71.4.1342.

[203] A. Deana and J. G. Belasco. "Lost in translation: the influence of ribosomes on bacterial mRNA decay". In: *Genes Dev* 19.21 (2005), pp. 2526–2533. DOI: 10.1101/gad.1348805.

[204] S. Westerhausen, M. Nowak, C. E. Torres-Vargas, U. Bilitewski, E. Bohn, I. Grin, and S. Wagner. "A NanoLuc luciferase-based assay enabling the real-time analysis of protein secretion and injection by bacterial type III secretion systems". In: *Mol Microbiol* 113.6 (2020), pp. 1240–1254. DOI: 10.1111/mmi.14490.

A. Appendices

A.1. Supporting material for chapter 3.1

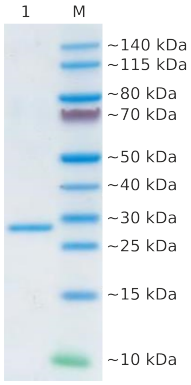

Fig. A.1. Purified GFP1-10 detector solution analyzed by SDS-PAGE. GFP1-10 was produced intracellularly by *E. coli* pET22b-sfGFP in a flask and the detector protein was purified from the inclusion body fraction. Ready-to-use detector solution with 1x Laemmli sample buffer, boiled and 10 µL were analyzed on a 4–12% Criterion™ XT Bis-Tris Protein Gel (1). 7 µL PageRuler™ Prestained Protein Ladder (10 to 180 kDa) were added to the SDS gel for size comparison (M)

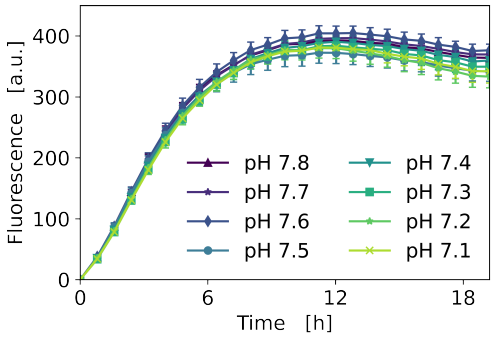

Fig. A.2. Impact of supernatant pH on split GFP assay. Original pH of *C. glutamicum* pPBEx2-NprE-Cutinase-GFP11 supernatant containing cutinase-GFP11 was 7.5. Acid (10 M HCl) or base (8 M NaOH) was added to change pH of supernatant to 7.1–7.8 before split GFP assay. Data is shown as mean of three technical replicates with standard deviation. Modified from [89]

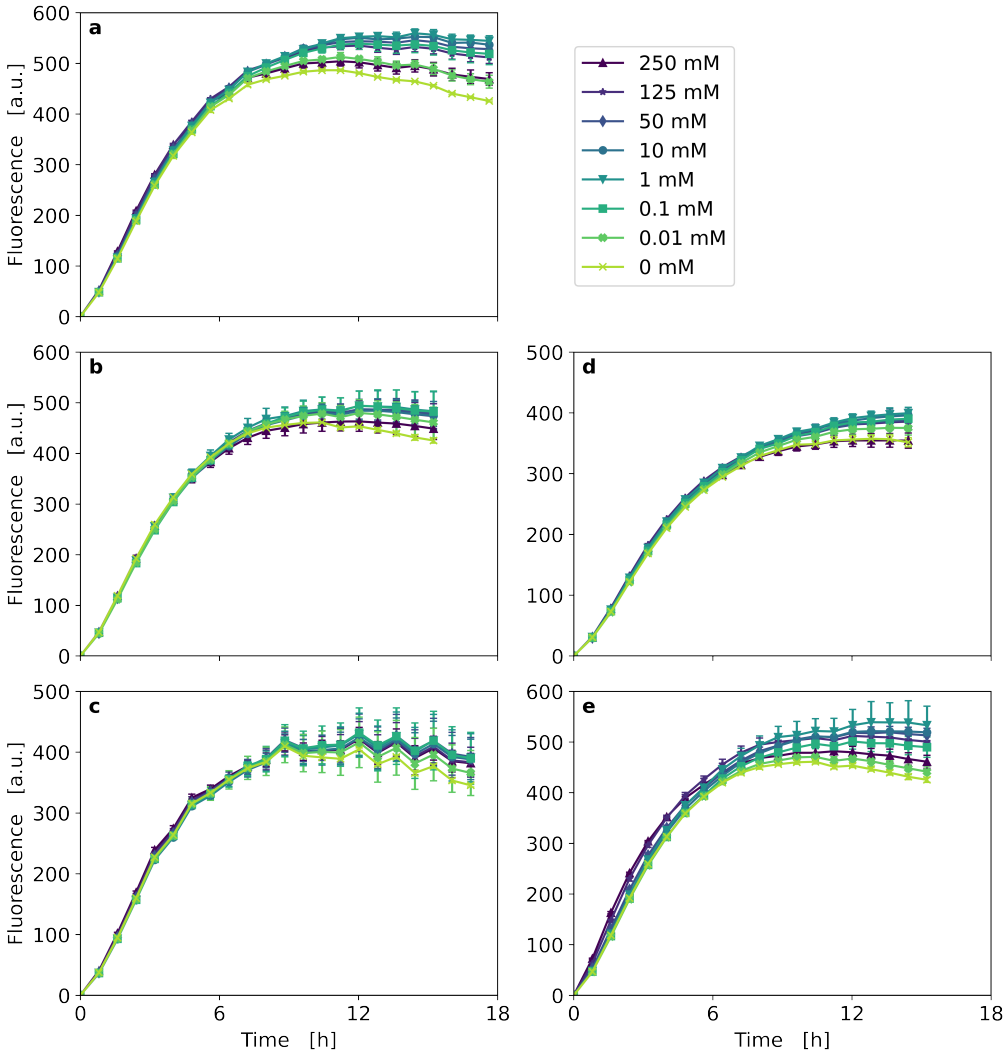

Fig. A.3. Impact of different metabolites in *C. glutamicum* supernatant on split GFP assay. (a) succinate, (b) lactate, (c) glutamate, (d) ketoglutarate and (e) acetate were added with final concentrations of 250–0.1 mM to *C. glutamicum* pPBEx2-NprE-Cutinase-GFP11 supernatant containing cutinase-GFP11. Data is shown as mean of three technical replicates with standard deviation. Modified from [89]

A.2. Supporting material for chapter 3.2

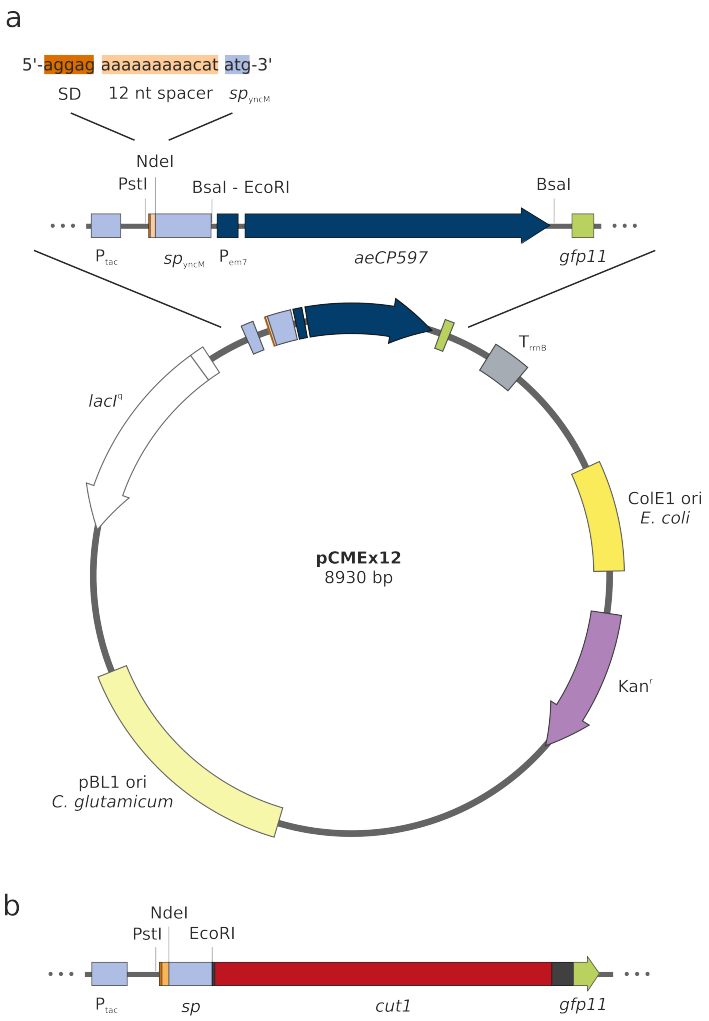

Fig. A.4. Sequence features of pCMEx-based plasmids. Plasmid map of pCMEx12 (a). The expression cassette contains a tac promoter, a 12 nt RBS spacer between the Shine-Dalgarno sequence (SD) and the *B. subtilis* signal peptide sequence from YncM, the GFP11-tag sequence and a *rrnB* terminator. The *Actinia equina blue chromoprotein aeCP597* under the control of the em7 promoter between the signal peptide sequence and the GFP11-tag sequence is constitutively expressed. After Golden Gate assembly, the cutinase gene *cut1* is in frame with the signal peptide and GFP11-tag sequence under the control of the IPTG-inducible tac promoter (b). Two amino acids (Glu, Phe) connect the signal peptide with the target protein after translation. The GFP11-tag is attached to the target protein via a polypeptide linker consisting of 14 amino acids. Partially created with SnapGene® software (from Insightful Science; available at snapgene.com) [175]

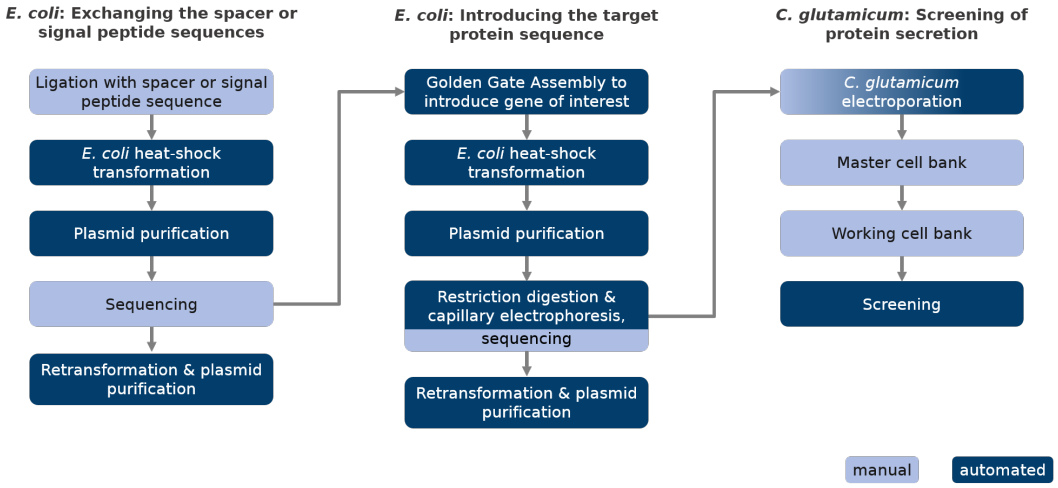

Fig. A.5. Workflow from exchanging plasmid sequences to automated secretion screening. Automated steps are highlighted in dark blue and manual steps in light blue. Molecular cloning is done using *E. coli* and steps can be divided into the exchange of RBS spacer or signal peptide sequences by cassette mutagenesis and introduction of the target gene by Golden Gate assembly. Only sequence verified expression plasmids are introduced in *C. glutamicum* by electroporation, which cannot be automated but parallelized by using a 96-well electroporation device. Only the screening is automated using a Tecan Freedom EVO® 200 with integrated BioLector® Pro, centrifuge and microplate reader. All other steps were automated using the Opentrons OT-2 system with additional Thermocycler and Magnetic Module [175]

Tab. A.1. Golden Gate assembly. Categories are M: manual step, I: manually timed incubation and A: automated step [175]

Step	**Automated [min]**			**Manual [min]**		
	M	**I**	**A**	**M**	**I**	**A**
Prepare robotic	10	-	-	-	-	-
Prepare reaction mix	5	-	-	5	-	-
Add pre-diluted DNA to plate	-	-	5	5	-	-
Mix reaction mix with DNA	-	-	10	10	-	-
Thermocycler protocol	-	-	210	-	-	210
Finish and take plate	5	-	-	5	-	-
Sum [min]	20	0	225	25	0	210
Total time [min]		245			235	

Tab. A.2. Heat-shock transformation. Categories are M: manual step, I: manually timed incubation and A: automated step [175]

Step	**Automated [min]**			**Manual [min] (12 samples)**			**Manual [min] (2x 12 samples, nested)**		
	M	**I**	**A**	**M**	**I**	**A**	**M**	**I**	**A**
Prepare robotic	20	-	-	-	-	-	-	-	-
Mixing cells and DNA	-	-	10	10	-	-	20	-	-
Incubation on ice	-	-	30	-	20	-	-	40	-
Heat-shock and cooling	-	-	3	5	-	-	10	-	-
Regeneration	-	-	70	5	60	-	10	401	-
Streaking or plating out	5	10	7	20	-	-	40	-	-
Sum [min]	25	10	120	40	80	0	80	80	0
Total time [min]		155			120			160	

Tab. A.3. Plasmid preparation. Categories are M: manual step, I: manually timed incubation and A: automated step [175]

Step automated	**Automated [min]**			**Manual [min] (12 samples)**			**Step manual**
	M	**I**	**A**	**M**	**I**	**A**	
Prepare robotic, cell harvest	20	-	-	25	-	-	Cell harvest
Automated protocol part I	-	-	70	15	-	-	Resuspend cells
Tip refill exchange of plates	5	-	-	10	-	-	Precipitation
Automated protocol part II	-	-	90	10	-	-	Pellet cell debris
Drying samples	-	35	-	25	-	-	Washing and elution
Automated protocol part III	-	-	30	5	-	-	Label and store tubes
Seal and store plate	5	-	-	-	-	-	-
Sum [min]	30	35	190	90	0	0	Sum [min]
Total time [min]		255			90		

Tab. A.4. Test digestion. Categories are M: manual step, I: manually timed incubation and A: automated step [175]

Step	**Automated [min]**			**Manual [min]**		
	M	**I**	**A**	**M**	**I**	**A**
Prepare robotic	10	-	-	-	-	-
Prepare reaction mix	10	-	-	10	-	-
Mix DNA and reaction mix	-	-	8	25	-	-
Digestion and heat inactivation	-	-	92	-	80	-
Dilution of samples	5	-	15	15	-	-
Sum [min]	25	0	115	50	80	0
Total time [min]		140			130	

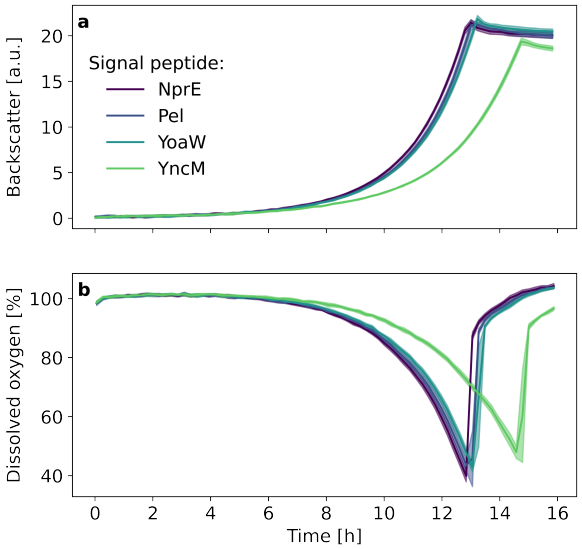

Fig. A.6. Impact of IPTG on growth of *C. glutamicum*. CGXII with 20 g L^{-1} glucose and 100 µM IPTG was inoculated to an $OD_{600\,nm}$ of 0.2 from pre-cultures in flasks that were harvested before reaching the stationary phase. Error tubes deviate from 12 replicates per *C. glutamicum* pCMEx8-[SP]-cutinase with *B. subtilis* signal peptides NprE, Pel, YoaW and YncM

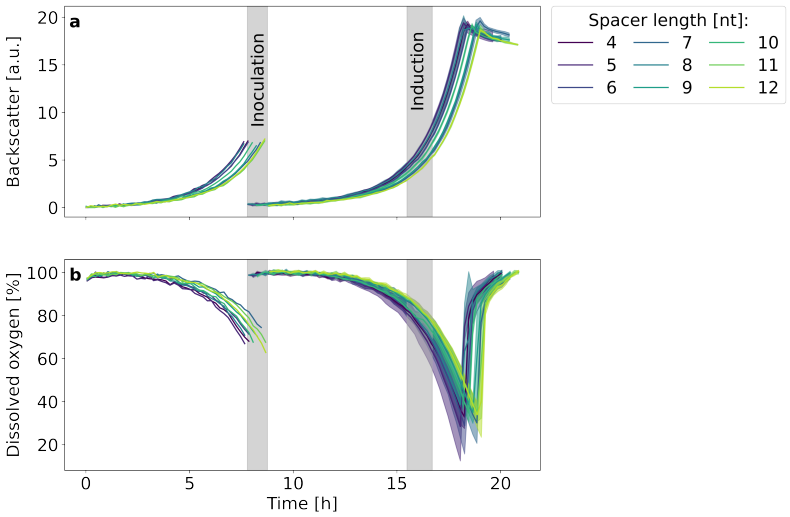

Fig. A.7. Pel-Cutinase-GFP11 secretion with RBS spacer lengths from 4–12 nt. Backscatter (a) and DO (b) were measured during cultivation of *C. glutamicum* pCMEx[4-12]-Pel-Cutinase. Precultures inoculated from cryo cultures were used to inoculate three main cultures that are shown as mean with standard deviation in confidence tubes. Inoculation and induction of main cultures with IPTG to a final concentration of 200 µM were each triggered by a device-dependent backscatter signal in the exponential phase. Cells were harvested 4 h after induction with main culture durations of 12–12.2 h [175]

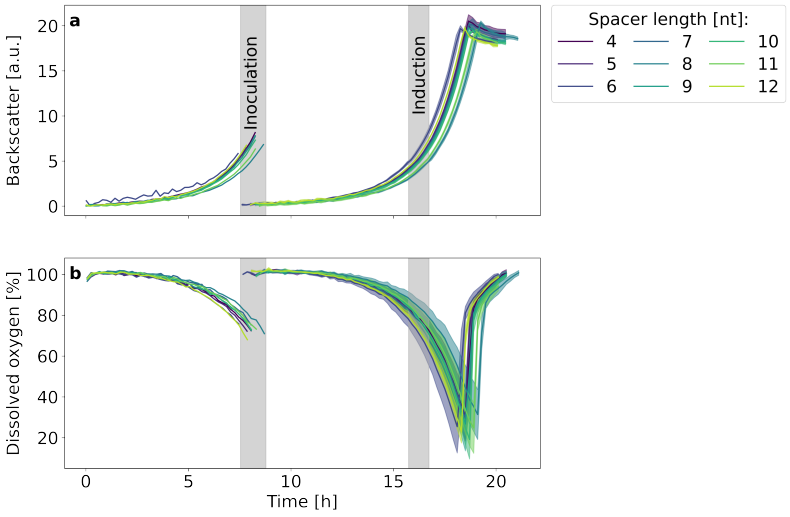

Fig. A.8. Epr-Cutinase-GFP11 secretion with RBS spacer lengths from 4–12 nt. Backscatter (a) and DO (b) were measured during cultivation of *C. glutamicum* pCMEx[4-12]-Epr-Cutinase. Precultures inoculated from cryo cultures were used to inoculate three main cultures that are shown as mean with standard deviation in confidence tubes. Inoculation and induction of main cultures with IPTG to a final concentration of 200 µM were each triggered by a device-dependent backscatter signal in the exponential phase. Cells were harvested 4 h after induction with main culture durations of 12–12.4 h [175]

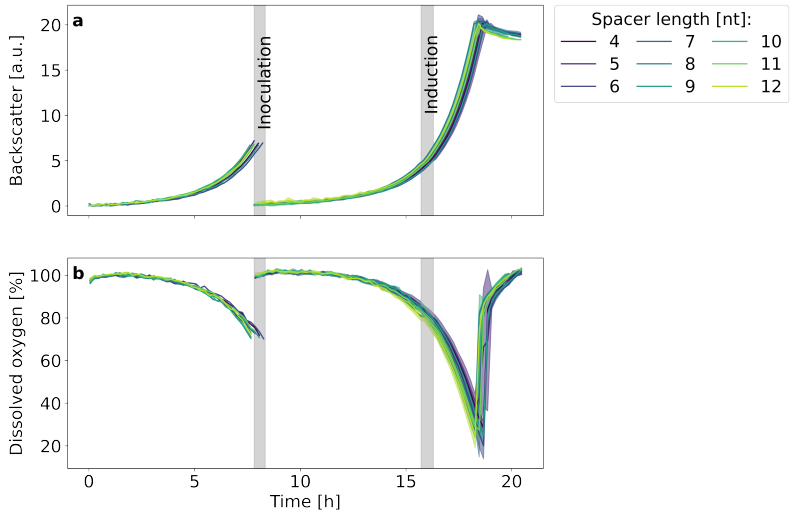

Fig. A.9. Bsn-Cutinase-GFP11 secretion with RBS spacer lengths from 4–12 nt. Backscatter (a) and DO (b) were measured during cultivation of *C. glutamicum* pCMEx[4-12]-Bsn-Cutinase. Pre-cultures inoculated from cryo cultures were used to inoculate three main cultures that are shown as mean with standard deviation in confidence tubes. Inoculation and induction of main cultures with IPTG to a final concentration of 200 µM were each triggered by a device-dependent backscatter signal in the exponential phase. Cells were harvested 4 h after induction with main culture durations of 11.9–12.4 h [175]

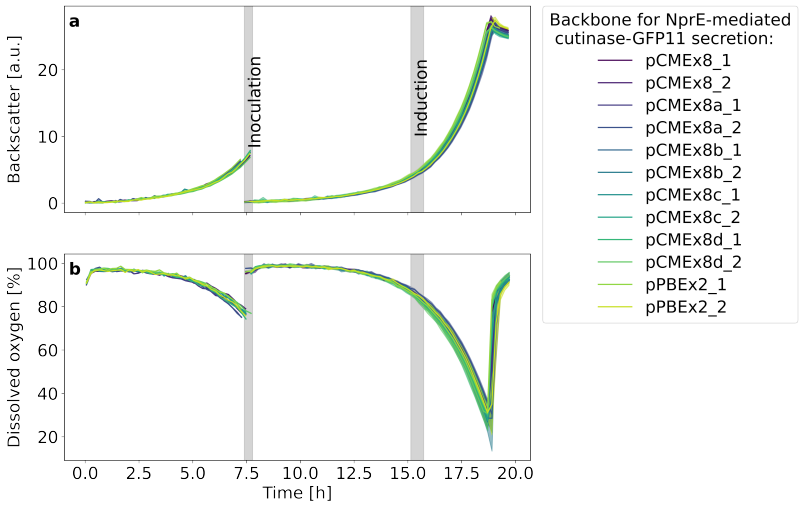

Fig. A.10. Cultivation of *C. glutamicum* RBS variants for NprE-Cutinase-GFP11 secretion. Two pre-cultures per strain were inoculated from cryo-conserved cultures. Triggered by backscatter signals, three main cultures were inoculated per pre-culture. Cutinase-GFP11 secretion with signal peptide NprE was induced with IPTG to a final concentration of 200 µM as soon as the backscatter threshold was reached. Cells were harvested 4 h after induction and supernatant was stored for detection of target proteins in the supernatant. Error tubes deviate from 3 main culture replicates

A.3. Supporting material for chapter 3.3

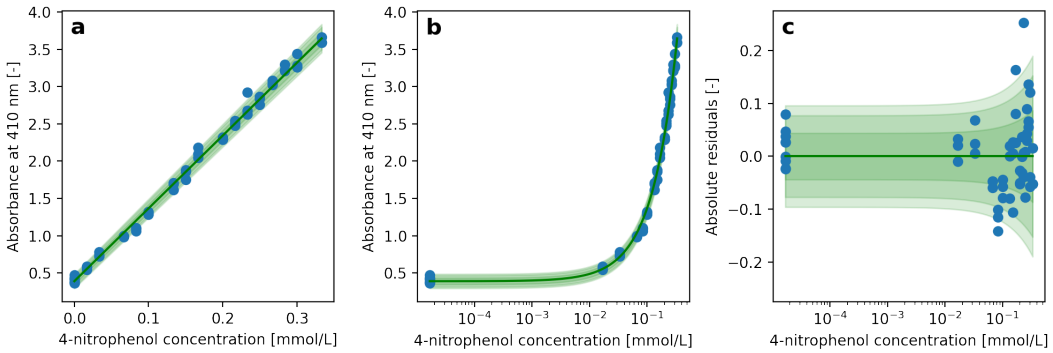

Fig. A.11. Calibration model for the cutinase assay. 4NP formation was measured at 410 nm and 37 °C for 40 min in a microplate reader. The model is describing the relationship between absorbance at 410 nm and the 4NP concentration in mM (a). The same relationship can be seen on a logarithmic scale (b). The residuals between model and data are shown for the 68%, 90% and 95% likelihood bands (c) [181]

$$
\begin{aligned}
k_{\text{strain}} &\sim \text{HalfNormal}(\sigma = 3) \\
\text{batch\_effect}_{\text{culture\_well}} &\sim \text{LogNormal}(\mu = 0, \sigma = 0.3) \\
\text{assay\_effect}_{\text{mtp\_column}} &\sim \text{LogNormal}(\mu = 0, \sigma = 0.1) \\
\text{cf\_cutinase\_assay}_{\text{mtp\_well}} &\sim \text{LogNormal}(\mu = \log(\text{cf\_input}_{\text{mtp\_well}}), \sigma = 0.3) \\
S_0 &\sim \text{Uniform}(\text{lower} = 0.5,\ \text{upper} = 0.7)) \\
\text{absorbance\_intercept} &\sim \text{Normal}(\mu = \text{intercept}_{\text{calibration model}}, \sigma = 0.1)
\end{aligned}
$$

$$
\begin{aligned}
k_{\text{batch}} &= k_{\text{strain}} \cdot \text{batch\_effect} \\
k_{\text{assay}} &= \text{cf\_cutinase\_assay} \cdot k_{\text{batch}} \cdot \text{assay\_effect}/\text{dilution\_factor} \\
Y_{\text{pred}} &= P_{t,\text{mtp\_well}} = S_0 \cdot \left(1 - e^{(-k_{\text{assay}} \cdot t)}\right) \\
\mathcal{L}(\theta_{\text{pm}} \mid Y_{\text{obs}}) &= p\left(Y_{\text{obs}} \mid \phi_{\text{calibration model}}(Y_{\text{pred}})\right)
\end{aligned}
\tag{A.1}
$$

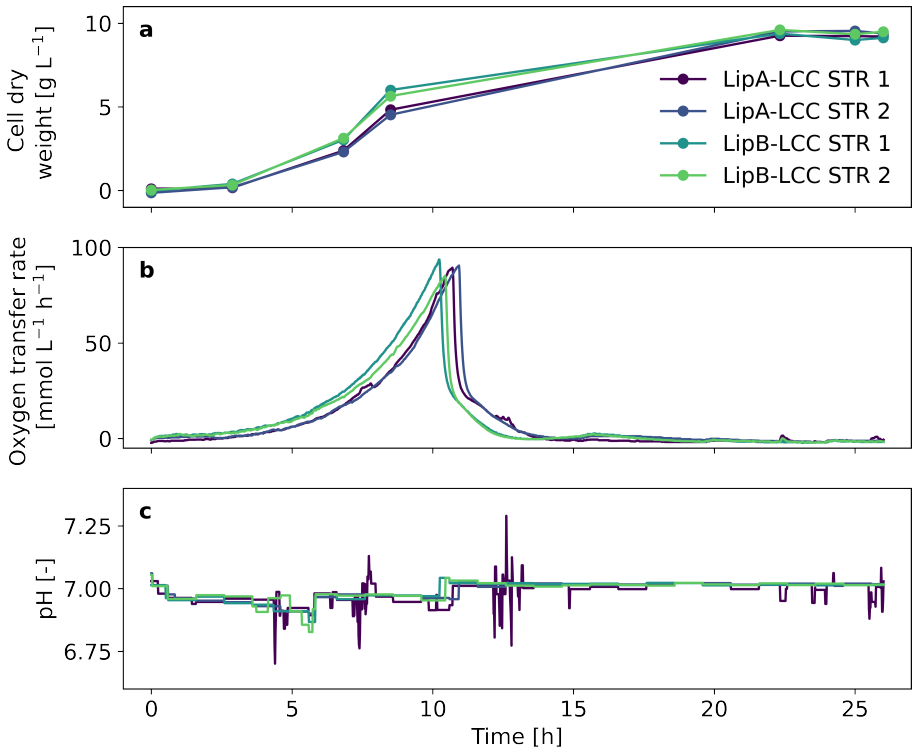

Fig. A.12. *C. glutamicum* LCC secretion mediated with signal peptide LipA or LipB in duplicates (STR 1 and 2). Samples from all bioreactors were taken for determination of cell dry weight (a). The oxygen transfer rate (b) and pH (c) signals were measured online during cultivation. LCC secretion was induced by adding IPTG to a final concentration of 200 µM at the second sampling point for CDW determination at an $OD_{600\,nm}$ around 1 and from here on additional samples were taken for activity measurements with the cultivation supernatants [181]

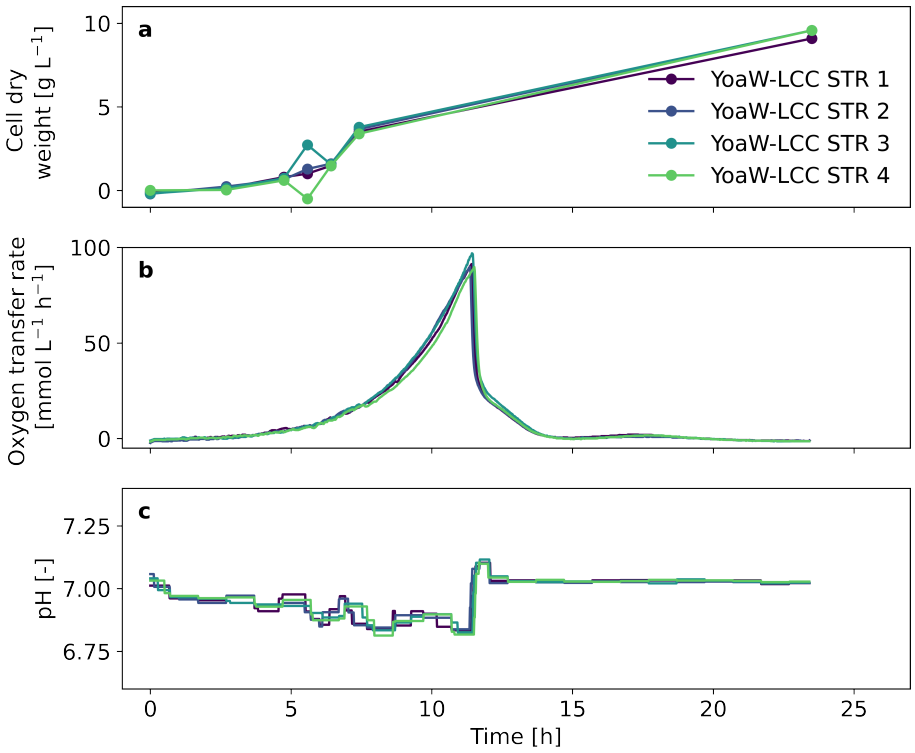

Fig. A.13. *C. glutamicum* LCC secretion mediated with signal peptide YoaW in quadruplicates (STR 1–4). Samples from all bioreactors were taken for determination of cell dry weight (a). The oxygen transfer rate (b) and pH (c) signals were measured online during cultivation. LCC secretion was induced by adding IPTG to a final concentration of 200 µM at the second sampling point for CDW determination at an $OD_{600\,nm}$ around 1 and from here on additional samples were taken for activity measurements with the cultivation supernatants [181]